DEVELOPMENT OF CONTINUOUS SOLVENT EXTRACTION PROCESSES FOR COAL DERIVED CARBON PRODUCTS

DE-FC26-03NT41873

Quarterly Report

PERIOD OF PERFORMANCE:
April 1, 2006 – June 30, 2006

Submission date:
August 1, 2006

Principal Investigator:
Elliot B. Kennel

Co-Investigators:
Dady B. Dadyburjor, Mark E. Heavner, Manoj Katakdaunde, Liviu Magean, J. Joshua Maybury, Alfred H. Stiller, Joseph M. Stoffa, John W. Zondlo

West Virginia University
Department of Chemical Engineering
College of Engineering and Mineral Resources
PO Box 6102
Morgantown WV 26506

Subcontractors:
GrafTech International
12900 Snow Road
Parma, OH 44130

Koppers Inc.
1005 William Pitt Way
Pittsburgh, PA 15238

DISCLAIMER:

ABSTRACT

The purpose of this DOE-funded effort is to develop continuous processes for solvent extraction of coal for the production of carbon products. The largest applications are those which support metals smelting, such as anodes for aluminum smelting and electrodes for arc furnaces. Other carbon products include materials used in creating fuels for the Direct Carbon Fuel Cell, and porous carbon structural material referred to as “carbon foam” and carbon fibers.

During this reporting period, hydrotreatment of solvent was completed in preparation for pitch fabrication for graphite electrodes. Coal digestion has lagged but is expected to be complete by next quarter. Studies are reported on coal dissolution, pitch production, foam synthesis using physical blowing agents, and alternate coking techniques.

Table of Contents

List of Figures

List of Tables

1.0 Executive Summary

Carbon foam is a material with many unique characterizes and proposed applications. Yet, the production process is pressure and temperature intensive. This study investigates the possibility of using pitch to form pitch foam, a precursor to carbon foam, through the use of physical blowing agents, specifically, CO_2, N_2 and water. Pitch has been characterized as behaving as a thermoplastic similar to organic polymers. Measurements of viscosity, transition temperatures, and heat capacity were taken for comparison of pitch and various polymers. Physical blowing agents are often used to produce cells within the polymer melt resulting in foam. The introduction of physical blowing agents into pitch melts yields similar results. Variations of three process parameters, temperature, saturation pressure, and pressure drop rate, in a batch process were examined to see if these parameters qualitatively yield the same trends for pitch foam as they do for polymer foam. It was found that the cell density of the resulting pitch foam varies proportionately with temperature, saturation pressure, and pressure drop rate; and cell size varies inversely with temperature, saturation pressure, and pressure drop rate, in the same manner as polymeric foam. The investigation could lead to a novel and inexpensive route to the production of carbon foam.

2.0 Technical

2.1 Synpitch Fabrication

In this reporting period, the production of ten drums of hydrotreated coal tar distillates was completed. However, coal digestion has yet to be completed. The current protocol for coal digestion calls for coal to be dispensed in the reactor in the form of a -50 mesh granular solid. This requires the system to be opened while coal is loaded, which in turn requires that the system be cool enough such that excessive volatile vapors are not released.

In addition, nitrogen pressurized filtration requires that the extract be cooled to about 200 ^{o}C. This requires time to cool down.

Modifications are planned for the next iteration of pitch production. Specifically, an intermediate holding tank will be used to permit the extract to be cooled (or alternatively, heated) to the desired temperature for filtration/centrifugation, thus permitting the reactor to be simultaneously re-loaded.

The system for hot loading, developed originally for the hydrotreatment process, will also be used for coal digestion. The primary modification is that the inlet feedstock will be a slurry rather than a true liquid. However, a diaphragm pump is adequate to handle a slurry of this type.

Figure 1 illustrates the modified digestion reactor. Key improvements are the use of a Lightnin^{TM} mixer to ensure that a coal slurry is formed; a separate holding tank to allow hot liquid to be transferred from the reactor; and a nitrogen ram system to remove plugging from the reactor outlet.

Figure 1. Modified reactor system for carrying out digestion.

2.2 Digestion (Joseph M. Stoffa)

The research detailed herein observed the swell and extraction of a bituminous coal in the super solvent n-methyl-pyrrolidone (NMP). NMP is no longer the solvent of choice for producing The swell and extraction was described as a function of process parameters, the extraction temperature and extraction time. The relationship between swell and extraction was examined, and the effect of coal size was quantified. Additionally, mercury porosimetry was performed to examine the porosity of the bituminous coal used in the research. The porosity of the bituminous coal and its relationship to solvent extraction and solvent swelling of coal was examined.

2.2.1. Functional Groups of Coal

In addition to carbon, the organic portion of coal contains hydrogen, oxygen, and nitrogen. These are the elements necessary to form the functional groups defined by organic chemistry. Organic chemistry is useful for predicting the behavior of coal in lesser known systems. Petrography, while useful for classifying coal, is inadequate for making novel predictions about coal systems. To determine what functional groups are appended to coal molecules, researchers use FTIR (Fourier Transform Infrared Analysis), NMR (Nuclear Magnetic Resonance), and XRD (X-ray Diffraction). The relevance of specific functional groups to coal chemistry is summarized below.

R-OH (Hydroxyl)

Hydroxyl groups in coal are interaction sites that solvents use to form hydrogen bonds. Solvent-coal hydrogen bonds are of interest because many solvents are thought to dissolve coal through a process requiring hydrogen bonding. FTIR studies of various coal ranks suggest that as coal rank increases from lignite to bituminous, there is a decrease in oxygen and hydroxyl content[1]. This implies that higher rank coals contain fewer interaction sites with which to form hydrogen bonds with solvents.[2]

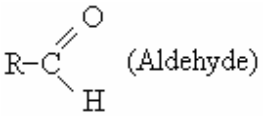

(Aldehyde)

Aldehydes are polar functional groups. The electronegative oxygen pulls the bonding pair of electrons towards itself, creating an electron deficiency at the carbon atom. Treatment of aldehydes with oxidizing agents, such as nitric acid, transforms the aldehydes to carboxylic acids. Coal researchers transform aldehydes to carboxylic acids using oxidizing chemicals such as hydrogen peroxide. Pretreatment of coal with oxidizing agents often results in increased extraction yields.

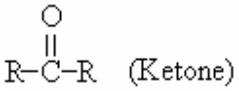

Ketones are hydrogen bond acceptors, but not hydrogen bond donators. Therefore, ketones can not form hydrogen bonds with themselves. This makes ketones more volatile than alcohols or carboxylic acids of similar molecular weight.[3] A ketone can combine with an electrophile to form resonance stabilized cation.

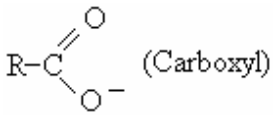

Carboxyl groups are characteristic constituents of more complex functional groups such as carboxylic acids and amides.[4]

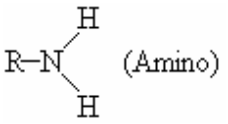

The amino functional group is of interest because the nitrogen can donate its electron pair to the proton of an acid.[5] When the nitrogen donates its electron pair, it becomes positively charged.

R-SH (Sulfhydryl)

In organic chemistry the sulfhydryl group is a functional group composed of a sulfur and a hydrogen. When the sulfhydryl group is connected to a carbon atom, it is known as a thiol, formerly called by the name mercaptan.

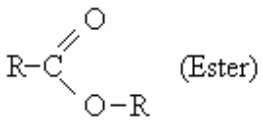

Esters can participate in hydrogen bonds as hydrogen bond acceptors, but cannot act as hydrogen bond donors, unlike their parent alcohols. and acids.

Examples of the functional groups mentioned can be observed in the Wiser Model of bituminous coals, illustrated in Figure 2.

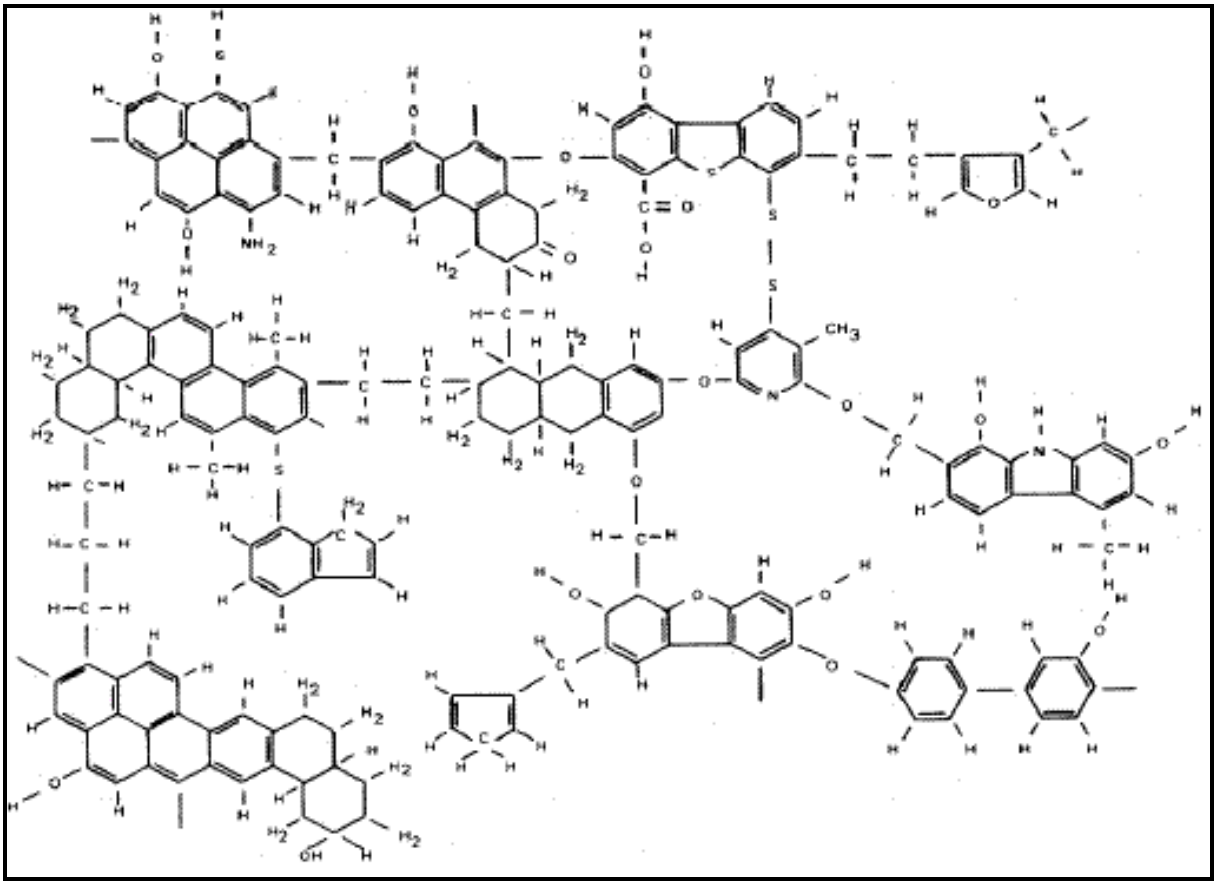

Figure 2. Wiser Macromolecular network model of bituminous coals[6]

2.2.2. Solvent Classification

In 1951, Oele et al. proposed a system for the classification of coal solvents based on four general types.[7]

a. Group 1, Non-specific solvents – Extract a small amount of coal (up to 10 %) at temperatures up to 135 °C. These solvents extract the resins and wax residues found in coal. The material extracted with Group 1 solvents is typically aliphatic in nature. Examples of Group 1 solvents include acetone, alcohols, benzene, chloroform, and ethers.

b. Group 2, Specific solvents – Specific solvents dissolve a larger portion of coal (20 to 40 %) than non-specific solvents, and are used at temperatures below 230 °C. Specific solvents extract coal by a process of physical dissolution. Dryden showed that effective specific solvents are those that contain a nitrogen atom and an oxygen atom with unshared electrons as a lone pair.[8] This lone pair of electrons tends to affect the solvent polarity and the coal swelling

characteristics of the coal. The nature of the extracted coal is virtually indistinguishable from the original coal.

c. Group 3, Degrading solvents – Degrading solvents extract the majority of coal (up to 90 %) at temperatures up to 425 ℃. The solvent can be recovered from the solution substantially unaltered. This action is presumed to depend on the mild thermal degradation of coal which produces smaller, more soluble, coal fragments. Anthracene oil and phenanthrene and examples of degrading solvents.

d. Group 4, Reactive solvents – Reactive solvents extract coal by chemical interaction. The chemical interaction of the solvent promotes degradation during coal extraction. The structure of both the coal and coal solvent change during this process. Examples of reactive solvents include; low temperature alkali hydrolysis of coal by alkaline-alcoholate resulting in partial depolymerization of the coal matrix."[9]

There is another class of solvents, not considered by Oele, known as super solvents. Super solvents are unique in that they can dissolve of many substances, both polar and non-polar. In 1981 Stiller showed that super solvents are capable of dissolving large amounts of organic material. Super solvents are a class of dipolar aprotic solvents that are capable of dissolving a large amount of the organic material in coal.[10]

Super Solvents have the general formula.

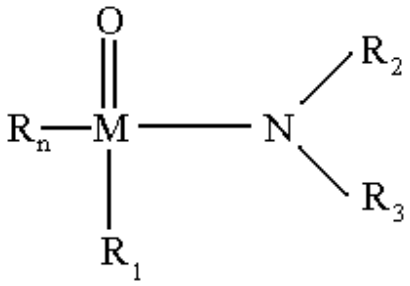

Functional representation of a super solvent

where M is a carbon, sulfur, or phosphorus atom, R2 and R3 are either a hydrogen or lower alkyl group, and R1 and Rn are either each a lower alkyl group, another

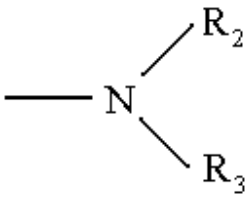

group, a monocyclic group or R1 can be another

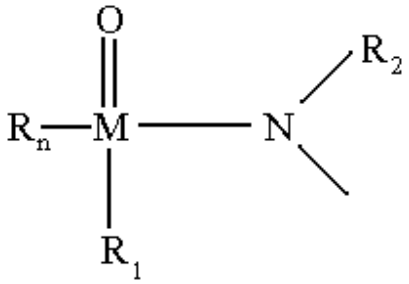

group, or R1 and R3 can represent the atoms necessary to close a heterocyclic ring, and n = 1 where M = Phosphorus and is otherwise 0. Where Rn and R1 are either or both lower alkyl groups in this formula alkyl can apparently have a carbon content in the range of C1-C4, or possibly C5, of which C1 and C2 are preferable. Preferred substituents for R2 and R3 are methyl and ethyl groups, although it is produced that homologs up to about C4 or possibly higher would produce more or less useful solvent compounds, and the replacement of such groups with one or more hydrogen atoms also appears to be an acceptable alternative. Monocyclic aromatic groups such as benzyl radical might also prove useful as the substituent Rn and R1, because the structure of this group is favorable to the resonance stabilizing function of the solvent. Either or both of Rn and R1 can be another amino group.[11]

Dimethyl-sulfoxide (DMSO), N-N-dimethyl-acetamide (DMAA), N-methyl-2-pyrrolidone (NMP), hexamethyl phosphoramide (HMPA), and tetra-methyl-urea (TMU) are some commonly used super solvents.

NMP extraction has been extensively trialed in previous coal solvent extraction experiments at WVU. Solvent extraction refers to a process where coal is refined by dissolution in a solvent, usually at elevated temperatures, followed by filtration. The filtration or centrifugation step separates the soluble carbonaceous portions of coal from the insoluble organic portions of coal. During solvent extraction, it is hypothesized that coal undergoes no chemical change; therefore, solvent extraction is more of a cleaning process than a chemical upgrading process.

Solvent extraction, like any coal cleaning technology, operates by exploiting differences between the desirable and undesirable portions of coal. The soluble portions of coal are typically carbonaceous aromatic macromolecules trapped within the 3-dimensional cross linked lattice of coal as illustrated in the Wiser Model for bituminous coals.[12] The insoluble inorganic portion of the coal consists mainly of pyrite, quartz, and clays. These inorganic materials become ash after the coal is combusted, and are the major source of particulate emissions from the combustion of coal. The temperature and pressures at which solvent extraction operates occupies a large range. Some studies have used extraction temperatures as low as room temperature, while others have employed temperatures up to 300 °C.

NMP is used as an extraction solvent because it is effective, relatively safe, and widely used in research. NMP is a super solvent. summarizes the physical and chemical properties of NMP.[13]

Table 1. Physical and chemical properties of NMP[14]

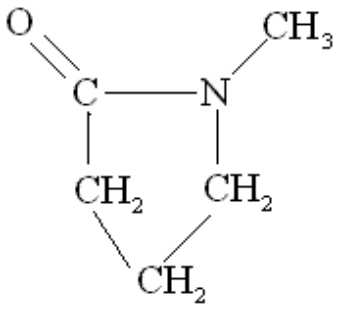

Empirical Formula:	C_5H_9NO
Molecular Weight:	99.13
Physical form:	Liquid with mild amine-like odor.
Color (APHA):	50
Melting Point:	-24 ºC (-11.9 ºF)
Boiling Point:	202 ºC (395 ºF) @ 760 mmHg 150 ºC (302 ºF) @ 162 mmHg 100 ºC (212 ºF) @ 24 mmHg Tsat = {ln (Psat) + 0.2349} / 0.0156 (Tsat [ºC], Psat [mmHg])
Viscosity (25 ºC)	1.65 cp
Specific Gravity:	1.027 @ 25 ºC 0.987 @ 75 ºC 0.969 @ 100 ºC
Specific Heat (Cp):	0.40Kcal/kg at 20 ºC CpNMP = 8.04*10^-4 *(T) + .38 (Cp [cal/gm* ºC], T [ºC])
Thermal Conductivity (kNMP):	kNMP = -1*10^-4(T) + 0.1954 (T [ºC], kNMP [W/M/ºC])
Heat of Vaporization	127.3 K cal/kg at 20 ºC
Interfacial Surface Tension	(25 ºC): 40.7 dynes/cm
Flash Point (open cup):	95 ºC (204 ºF)
Dipole Moment	4.09+0.04 Debye
Dielectric Constant (25 ºC):	32.2
Solubility parameter (d):	11.0
Miscibility with Other Solvents:	completely miscible with water and most organic solvents including alcohols, esters, ketones, aromatic and chlorinated hydrocarbons and vegetable oil.

2.2.3. Coal Dissolution via NMP

As discussed previously, models typically treat coal as a large 3-dimensional macromolecular network, with extractable carbonaceous substances occluded in the pores in between the macromolecular network. Research by Takanohashi differed in that it concluded coal was a large aggregate, and Takanohashi proposed different mechanisms for describing coal dissolution.[15] Thus, Takanohashi's research suggested that coal is solubilized without breaking covalent bonds.

The most common model of solvent extraction treats extraction in terms of the electron donor and acceptor interactions in the solvent coal system.[16] This model assumes that donor-acceptor bonds in coal are responsible for binding together the macromolecular network and the extractable carbonaceous materials that fill the pores of the network.[17] According to this model, "Extraction is in principle, a substitution reaction: pore substances are replaced by a solvent molecule in their $Donor_{network} \rightarrow Acceptor_{pore\ substance}$ or $Donor_{pore\ substance} \rightarrow Acceptor_{network}$ bonds that bind together structural elements of an original coal."[18]

Solvent swelling of coal occurs when the physical dimensions of coal increase due to the presence of a solvent. Researchers study coal swelling to elucidate coal structure. Additionally, researchers correlate or relate coal swelling with other coal properties; such as coal extraction yield or coal surface area. The hypothesis of why coal swells in a solvent is adapted from polymer research. For this reason, coal swelling studies tend to be more interdisciplinary than other coal studies. This leads to a wealth of coal swelling studies, the main points of which appear in summary below.

The amount of coal swelling is measured by the swelling ratio, represented by the symbol Q. The swelling ratio is defined as the volume of the swollen coal divided by the volume of the original coal. Coal begins to swell as it imbibes a solvent for which it has an affinity. As the coal absorbs solvent, it grows in size, while maintaining its original shape. When the solvent is removed the coal shrinks to near its original size and shape. Some destruction of coal samples occurs after swelling and shrinking, but this destruction seems due to mechanical stresses rather than chemical changes.[19] It is important that coal retains its original shape after swelling and shrinking because coal swelling models assume that swelling is a reversible process.[20] Solvents for which coal has a high affinity are referred to as "good swelling solvents." Swelling in good swelling solvents is found to be independent of the solvent to coal weight ratio and grinding direction.[21,22] In good swelling solvents such as NMP and pyridine, coal is capable of swelling to over twice of its original volume, while still retaining its original shape.[23]

Good extraction solvents are usually good swelling solvents. Thus, n-methyl pyrrolidone (NMP) and carbon disulfide (CS_2) are expected to be good swelling solvents.[24] The ability of a solvent to swell coal is a strong function of the electron donating ability of the solvents.[25] Painter and Shenoy proposed that the swelling of coal takes place by a process of chain disinterspersion.[26] It is postulated that the covalent bonds in the coal matrix act as chains that are stretched by solvents. In this model, the solvent dissociates the non-covalent cross-links of the coal matrix resulting in a swollen coal sample.

Because of the anisotropic nature of coal, coal swells preferentially in a direction perpendicular to the bedding plane of the coal seam.[27] This directional swelling is observed because coal appears to be more highly cross-linked in the bedding plane than perpendicular to it.[28] This directional swelling of coal is not noted in most studies because only bulk swelling is measured, not the swelling of individual oriented coal pieces. Measuring the swelling ratio of

individual coal pieces yields clues to the structure of coal not provided by the bulk swelling behavior of coal. "The perpendicular/parallel swelling ratios are highest in pyridine and lowest in chlorobenzene, indicating a highly anisotropic arrangement of covalent bonds."[29] Also, the time to reach maximum swell parallel to the bedding plane is shorter than the time to reach maximum swell perpendicular to the bedding plane.[30] Cody et al also discovered that swelling measured as a function of time passes through a maximum due to the formation of a metastable state.

Other clues about the structure of coal may be obtained by studying the swelling of different ranks of coal in various solvents. Observing the swelling ratios of different ranks in different solvents may provide information about the structural changes across varying ranks. Rincon et al found that swelling ratios are higher for lower ranked coals.[31] Rincon also found that swelling could be used to improve THF (tetrahydrofuran) soluble materials after liquefaction with H-donor solvents.[32] The trend of increased THF soluble materials correlated with coals of increased swelling ratios.[33] Rincon et al postulated that that liquefaction of coal by H-donor solvents is a surface area dependent reaction, and that pre-swelling the coal is a good method for producing greater penetration and diffusion of reactants, increasing the liquefaction yield.[34]

How quickly coal swells is controlled by how quickly the solvent can diffuse into the coal. This is controlled by solvent properties, the size of the coal particles, and the average molecular weight between the crosslinks of the coal matrix.[35] The diffusion of solvent into coal is modeled by either Fickian diffusion or anomalous transport.[36] Coal is a glassy solid at room temperature, but transitions to a flexible state as it absorbs solvent. The flexible nature of the swollen coal suggests lower effective crosslink density, and suggests that the elasticity of the solvent swollen coal may be predominantly rubber-like.[37] The transition from the glassy to rubbery state is generally very sharp.[38]

When discussing how swelling affects dissolution, if at all, it may be helpful to break coal constituents into soluble and non-soluble materials. Current models for coal dissolution postulate that the soluble portions of coal occupy the pore space of coal and extraction more or less leaves the existing macro molecular network intact.[39] An aggregated structure of coal would imply a model where the coal structure is irrefragably lost upon dissolution.

2.2.4 Experimental Studies of NMP-Coal Interactions

By examining process parameters and coal properties, and their effect on the extraction and swelling of bituminous coal, it was possible to develop a correlation describing the solvent extraction and solvent swelling of high-volatile bituminous coal in the super solvent n-methyl-pyrrolidone. It is hypothesized that the developed correlation is general enough to apply to all bituminous coals in super solvent systems.

The experimental matrix is a summary of experiments that were performed during the research. The experimental matrix dictated the values of the independent variables during a particular experiment. These variables were manipulated to determine their effect on solvent extraction and solvent swell. The independent variables which the experimental matrix controlled are system temperature, time at temperature, and coal size.

The system temperature may determine how quickly solvent extraction proceeds. There are several temperatures of interest ranging from 50 °C to 200 °C. The time at temperature may determine how far solvent extraction proceeds and to what extent the coal swells. There are

several times of interest, from 2 minutes to 270 minutes. The coal size may affect the rate of solvent extraction and coal swell, and or the extent of solvent extraction and coal swell. There are three coal sizes of interest, a relatively large, medium, and small, ranging from 40 Tyler Mesh (355 μm) to sub 150 Tyler Mesh (less than 106 μm). These variables and their ranges are illustrated graphically in the experimental matrix, which appears below as Table 2.

Table 2. Experimental Matrix.

Size	
s1	Small
s2	Medium
s3	Large

Temperature (°C)	
m1	50
m2	80
m3	100
m4	120
m5	140
m6	170
m7	200
m8	140
m9	140
m10	185

Time (minutes)		
t1	5	Temperatures 140°C or Less
t2	15	
t3	30	
t4	60	
t5	90	
t6	120	
t7	150	
t8	180	
t9	210	
t10	240	
t11	270	
t1	2	Temperatures Above 140°C
t2	4	
t3	6	
t4	8	
t5	10	
t6	12-14	
t7	14-16	
t8	16-18	
t9	18-20	
t10	20-22	
t11	22-24	
t12	60	

Coal swells when imbibing a solvent. The amount a coal swells, known as the swelling ratio, is the volume of the swollen coal divided by the volume of the original coal, minus one. The swelling ratio, Q is given by

$$Q = \frac{h_f}{h_i} - 1 \quad . \qquad \text{(Equation 1)}$$

Following solvent extraction, it is necessary to determine how much coal is dissolved in solution. The amount of coal dissolved in the coal-NMP solution is directly proportional to the absorbance of the coal-NMP solution. The absorbance of the coal-NMP solution is measured using a UV-Vis spectrophotometer. Beer's Law is used to calculate the amount of coal in solution,

$$A = ebc \qquad . \qquad \text{(Equation 2)}$$

In Equation 2, A represents the absorbance of the solution, ε is the molar absorptivity, b is the path length, and c is the concentration. A solution exposed to UV-VIS spectroscopy must be absorbent enough to absorb some light, but not so absorbent that too little light is transmitted. Without the proper absorbance, useful data will not be obtained. The absorbance equals the logarithm of the ratio of the power of the light source before and after passing through the solution. The equation used to calculate absorbance A is

$$A = \log \frac{P_0}{P} \qquad . \qquad \text{(Equation 3)}$$

where P_0 and P are, respectively, the power of a beam of monochromatic radiation before and after passing through the solution. Another variable in Beer's Law is the path length, represented as term b. The path length is the length of solution that the UV-Vis monochromatic beam must pass through. Figure 3 is a graphical illustration of these properties.

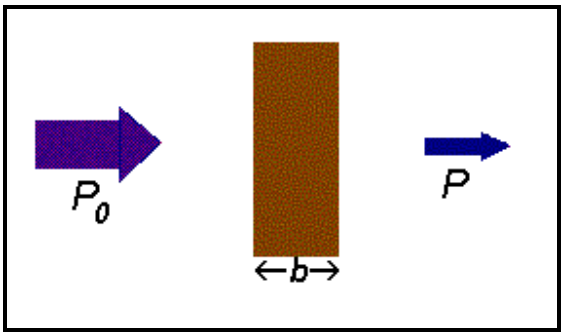

Figure 3. Radiation passing through solution of path length b.

This is not a linear relationship at higher concentrations, only at lower concentrations. For this reason, it is necessary to keep the absorbance of the coal-NMP solutions at or below three. There are two controllable parameters that determine solution absorbency. The first parameter is the path length of the cell that holds the coal-NMP solution. If cell A is ten times the width of cell B, the solution in cell A will appear to have one tenth of the transmittance ($T = P / P_0$) of the solution in cell B. The second adjustable parameter is the dilution of the solution. A relatively dilute solution will absorb less (have a higher transmittance) than a relatively concentrated solution.

It is necessary to know the molar absorptivity of the coal NMP-solution before the concentration of the coal-NMP solution can be calculated. The molar absorptivity, a measure of the amount of light absorbed per unit concentration, is calculated as follows. A Soxhlet Extraction is performed on all coal samples, small, medium, and large. Soxhlet extraction is performed for 24 hours at reflux under vacuum, to ensure complete extraction. The product is filtered and vacuum dried at ambient temperature. The product and residue weights is added and mass closure is achieved. A known amount of extract is dissolved in a known amount of NMP. The extract is dissolved fully in the NMP, and will then be diluted 100:1. The absorbance is

measured and plotted as a function of concentration. A linear regression is performed and the slope is the product of the molar absorptivity and the path length.

Porosimetry is the measurement of pore size, pore volume, pore size distribution, density, and other porosity related characteristics. The adsorption, permeability, strength, and density of a material are often influenced by its pore structure. The porosity of the Lower Powellton coal used in this research was characterized via mercury porosimetry. Mercury porosimetry is based on the capillary law governing liquid penetration into small pores. This law, in the case of a non-wetting liquid like mercury, is expressed by the Washburn equation,

$$D = \left(\frac{1}{P}\right) 4g \cos f \quad . \qquad \text{(Equation 4)}$$

where D is the pore diameter, P is the applied pressure, γ the surface tension of the mercury, and ϕ the contact angle between the mercury and the sample, all in consistent units. The volume of mercury V penetrating the pores is measured directly as a function of applied pressure. This P-V information serves as a unique characterization of pore structure.[40] Mercury porosimetry is capable of observing pore sizes over five orders of magnitude, from 0.003μm to 360 μm.

The experimental procedure consisted of the methods necessary to perform extraction of coal with NMP, measure coal swell, quantify coal solubility, and analyze coal porosity.

Solvent extraction experiments were run in batches. Each batch was performed at a temperature of interest. For example, the first batch was run at 50 °C, and contained samples of small coal in NMP. In this particular batch, there were eleven samples, one sample for each of the eleven times of interest as illustrated in the experimental matrix. Experimental batches at temperatures above 140 °C had twelve time levels. All extraction runs were performed individually in a set of 10ml graduated test tubes.

To begin an experimental batch, each empty test tube was numbered and weighed to one milligram accuracy. The test tube was then filled with 1ml of Lower Powellton coal of the appropriate size, and again weighed to the nearest milligram. The graduated test tube was then filled to the 6 ml graduated mark with NMP, and again weighed to the nearest milligram. After the above procedure was complete for all samples in an experimental batch, the set of test tubes were placed in a test tube rack, and lowered into a fluidized sand bath preheated to the batch temperature.

Once a time of interest was reached, a test tube was removed from the sand bath and allowed to air cool. Test tubes were continually removed at the experimental times until no more test tubes remained. Once the test tubes were removed and cooled the solvent extraction was complete. With solvent extraction complete, the next tasks were to quantify the amount that coal swelled during extraction, and to quantify the amount of coal dissolved in NMP.

After the test tubes were air-cooled, the extraction runs were complete. At this time the test tubes were centrifuged. The graduation mark to which the coal had swollen was noted. The swelling ratio was calculated as the ratio of the post-extraction volume of the coal divided by the pre-extraction volume of the coal, minus one, in accordance with Equation 1. For example, if the coal had expanded to the 2.5 ml mark (from the original 1.0 ml mark), that would indicate a swelling ratio of 150 %. After all the swelling ratios in a particular experimental batch were measured, the next step is to quantify coal solubility.

After the swelling ratio was recorded, one or two milliliters (depending on solution darkness) of the coal-NMP solution were withdrawn from the test tube via a graduated pipette. The one or two milliliters of the coal-NMP solution were placed in a 100 ml Erlenmeyer Flask. NMP was added to the flask until the 100 milliliter mark was reached. This resulted in either a 50:1 or 100:1 dilution of the coal-NMP solution. A portion of the diluted solution was placed in a small polyethylene bottle, and stored in a refrigerated room until ready for analysis.

Coal solubility was quantified by analyzing the absorbance of the coal-NMP solution. The absorbance of the coal-NMP solution is measured in a UV-Vis spectrophotometer.

Adjustment of both of the coal-NMP solution darkness and cell path length were necessary to obtain solutions with the proper absorbance. A cell width (path length) of 0.1 mm was required, which is small compared to most cells. Dilution of the coal-NMP solution was necessary as well. Some coal-NMP samples were diluted by a factor of 50, while most were diluted by a factor of 100. The dilution factor was chosen depending on the darkness of the coal-NMP solution. Light solutions had a dilution factor of 50:1, while average and dark solutions had a dilution factor of 100:1. These dilution factors placed absorbance readings in an acceptable range.

Porosity measurements were made to determine is they could be related to coal extraction and coal swelling. Porosity measurements were made via an AutoPore 9220 Mercury Porosimeter. The mercury porosimeter analyzes samples in a sample holder known as a penetrometer. The penetrometer is cleaned and weighed to the nearest milligram. A small amount of coal, approximately 2 grams, is placed in the penetrometer. The penetrometer is weighed again to the nearest milligram, and the difference is the sample weight. The penetrometer is placed in the mercury porosimeter for analysis. The mercury porosimeter contains its own dedicated vacuum pump, and the sample penetrometer is evacuated to a pressure of 10 μm Hg, well below the vapor pressure of water at room temperature. Once the evacuation pressure is reached, the porosimeter evacuates the sample for an additional hour to ensure a dry sample. Then the penetrometer is filled with mercury under a pressure 0.5 psia and the analysis can begin. The mercury pressure slowly increases and the intrusion of mercury is measured at various pressures. The penetrometer, filled with mercury, is removed from the low pressure ports and again weighed to the nearest milligram. From this information the density of the coal sample is calculated. Then the penetrometer is placed in the high-pressure test station of the mercury porosimeter, which varies the pressure from 30 psia to 60,000 psia. After the pressure increases to 60,000 psia, the sample is depressurized from 60,000 psia to atmospheric pressure. Whereas the increasing pressure is used to measure mercury intrusion, the decreasing pressure is used to measure mercury extrusion. The amount of mercury extruded relative to the amount intruded quantifies the amount of “ink bottle” type porosity.

2.2.5 Coal Dissolution Experimental Results

Mercury porosimetry was used to determine the porosity characteristics of coal. To ensure accurate data, there was one sample and three replicates ran for each coal size, a total of four analyses. The data for the four small coal samples follows in Figure 4.

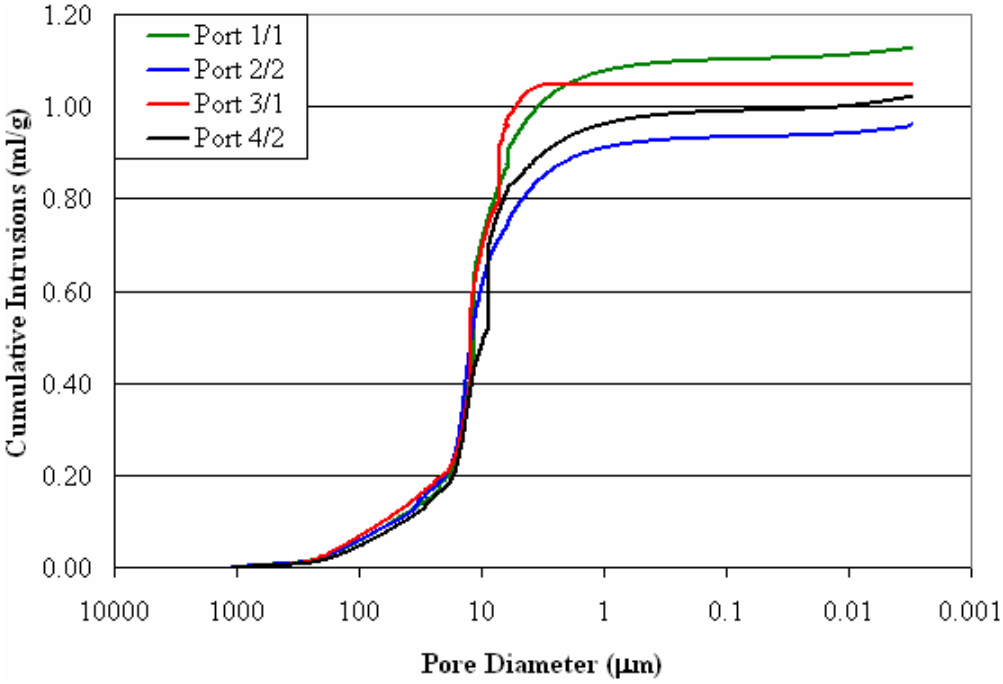

Figure 4. Porosity of small (sub 106 µm) coal

The cumulative intrusion as measured by the mercury porosimeter, in units of ml of mercury per gram of coal sample, is represented by the y-axis. The pore diameter of the coal sample, which is proportional to the mercury over-pressure exerted on the sample by the porosimeter, is represented by the x-axis. The mercury porosimeter contained four low-pressure analysis ports and two high-pressure analysis ports. The low-pressure and high-pressure ports which the samples were analyzed in are represented by the key in the upper left hand of Figure 4. Mercury porosimetry results suggested that most of the porosity in small coal occurred between approximately 80 µm and 20 µm.

Medium sized coal and large sized coal was also analyzed via mercury porosimetry, and the results are represented as Figures 5 and 6.

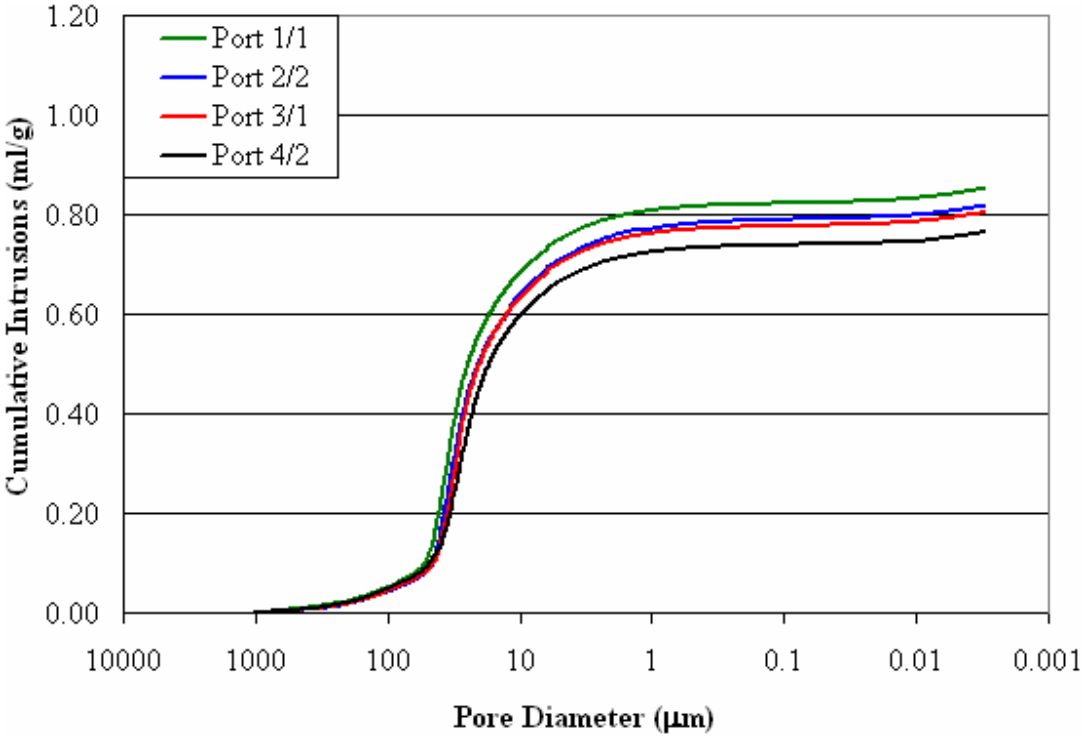

Figure 5. Porosity of medium (106 to 212 µm) coal

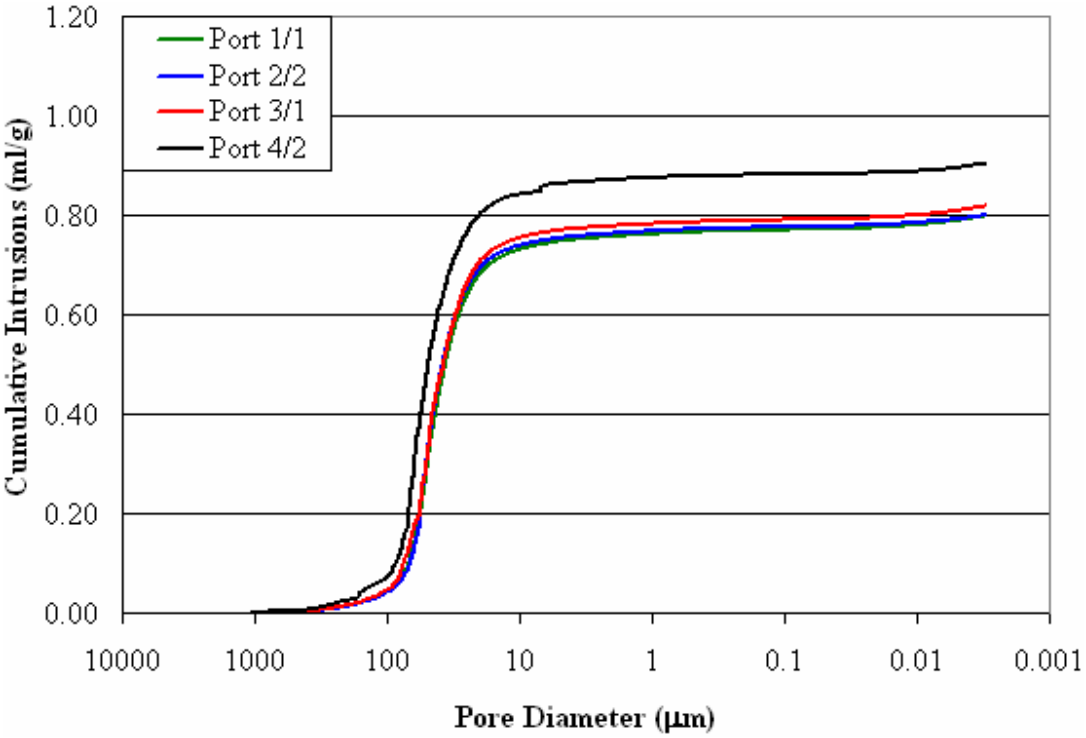

Figure 6. Porosity of large (212 to 355 µm) coal

As with the small coal, porosimetry results suggested that most porosity in medium and large coal occurred between 80 μm and 20 μm. However, medium and large coals exhibited less total porosity than small coals. The discrepancy in coal porosity across the different coal sizes could be explained several ways. The medium and large coal may have contained closed pores which were not opened until the coal was more finely ground. Additionally, the small coal may have had a different composition than the large and medium coals. Due to differences in the friability of coal macerals, grinding may have caused more porous macerals to be concentrated in the smaller coal sizes. This research suggested no difference in composition between the coal sizes – extraction yields were the same across all three sizes of coal. A difference in extraction yields would have suggested compositional differences. However, a difference in composition is not necessarily precluded by similar extraction yields. A graph illustrating the porosity differences between the three different coal sizes is presented below in Figure 7.

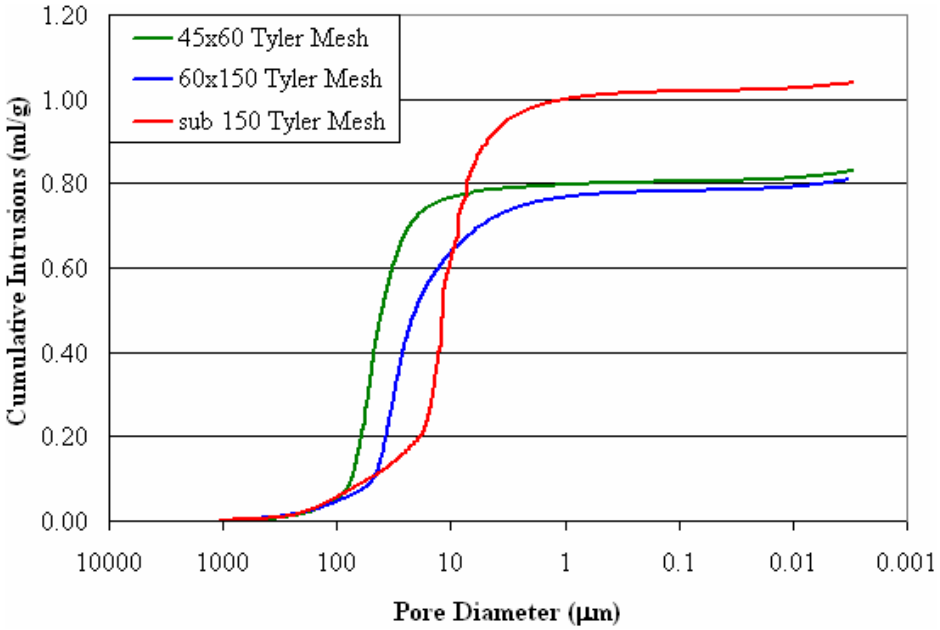

Figure 7. Pore distribution of the three coal sizes.

The amount of coal swell was measured for every solvent extraction run. The swelling ratio appeared to be a function of the extraction temperature, extraction time, and coal size. Coal swelled much more quickly for the higher temperature extractions (140 °C to 200 °C) than for the lower temperature extractions (50 °C to 120 °C). For this reason, there are two graphs for each coal size, one for lower extraction temperatures (longer time scales) and one for higher extraction temperatures (shorter time scales). The swelling ratio of small coals at lower extraction temperatures is presented below in Figure 8.

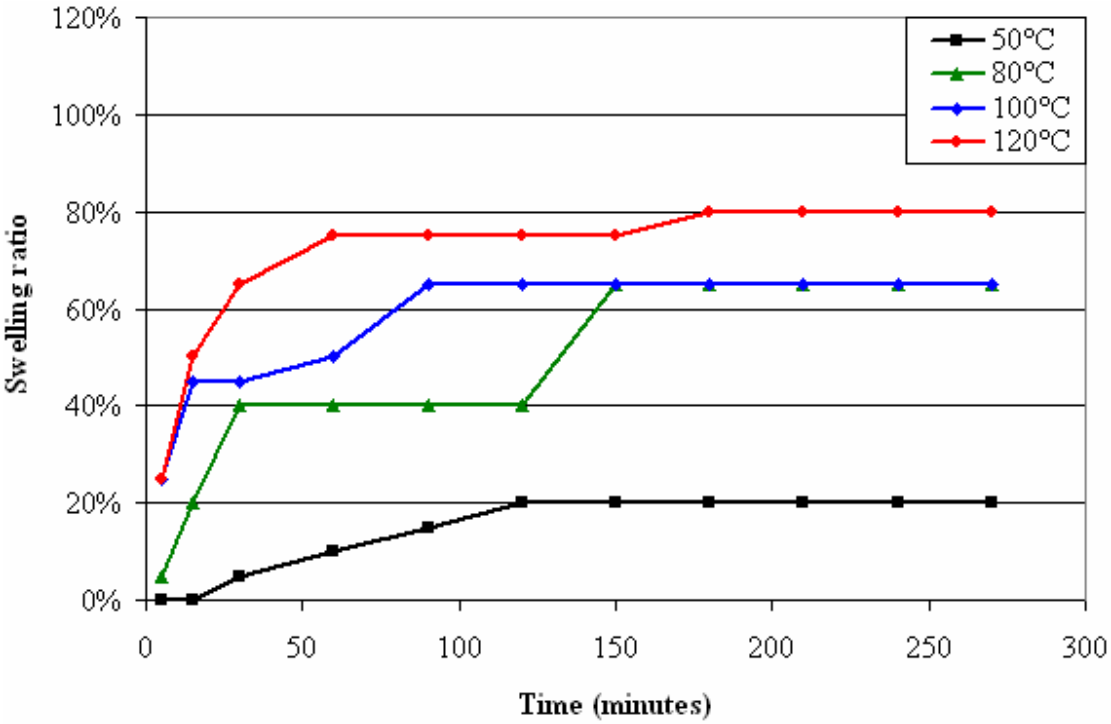

Figure 8. Swell of small coal (sub 106 μm) at low temperatures

Figure 8 suggests that appreciable coal swelling occurred at temperatures of 80 °C and higher. It was observed that coal swelling increased with increasing extraction time. It was also observed that for lower temperatures, coal swell increased with increasing temperature. This contrasted with the swell of small coal during high temperature extraction runs, which is presented below in Figure 9.

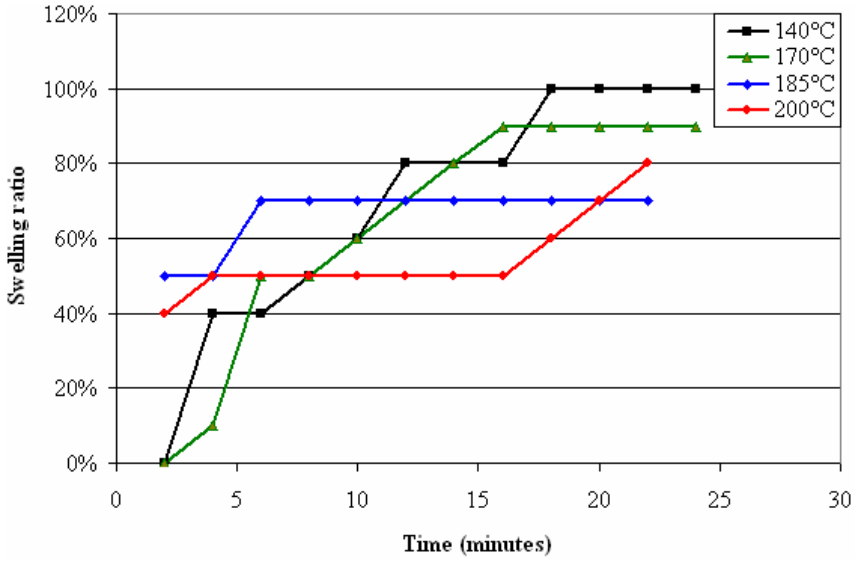

Figure 9. Swell of small coal (sub 106 μm) at high temperatures

Coal swelling passed through a maximum somewhere between 120 °C and 140 °C. Above 140 °C, the coal swelling ratio begins to decline with increased temperature. This may be due to dissolution, at higher temperatures more extractable material is removed from the coal matrix. The dissolution of extractable material from the coal matrix may counteract swelling. The next graph, Figure 10, illustrates the swelling of medium sized coal as a function of time, at different temperatures.

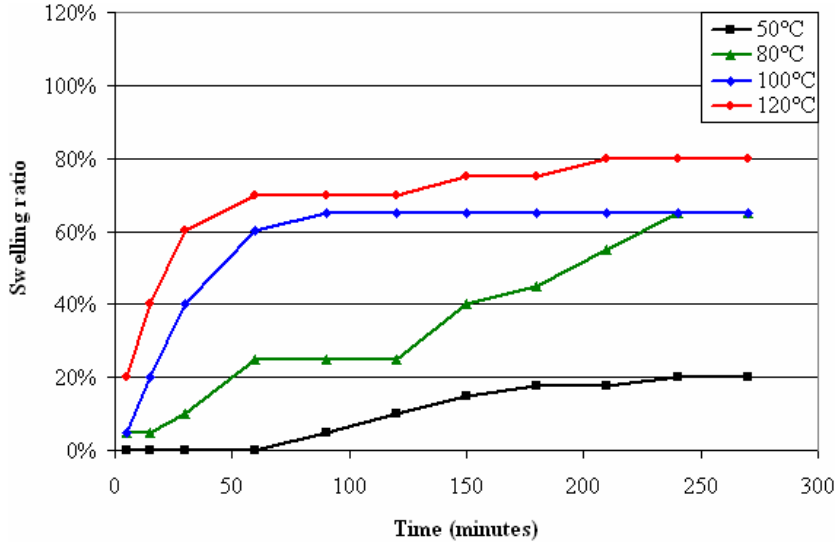

Figure 10. Swell of medium coal (106 - 212 µm) at low temperatures

As with the smaller coal samples discussed earlier, the swelling ratio increased with increasing temperature. Swelling also occurred more quickly for higher temperatures. The swelling ratio of the medium sized coal during high temperature extraction runs is represented by the next graph, Figure 11.

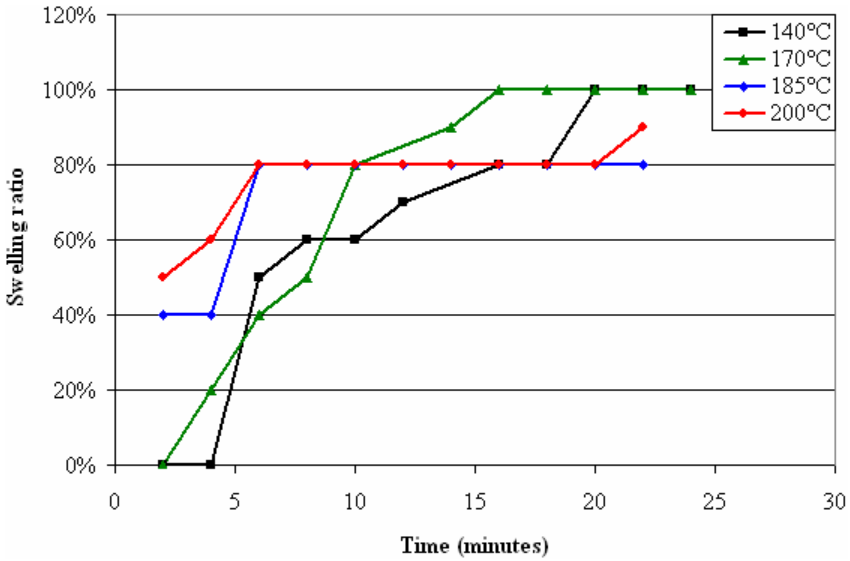

Figure 11. Swell of medium coal (106 - 212 µm) at high temperatures

Similar to the swelling of small coal discussed earlier, the swelling ratio reached a maximum somewhere between 120 °C and 140 °C. Again, the swelling ratio decreased with increasing temperature. As before, swelling occurred more quickly at higher temperatures, but ultimately lower temperatures swelled more. The amount of swell observed during the low temperature extraction of large coal is presented below as Figure 12.

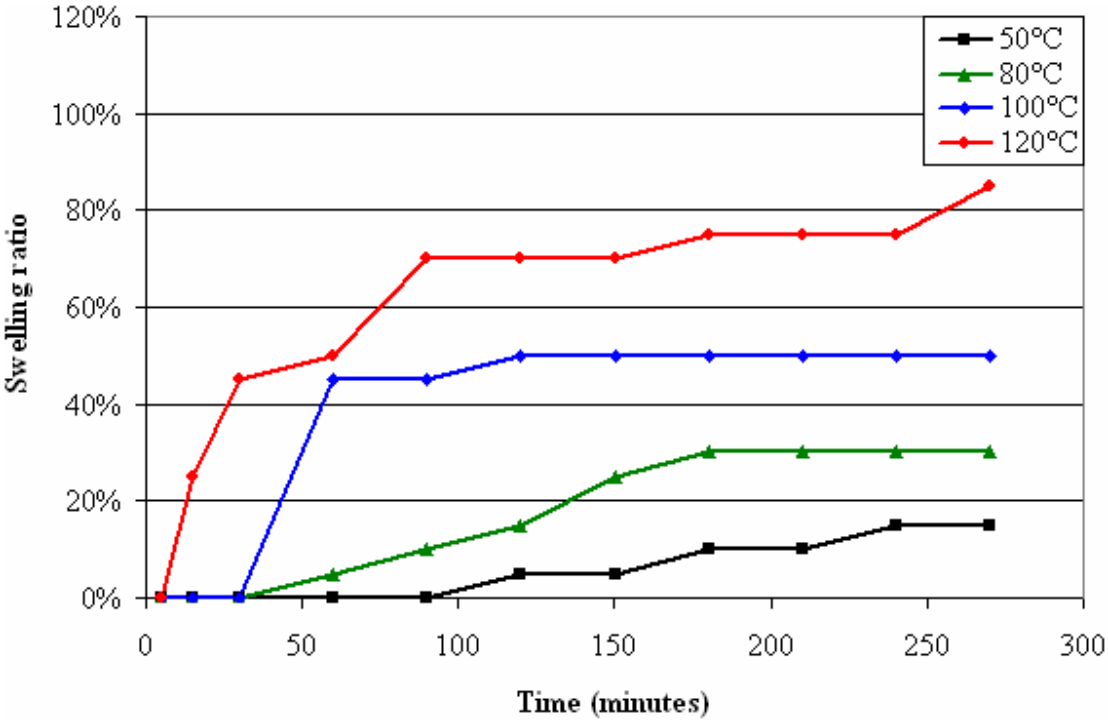

Figure 12. Swell of large coal (212 - 355 μm) at low temperatures

The swell of large coal at lower temperatures resembled the swell of small and medium coals at lower temperatures. The unique aspect of the swelling of large coal is the observed lag time between when extraction starts and when the coal begins to swell. This suggested that swelling is a diffusion controlled process. As with medium and small coals, the swelling ratio increased with increased temperature. The swelling of large coals during high temperature extraction runs is presented below as Figure 13.

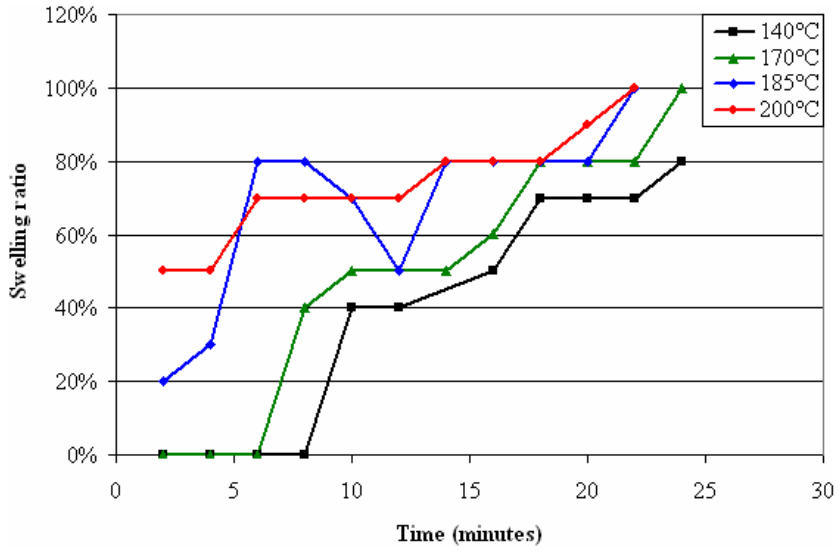

Figure 13. Swell of large coal (212 - 355 µm) at high temperatures

The swelling ratios for large coal at high temperatures differed from the swelling ratios for small and medium coals at high temperatures. Unlike small and medium coals, the large coal swelling ratio continued to increase with increasing temperature. This result was somewhat anomalous, as the maximum swelling (about 100 % swell) and extraction yield at higher temperatures were similar across all three coal sizes. The result may be due to a time scale that was too short to collect sufficient swelling data.

Coal solubility was measured using a UV-Vis spectrophotometer. The concentration (grams of coal dissolved per liter of NMP) of coal is NMP for low temperature (50 °C to 120 °C) extraction of small coal is presented below in Figure 14. Notice that the time scale ran from five minutes to four and a half hours. This data suggested that the extraction reached a maximum quickly, and that the temperature determined how much coal was dissolved. Relatively small extraction differences occurred across the temperature range.

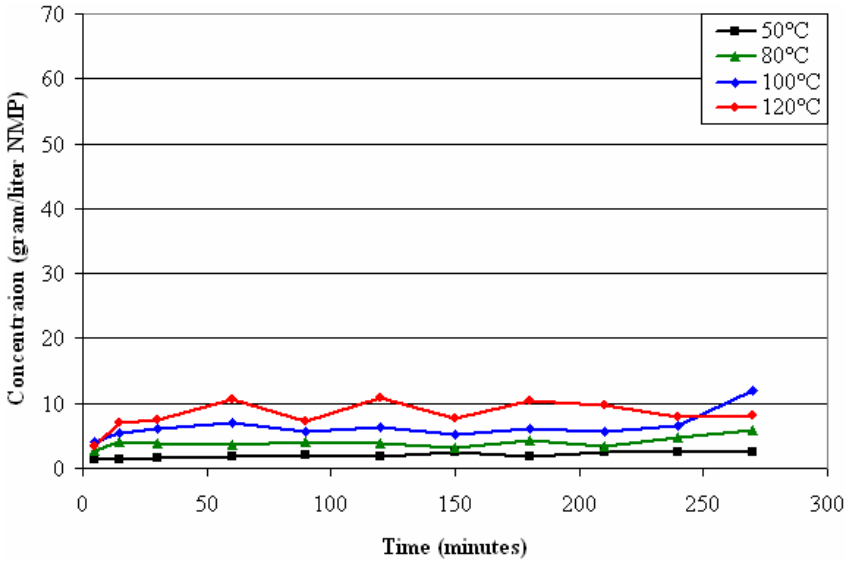

Figure 14. Small coal (sub 106 µm) in NMP at low temperatures

The next set of experimental conditions focused on higher temperature extraction runs, from 140 °C to 200 °C. During the higher temperature runs, extraction was negligible, until the temperature reached approximately 185 °C. At 185 °C, a spike in concentration appeared. Extraction yield data for the higher temperature runs appears below in Figure 15.

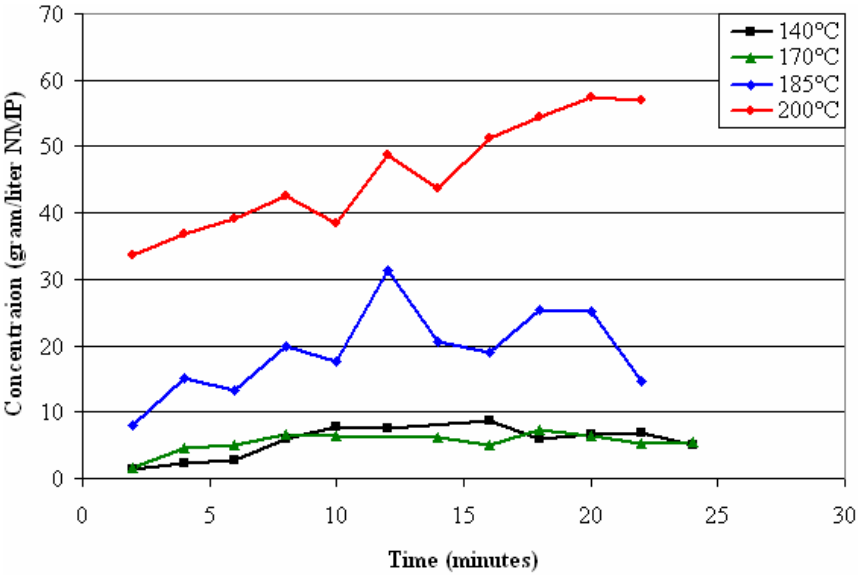

Figure 15. Small coal (sub 106 μm) in NMP at high temperatures

Little extraction occurred before 170 °C, significant extraction occurred at 185 °C, and maximum extraction occurred at 200 °C. This contrasted with swelling – appreciable swelling occurred at all temperatures. This data suggested that swelling and extraction may be independent processes. Extraction yield data for the lower temperature extractions of medium sized coal is presented below in Figure 16.

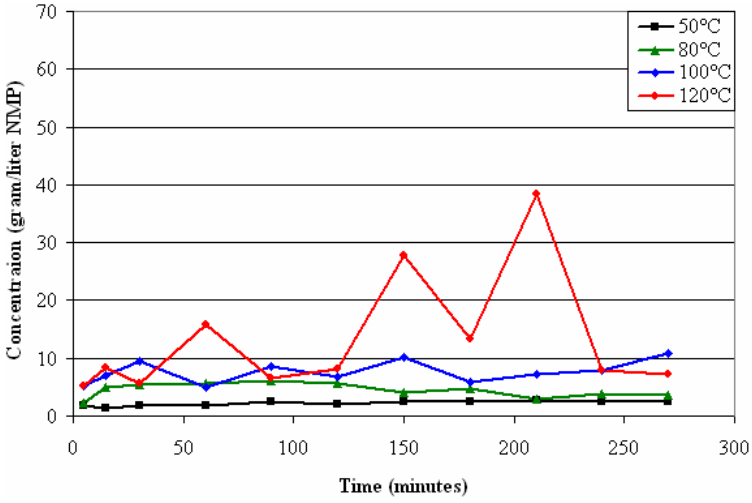

Figure 16. Medium coal (106 - 212 μm) in NMP at low temperatures

Similar to the lower temperature runs on small coal samples, little extraction was observed at the lower temperatures. Except for a few spikes in concentration, observed solubility was flat for most low temperature runs. The extraction yield for high temperature extraction of medium coal is presented below in Figure 17.

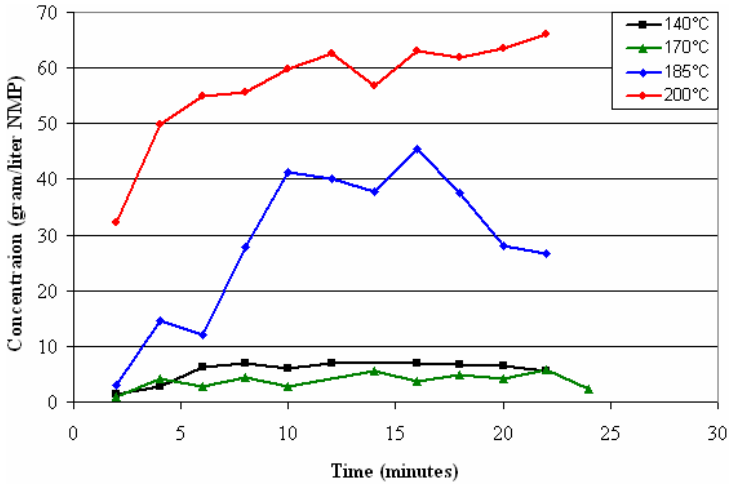

Figure 17. Medium coal (106 - 212 µm) in NMP at high temperatures

The concentration of medium coal at higher temperatures resembled the concentration of small coal at higher temperatures. Little extraction occurred at lower temperatures, 140 °C and 170 °C. Significant extraction did not occur until 185 °C. These parallels between the extraction of small and medium coals extended to the large coal sizes. The extraction of large coals at low and high temperatures is illustrated in the following two graphs, Figures 18 and 19.

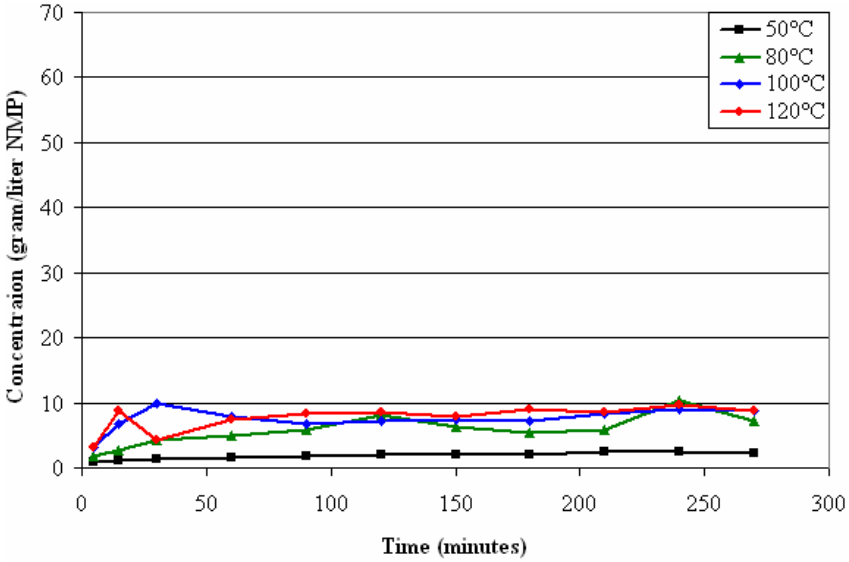

Figure 18. Large coal (212 - 355 µm) in NMP at low temperatures

The data represented in Figure 18 illustrate that the same trends observed in the extraction of small and medium coals extended to large coals. Very little extraction occurred at the lower temperatures of 50 °C to 120 °C. Data for the extraction of larger coal sizes at higher temperatures follows in Figure 19.

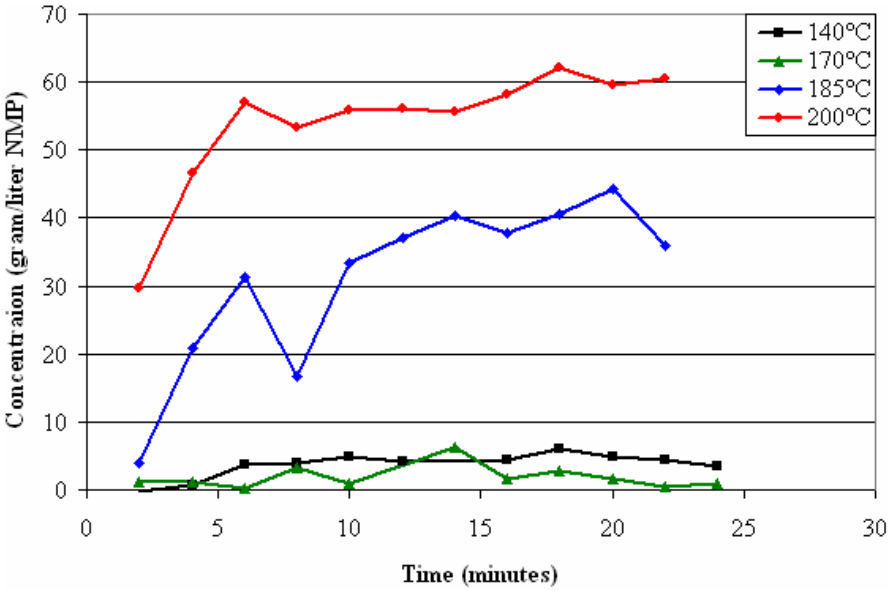

Figure 19. Large coal (212 - 355 μm) in NMP at high temperatures

The dissolution of large coal at higher temperatures resembled the dissolution of smaller and medium coals at lower temperatures. Little extraction occurred at the temperatures of 140 °C and 170 °C. Significant extraction when the temperature reached 185 °C and higher.

2.2.6 Correlation of Extraction and Swelling

It was desired to correlate swell data with process parameters. Several regressions of swelling data were performed. Polynomial, logarithmic, linear, and a reciprocal fits were all applied to swelling data. An example set of swelling data and various fits of the data are presented below as Figure 20.

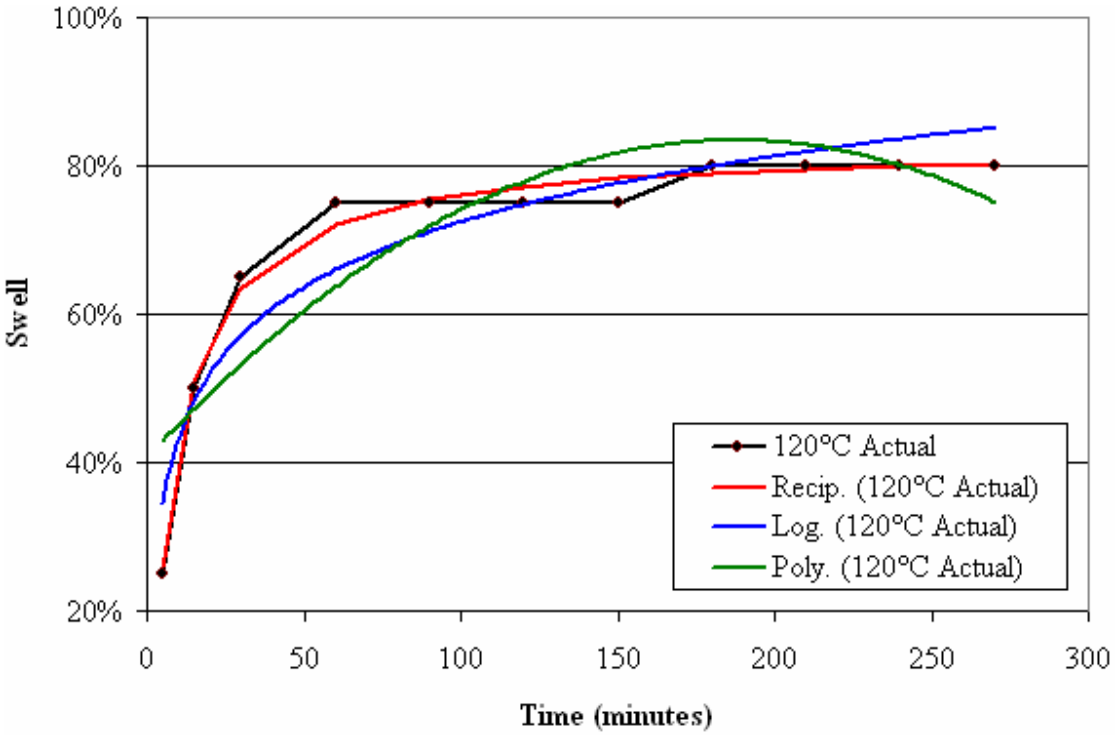

Figure 20. Various fits of swelling data

The reciprocal fit is a custom correlation that was developed during the course of research. The reciprocal fit was developed after it was observed that both swell and extraction data seemed to approach some maximum asymptotically. For almost all data, the reciprocal fit was superior. By superior, it is meant that the reciprocal fit most often minimized the sum of squares of the residuals between the actual data and predicted fit. The formula for the reciprocal fit appears below.

$$S_T = S_M\left(1-\frac{1}{C_S\left(t-\frac{t_l}{l}\right)}\right) \quad , \qquad \text{(Equation 5)}$$

where S_T = Swell at time t, S_M = Maximum predicted swell, C_S = Swelling curve factor, t = time t_l = lag time,

$$l = \frac{1}{1-\frac{1}{S_M C_S}}$$

The variable l ensured that the lag time, t_l, offset the curve by the desired time. The effects of the three adjustable parameters of the reciprocal fit, S_M, C_S, and t_l are illustrated below in Figures 21 and 22.

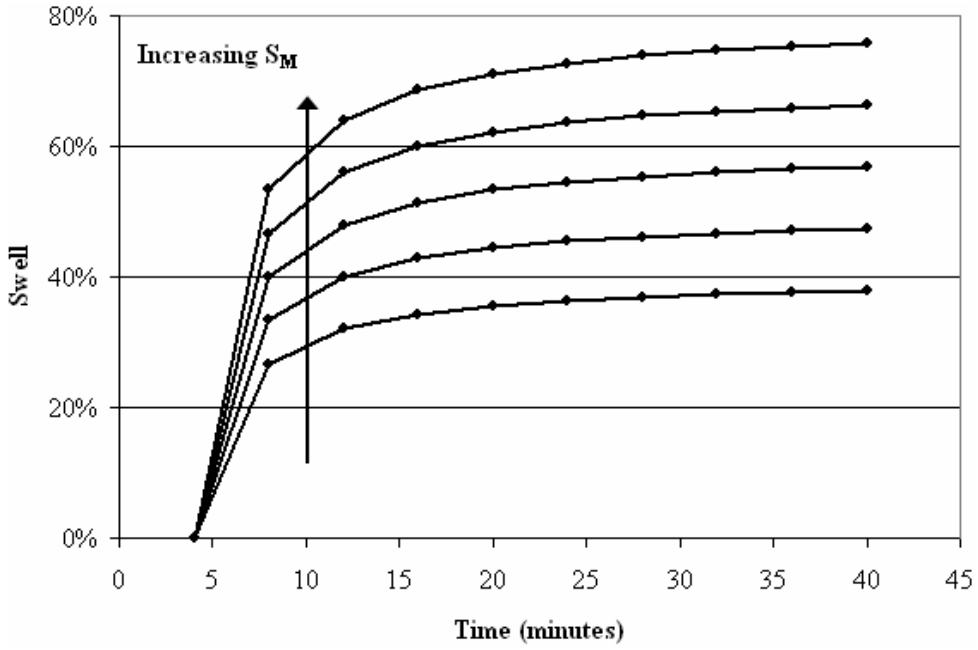

Figure 21. Effect of increasing S_M on reciprocal fit

Figure 21 was generated with C_S held constant at 0.5 and t_l held constant at 4. S_M was varied from 0.4 to 0.8. S_M is the maximum swell predicted by the correlation. The predicted swell will reach S_M at infinite time. As can be seen in Figure 21, S_M is simply a multiplier of the curve, it does not affect the general shape of the curve. The shape of the curve is affected by C_S, the swelling curve factor. The effect of C_S on the reciprocal fit is presented below as Figure 22.

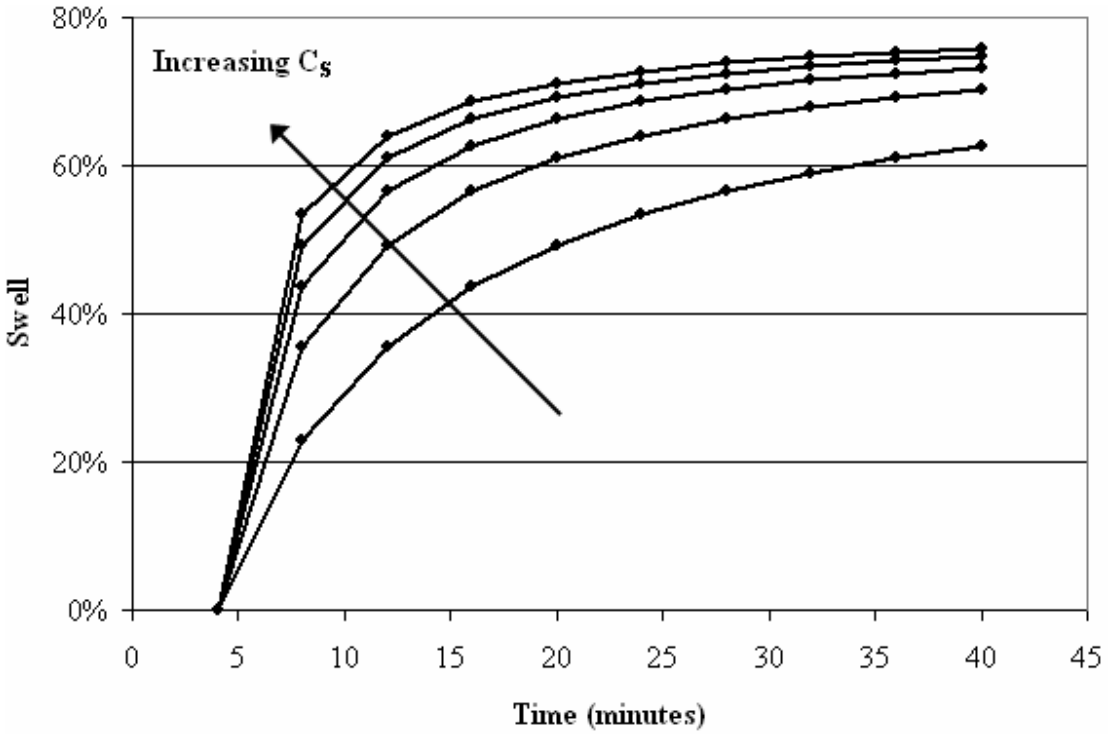

Figure 22. Effect of increasing C_S on reciprocal fit

Figure 22 was generated with S_M held constant at 0.8 and t_l held constant at 4. C_S was varied from 0.1 to 0.5. As illustrated in Figure 22, C_S represents the curve of the reciprocal fit. It could also be said that C_S determined how quickly the swell predicted at time t approached the maximum predicted swell. Linear data would be best approximated by an extremely small C_S, while step-function data would be best represented by an extremely large C_S. Note that changing both C_S and S_M has no effect on where the reciprocal fit intercepts the x-axis. This is controlled by the lag time parameter, t_l. The effect of various lag times on the reciprocal fit is presented below as Figure 23.

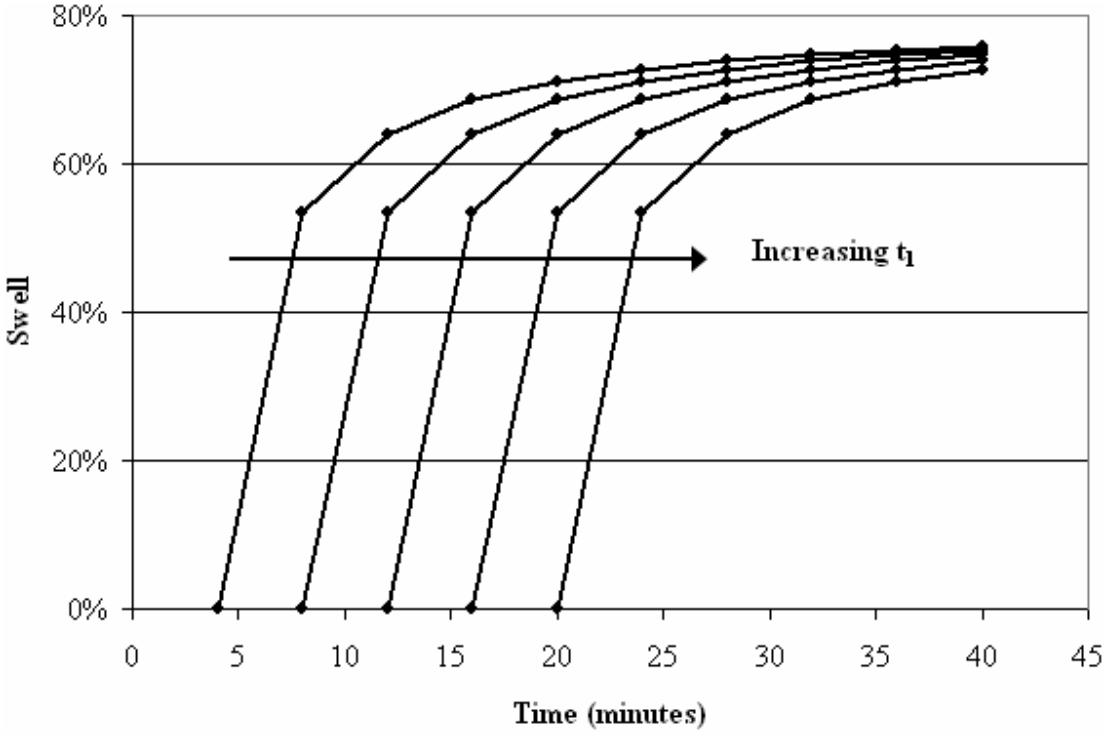

Figure 23. Effect of increasing t_l on reciprocal fit

Figure 23 was generated with S_M held constant at 0.8 and C_S held constant at 0.5. t_l was varied from 4 minutes to 20 minutes. As illustrated in Figure 23, varying t_l did not affect the shape of the curve or the maximum swell, but simply the x-axis offset of the curve.

The regression to determine the optimum values of S_M, C_S, and t_l operated as follows. A series of nested for loops were created, to exhaustively run all combinations of S_M, C_S, and t_l that were reasonable considering the data at hand. S_M was divided into 200 increments, from 0.01 to 2.00. C_S was divided into 250 increments, from 0.01 to 2.50. t_l was divided into 100 increments, from 0 to 100. These divisions resulted into a total of five million combinations of S_M, C_S, and t_l. SSR (the sum of squares of residuals) between the curve from the data and the reciprocal fit was calculated for all five million points. The one combination out of five million that minimized SSR was judged the best fit.

The extraction data was also best described by a reciprocal fit, fundamentally the same equation as Equation 6, but with different terms for the sake of clarity. The equation used to describe extraction data is

$$E_T = E_M \left(1 - \frac{1}{C_E \left(t - \frac{t_l}{l} \right)} \right) \quad , \qquad \text{(Equation 6)}$$

where E_T = Extraction at time t, E_M = Maximum predicted extraction, C_E = Extraction curve factor, t = time, t_l = lag time and

$$l = \frac{1}{1 - \frac{1}{E_M C_E}} \qquad .$$

Because the adjustable parameters E_M and C_E occupied different ranges than their counterparts S_M and C_S, the regression was similar but not exactly the same. E_M was divided into 800 increments, from 0.0 to 80.0. C_E was divided into 250 increments, from 0.00 to 2.50. t_l divided into 10 increments, from 0 to 10. This resulted in a total of two millions combinations. As before, the best fit was defined as the combination of parameters that minimized SSR.

Data for the extraction of small coal at low temperatures, along with reciprocal fits laid over the data, is presented below as Figure 24. Data for the high temperature extraction of small coal follows as Figure 25.

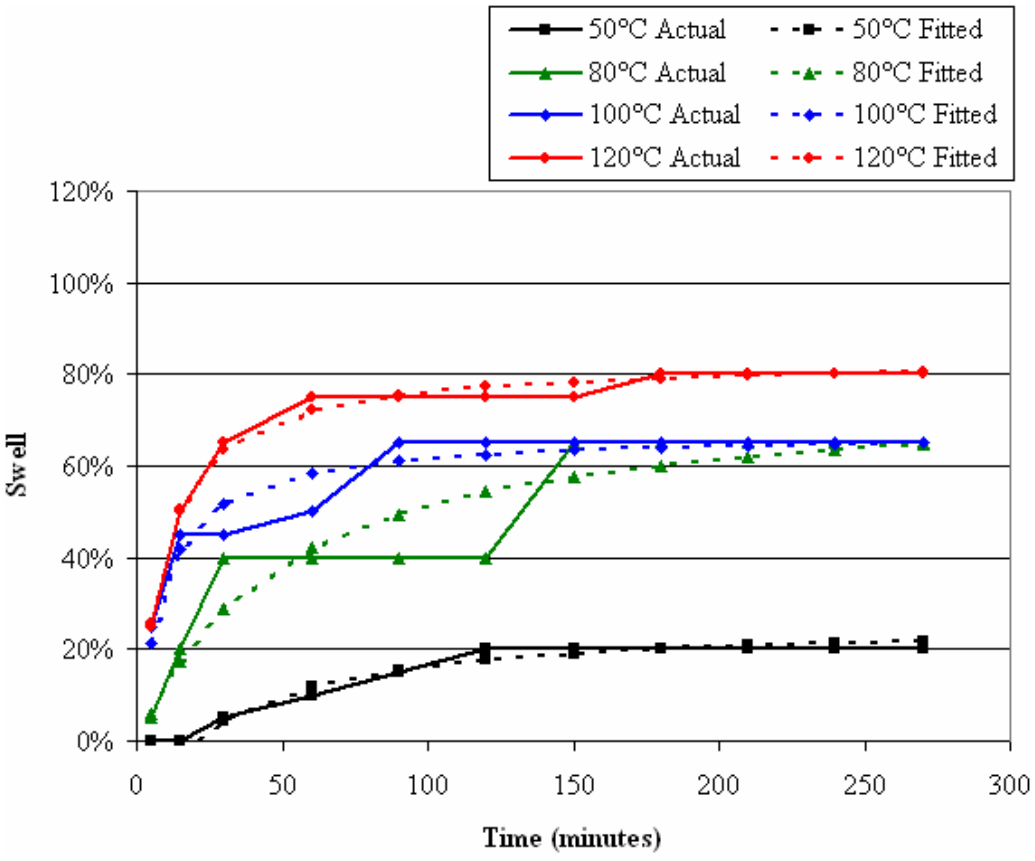

Figure 24. Fitting small coal (sub 106 μm) swell at low temperature

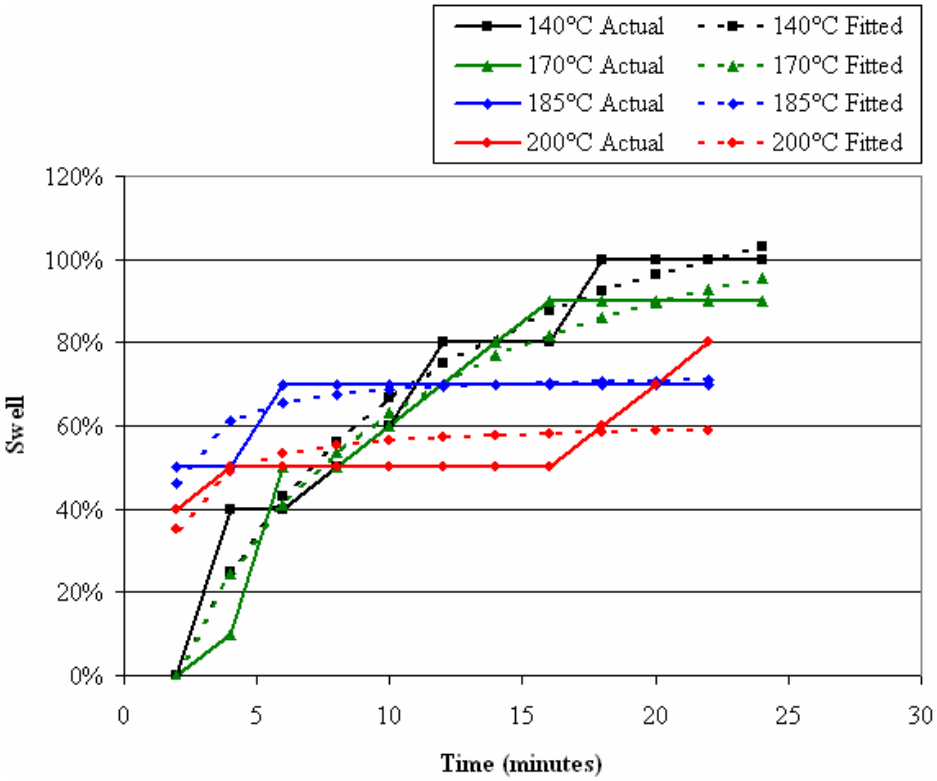

Figure 25. Fitting small coal (sub 106 μm) swell at high temperature

The reciprocal fits correlated well with the data. The reciprocal fit suggested maximum swell occurred at 140 °C to 170 °C, which is consistent with earlier conclusions. Swelling data and reciprocal fits for the low and high temperature extraction of medium sized coal follows as Figures 26 and 27, respectively.

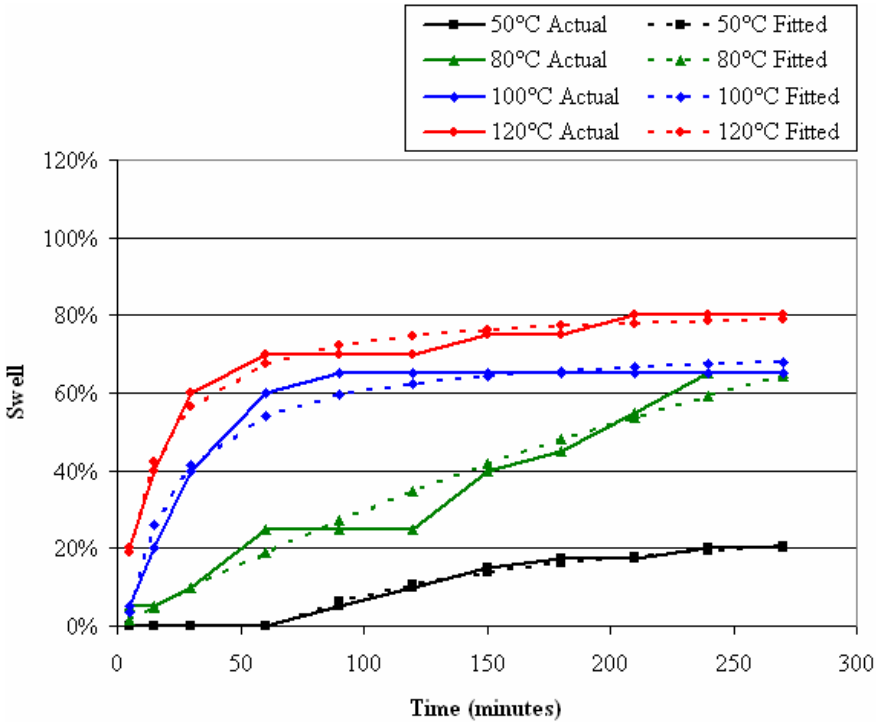

Figure 26. Fitting medium coal (106 - 212 µm) swell at low temperature

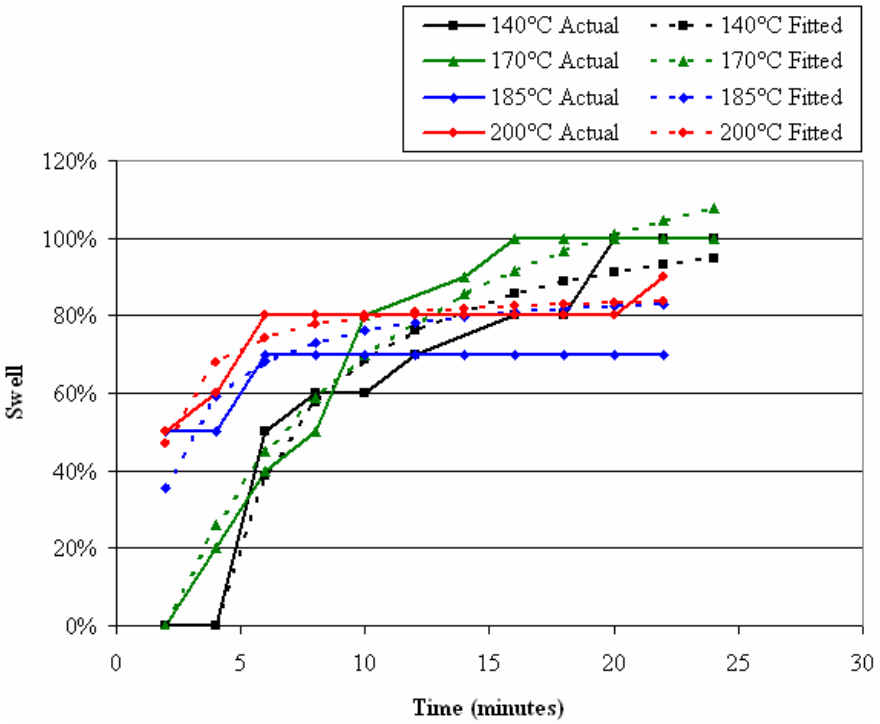

Figure 27. Fitting medium coal (106 - 212 µm) swell at high temperature

As before, swell increased with temperature, until it maximized around 170 °C. Swelling data and reciprocal fits for the low and high temperature extraction of large sized coal follows as Figure 28 and Figure 29, respectively.

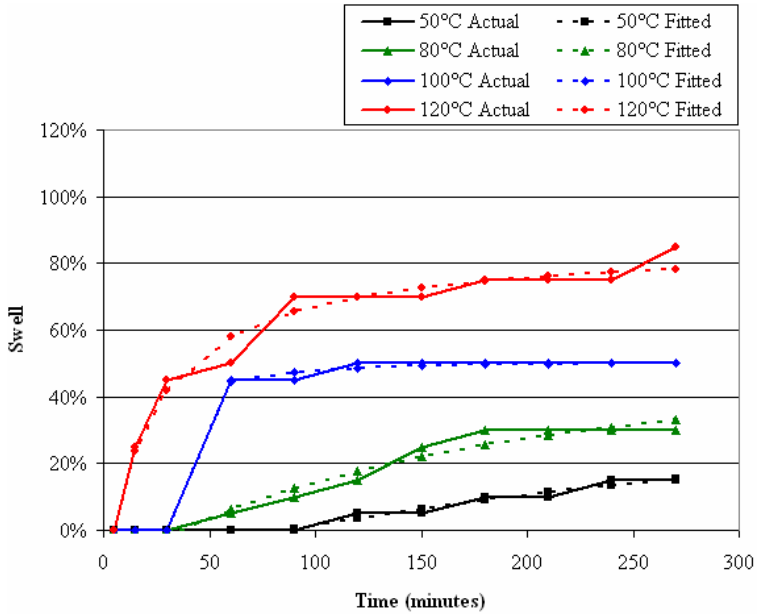

Figure 28. Fitting large coal (212 - 355 µm) swell at low temperature

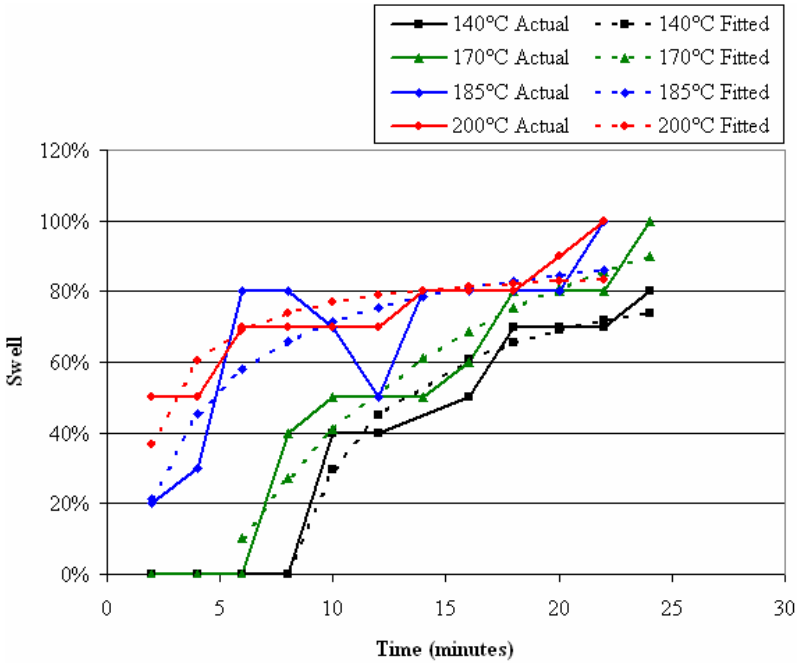

Figure 29. Fitting large coal (212 - 355 µm) swell at high temperature

The large coal followed the same trends as the small and medium coals. The difference was an increased lag time, large coals took longer to begin swelling, especially at lower

temperatures. Once swelling began, large coals swelled a similar amount to small and medium coals. Interestingly, the correlation predicted the highest maximum swell at 170 °C, which was not observed in the raw data. This supported the idea that maximum swell occurred around 170 °C regardless of coal size, but this was not observed in the high temperature extraction of large coals because the time scale was not sufficiently long.

With all six sets of swelling data fit, it was desired to graph the correlation's adjustable parameters, S_M, C_S, and t_l, as a function of temperature. S_M, C_S, and t_l graphed as a function of temperature are presented as Figure 30, Figure 31, and Figure 32, respectively.

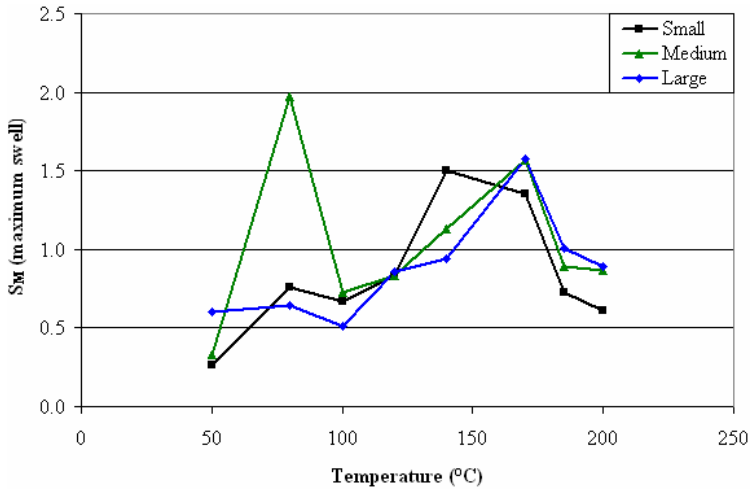

Figure 30. Predicted maximum swell as a function of temperature

As observed, maximum swell increased with temperature until it peaked at 170 °C, after which point the maximum swell decreased. The anomalous data point at 80 °C is attributed to the somewhat linear looking data of medium coal at that temperature. Linear data is best fit by a reciprocal fit with large S_M and small C_S. The swelling curve factor, C_S, was also graphed as a function of temperature, and follows as Figure 31.

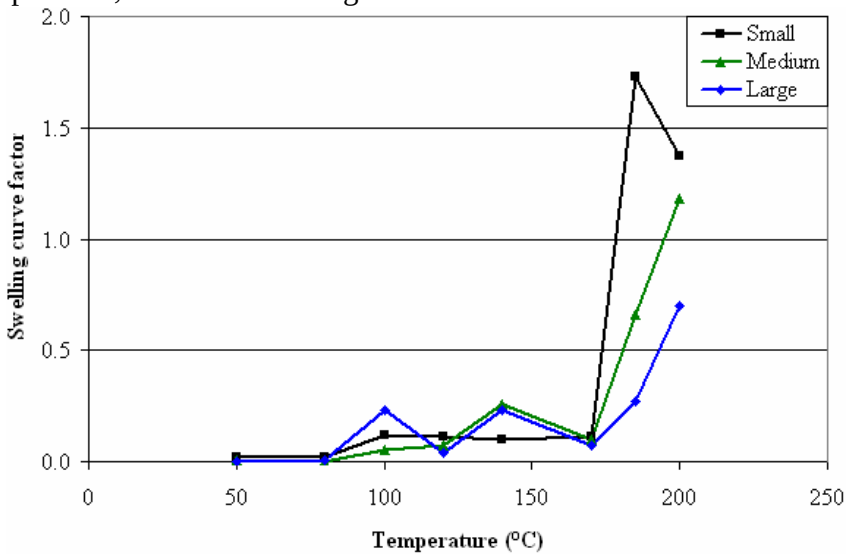

Figure 31. Swelling curve factor as a function of temperature

The swelling curve factor remained relatively flat until it spiked dramatically at a temperature of 185 °C. This sudden spike was reminiscent of the sudden spike in extraction yield, which was also observed at 185 °C (see Chapter 5 –

2.2.5 Coal Dissolution Experimental Results). The swelling curve factor for small coals was greater than the swelling curve factor for medium coals, which was greater than the swelling curve for large coals. This suggested that small coals approached their maximum swell more quickly, which suggested swelling was diffusion dependent. Next, the swelling lag time was graphed as a function of coal size and temperature, and appears as Figure 32.

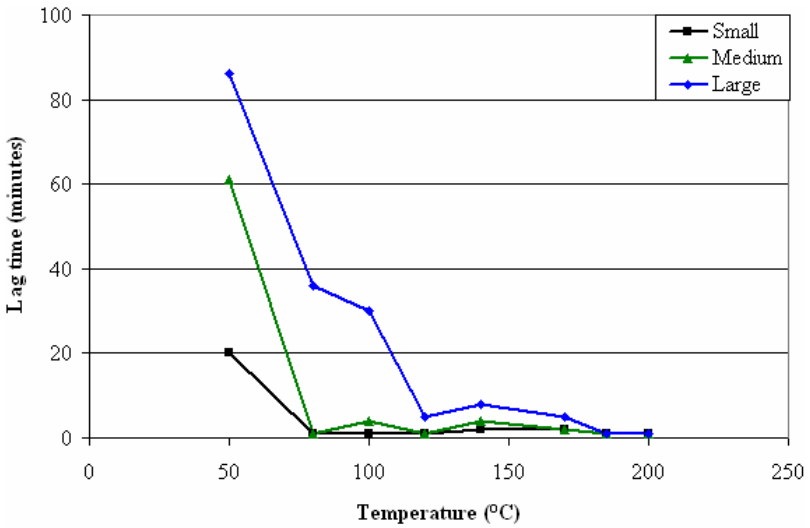

Figure 32. Predicted lag time as a function of temperature

As expected, larger coals had the highest lag times, and swelling lagged until a temperature of 185 °C. Medium coal initially had a larger lag time than small coal, but both quickly approached no lag time at 80 °C and higher. This data further supported the conclusion that swelling is at least somewhat diffusion controlled. Smaller coals began swelling sooner, and upon initiation of swelling, swelled at a faster rate.

The extraction data for low temperature and high temperature runs are presented below as Figure 33 and Figure 34, respectively.

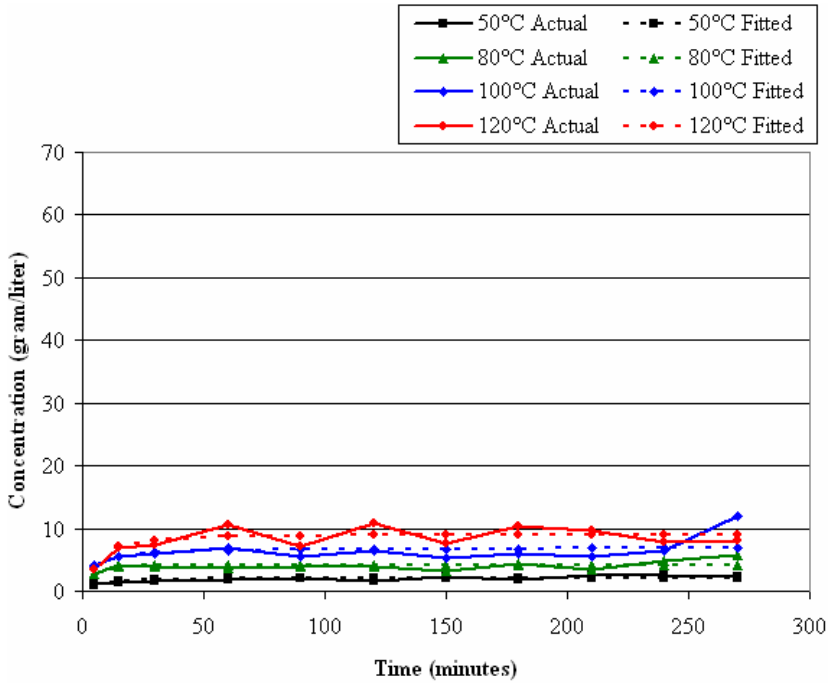

Figure 33. Fitting small coal (sub 106 µm) extraction at low temperature

Note that for the low temperature runs graphed in Figure 33, extraction was temperature dependent, but the total observed extraction was relatively small. This contrasted with the extraction of small coal at high temperature, which is presented below as Figure 34.

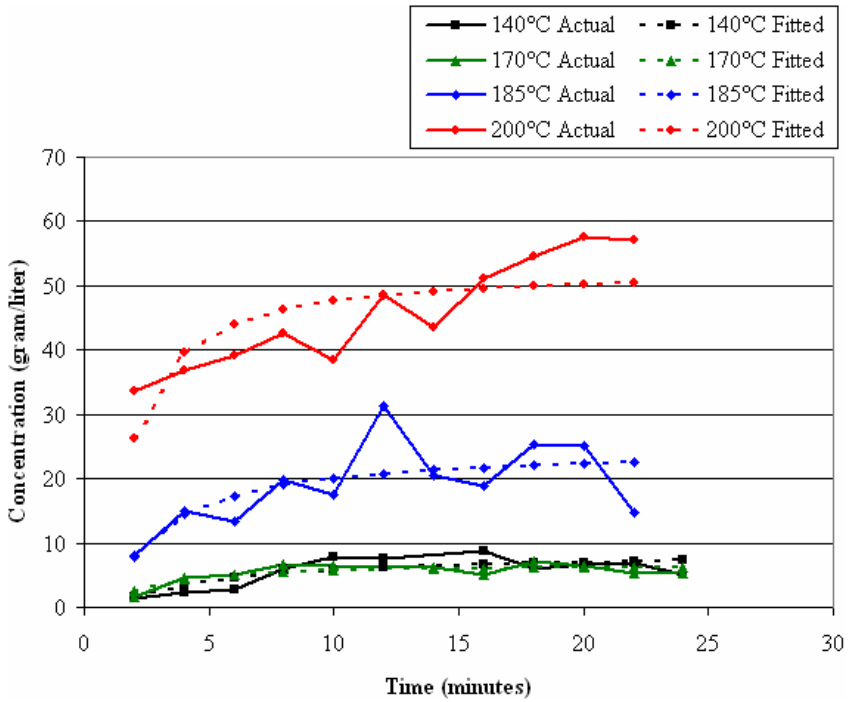

Figure 34. Fitting small coal (sub 106 µm) extraction at high temperature

Little extraction occurred at 140 °C and 170 °C. When the extraction temperature reached 185 °C, significant extraction occurred. The maximum extraction predicted at 200 °C was higher than the maximum extraction predicted at 185 °C – this was consistent with observed data. This trend was repeated with medium and large sized coal samples. Data for the low temperature and high temperature extraction of medium sized coal are presented below as Figures 35 and 36.

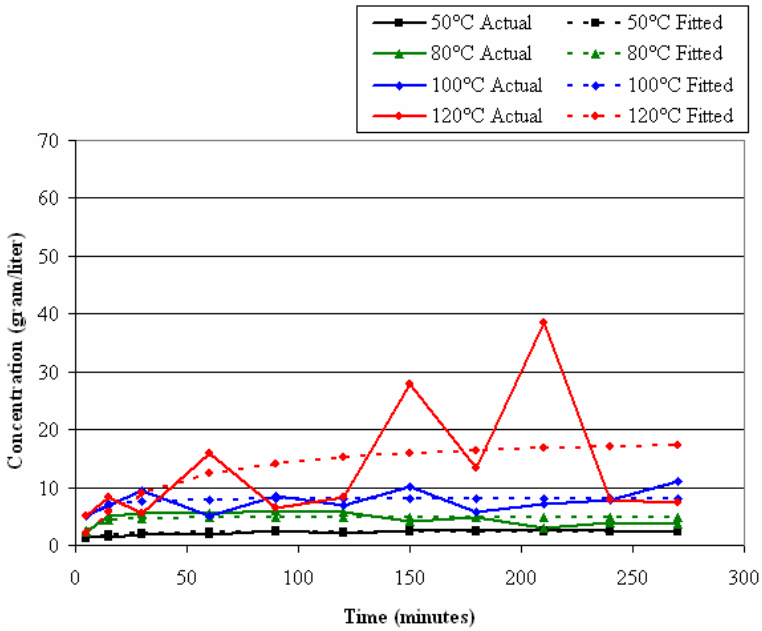

Figure 35. Fitting medium coal (106 - 212 µm) extraction at low temperature

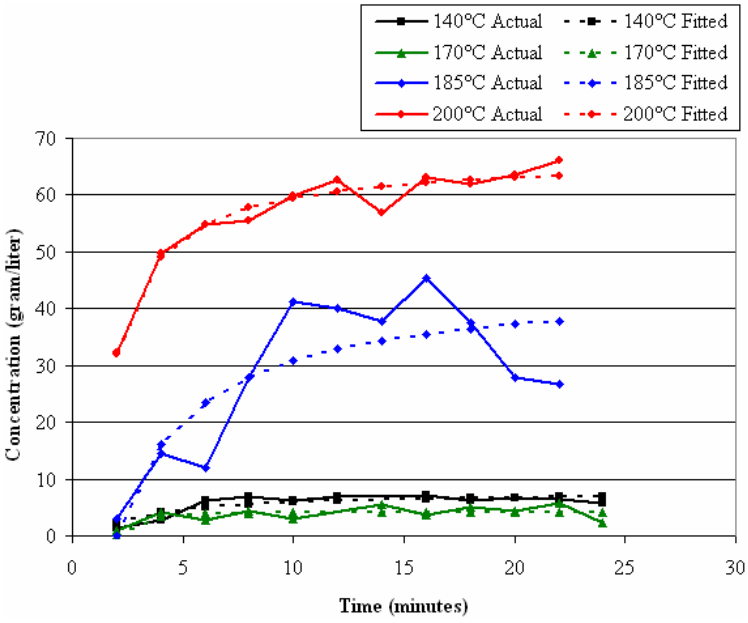

Figure 36. Fitting medium coal (106 - 212 µm) extraction at high temperature.

Similar to the small coal samples, little extraction occurred at temperatures up to 170 °C. At temperatures of 185 °C and higher, the extraction yield immediately spiked. The extraction yield at 200 °C was greater than the extraction yield at 185 °C. The same trend was observed for the large coal samples. Data for the low temperature and high temperature extraction of large coal are presented below as Figure 37 and Figure 38.

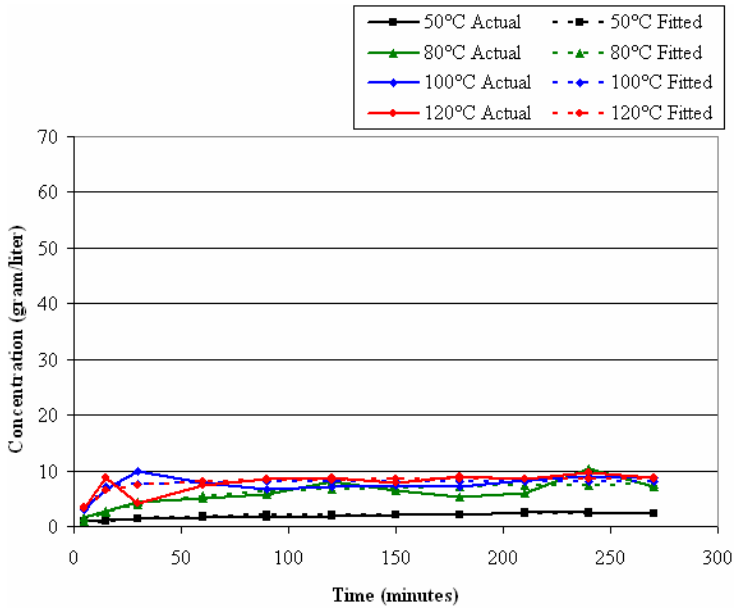

Figure 37. Fitting large coal (212 - 355 µm) extraction at low temperature

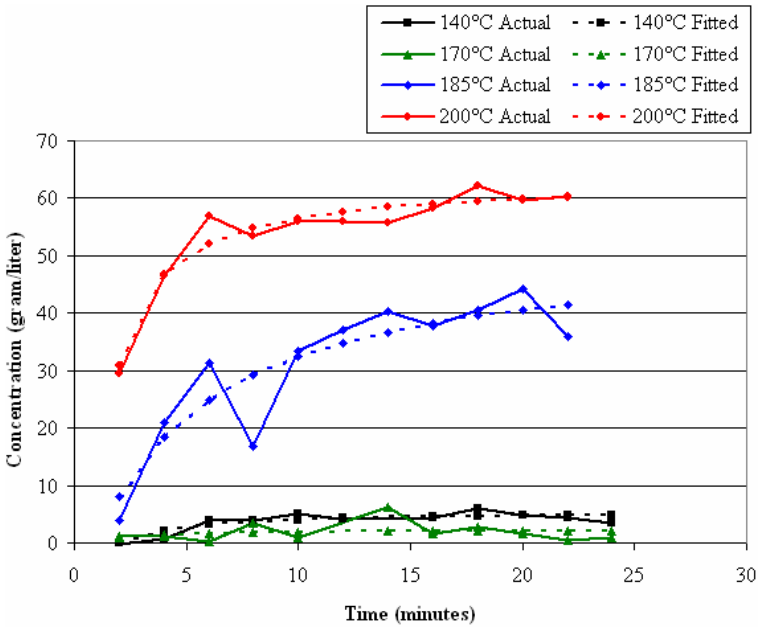

Figure 38. Fitting large coal (212 - 355 µm) extraction at high temperature

After the reciprocal fit was applied to all sets of extraction data, the adjustable parameters E_M and C_E were graphed as a function of temperature. The extraction lag time was not graphed because it was small, less than four minutes, for all extraction runs. The graphs of E_M and C_E are presented below as Figure 39 and Figure 40.

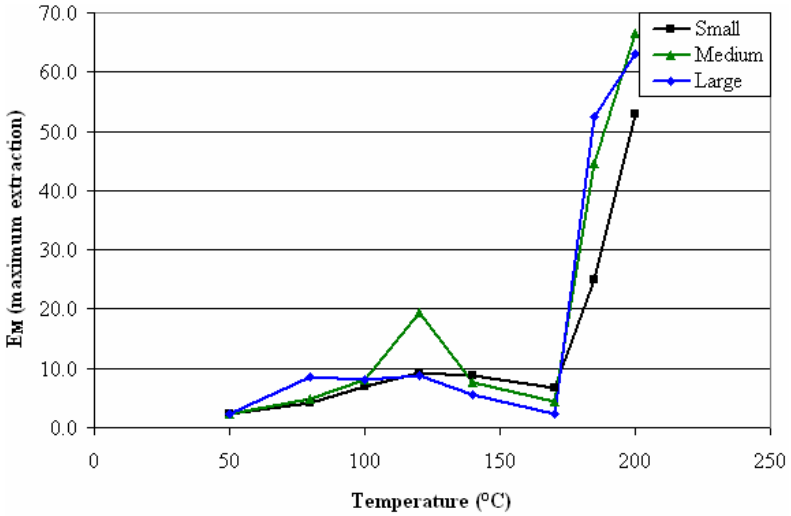

Figure 39. Predicted maximum extraction as a function of temperature

The maximum extraction predicted based on temperature was consistent with observed data. Extraction was relatively flat, until it spiked at a temperature of 185 °C. As the data suggested, the maximum extraction was predicted at 200 °C, which is near the boiling point of NMP, 202 °C. Extraction data contrasted greatly with swelling data. The maximum predicted swell changed relatively smooth with respect to temperature, where the maximum predicted extraction changes abruptly.

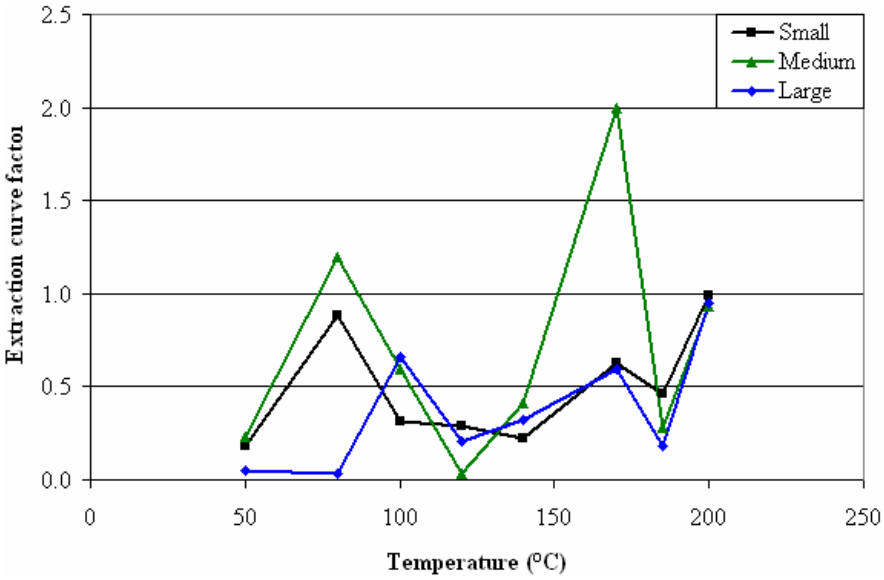

Figure 40. Extraction curve factor as a function of temperature.

The extraction curve factor, E_M, appeared erratic across the extraction runs. The extraction lag time, tl, was small for all runs. This suggested that, generally, low temperature extraction runs approached their maximum extraction as quickly as high temperature extraction runs approached their maximum. This contrasted sharply with swelling data, which suggested that lower temperature extractions (less than 185 °C) swelled much more slowly than higher temperature extraction runs.

2.2.7 Summary of Coal Dissolution and Extraction

The research collected data on the swelling, extraction, and porosity of high volatile bituminous coal (Lower Powellton seam). Swelling and extraction data were collected for over 300 extraction runs. These extraction runs varied temperature, which ranged from 50 °C to 200 °C, extraction time, which ranged from 2 minutes to 270 minutes, and coal size, which ranged from 355 μm to less than 106 μm. The swell of the bituminous coal post dissolution was measured via optical methods, while the extraction yield achieved during dissolution was measured via UV-Vis spectroscopy. The porosity of the coal was measured via mercury porosimetry. Swelling, extraction, and porosity data were examined independently, and a novel correlation was developed between swelling and process parameters, and between extraction and process parameters. Concurrent examination of swelling and extraction correlations suggested a relationship between swelling and extraction.

Data collected during researched showed that the maximum swell observed increased with increasing temperature, until 170 °C, after which maximum observed swell decreased. It is hypothesized that swell decreased after 170 °C due to the sharp increase in extraction yield that occurred at temperatures higher than 170 °C. Increased extraction resulted in significant material being removed from the coal matrix, which may have counteracted swelling. At higher temperatures, temperature weakly affected the maximum observed swell. However, the speed with which the coal swelled increased sharply with increasing temperature. The speed with which the coal swelled maximized at the highest extraction temperature, 200 °C.

Data collected during research showed that extraction was relatively negligible with respect to temperature, until a temperature of 185 °C, at which point extraction increased dramatically. It was not determined whether this sharp increased in solubility is due to the nature of the extractable material, the nature of the solvent extracting the material, or a combination of the two. All extraction runs showed very little lag time irrespective of coal size, which suggested that the onset of dissolution occurred quickly.

The relationship observed between swelling and extraction is the most significant research result. The research suggested that the maximum observed extraction, E_M, was proportional to the swelling curve factor, C_S. Both of these parameters were fairly flat, until they spiked dramatically at a temperature of 185 °C. This suggested that if material was not extracted from the coal matrix, swelling was a relatively slow process. However, when the extractable material was significantly soluble in the solvent, the coal swelled quickly. This result supported the "extraction is a substitution" mechanism proposed by Marzec.[41] It is hypothesized that, as the extractable material in the coal matrix became soluble (at and above 185 °C), extractable coal material was replaced with solvent. This sudden introduction of solvent into a coal matrix,

which is hypothesized to now be more porous due to the removal of extractable material, may have caused the coal to swell much more quickly.

One novel contribution of this research was the proposed proportionality between a swelling curve factor and the maximum observed extraction. The other result of this research is a new correlation, a reciprocal fit, used to relate coal swelling and extraction to processing time and temperature. The optimum parameters for these correlations were found through a "brute force" method, which found the combination of parameters that minimized the sum of squares of the residuals between the correlation and actual data. This research was also significant in that it supported existing literature. It appeared that the dissolution of bituminous coal in a super solvent does take place through a substitution mechanism.[42]

There is opportunity for further research into super solvent and bituminous coal systems. Research could be performed on other coals, to determine whether the previously developed correlation is general enough to apply to other bituminous coals, other solvents, and even perhaps other ranks of coal. Further research could be performed on the mechanism of the substitution process that is solvent extraction. Does the extractable material dissolve out of the coal matrix, leaving the matrix intact? Or, does the coal matrix cease to exist upon dissolution? The small lag time observed during extraction suggested the latter, but more extraction experiments employing larger coal sizes may be necessary to elucidate the extraction mechanism.

A remaining issue is why coal swelling and extraction change so dramatically at 185 °C, and furthermore, why swelling and extraction are best fit by a reciprocal correlation. Starting from first principles, it should be possible to develop a model describing coal extraction. This model would yield understanding of extraction phenomena observed during this research. Additionally, research could be performed to investigate the relationship between other coal properties and swelling and extraction. In addition to processing time, processing temperature, and coal size, it would be desirous to relate the maceral content of coal to its swelling and extraction behavior.

In summary, many research opportunities still exist concerning the solvent extraction of coal. The research completed herein has raised questions that could be the basis of further research.

2.3 Pitch Foam Production by Use of Physical Blowing Agents (Mark E. Heavner)

Coal-derived carbon foam has an advantage of low raw materials cost. Yet processing costs are currently much higher due to the high temperatures and pressures required, and the need for maintaining an inert or reducing atmosphere.

Thus, technical means are sought to produce carbon foams at near-ambient pressure and temperature in the same way that polymeric foams are produced. This can be accomplished by using physical blowing agents with an altered coal pitch such that foaming conditions can be accomplished at near-ambient pressure and temperature.

2.3.1. Nomenclature

A Area

b	Affinity respectively
c	Blowing agent concentration
c_1, c_2	WFL constants
CBA	Chemical blowing agents
C_L	Langmuir capacity
D	Diffusion coefficient
DCFC	Direct Carbon Fuel Cell
DSC	Differential Scanning Calorimetry
E	Elastic modulus
EOS	Equation of state
E_v	Activation energy for viscosity equation
f	Frequency factor
F	Surface energy
G	Gibbs free energy
k	Boltzmann constant
m	Mass of a gas molecule
N	Nucleation rate
N	Number of external contacts present in the system
P	Pressure
k_H	Henry's law constant
P*	Critical point characteristic pressure
P_1	Pressure within the melt
P_8	Bulk pressure
PAN	Polyarcrylonitrile
P_b	Pressure in the cell
PBA	Physical blowing agent
PEM	Proton exchange membrane
P_g	Initial pressure in a cell
P-V	Panayiotou-Vera EOS
q	Effective chain length
R	Gas-polymer interface radius
r	Radial coordinate
R_f	Cell outer radius,
R_g	Ideal gas constant
SEM	Scanning Electron Micrograph
SH	Superheat
S-L	Sanchez-Lacombe EOS
SP	Mettler softening point
t	Foam growth time
T*	Critical point characteristic temperature
T_c	Crystallization temperature
T_{foam}	Temperature foamed
T_g	Glass transition temperature
T_{g0}	Glass transition temperature without diluent
T_m	Melting temperature
T_{MS}	Mettler Softening Point Temperature

T_s	Reference temperature
v*	Critical point characteristic volume of a lattice site
V_r	Radial component of velocity
WFL	William-Landel-Ferry Equation
Z	Finite coordination number
z	Lattice constant
?	Surface tension
? C_p	Heat capacity
? G*	Activation energy to sustain a bubble
?	Viscosity
$?_0$	Viscosity
$?_s$	Reference viscosity
?	Fraction of total external contacts in the system that are mer-mer contacts in a random array of molecules and holes
?*	Critical point characteristic density
$?_f$	Density of foam
$?_g$	Density of the blowing agent
$?_p$	Density of the polymer
$?_s$	Density of original material
s	Rate of strain tensor
?	Shear rate
s	Shear stress
$t_{(1)}$	Convected time derived if stress tensor
$t_{??}$	Stress in the radial direction
$t_{??}$	Stress in the circumferential direction
f	Relative density
?	Mass fraction

2.3.2 Background on Pitch Foam

The use of carbon foam for structural applications leads to consideration of low-pressure, low-temperature applications, including the possibility of a spray-on foam that can be synthesized in ambient air. Some of the proposed applications include fire-proof ship decking and bulkheads, impact mitigation for aircraft and automobiles, structural panels and firewalls, low radar signature materials, Electromagnetic Interference (EMI) shielding, high-performance electrodes for fuel cells, abrasion resistant panels, composite tooling, and thermal management materials.[43]

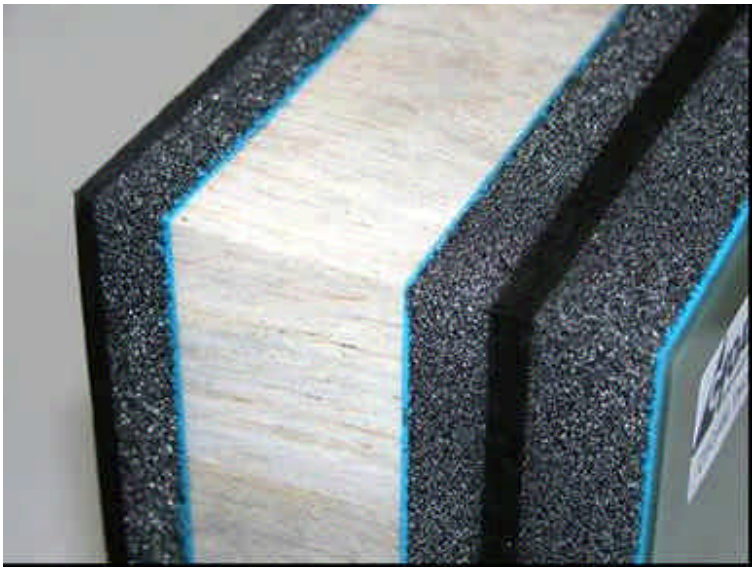

Figure 41. Composite consisting of carbon foam, balsa wood, fiberglass, and epoxy.

Cost is an important consideration for structural materials. Commercial carbon foam prices are in the range of several dollars per pound and increases depending on properties and processing. A number of the proposed applications may be commercially viable were carbon foam available at lower cost. Production of pitch foam may be an alternative that could be produced by less expensive methods.

One of the developments in material science during the 1930's was the production of synthetic urethane and vinyl polymeric foam.[44] Since that time, many other polymers have been successfully converted into foams and the processing steps have been further refined. Using polymer foaming developments, other materials were produced in foam form. Some of theses materials include metals and metal alloys, silicon oxide, carbon and graphite.

Carbon and graphite foams are of much interest due to their good mechanical performance and tailorable properties.[45] This has spawned a myriad of proposed applications that range from impact adsorptive panels to high performance heat sinks and nonconductive thermal insulation.

Currently, production of carbon foam is fairly specialized and capital intensive. This is manly due to the high thermal and pressure requirements. Carbon foam is produced by two different methods. The first uses suitable polymeric foam which is subsequently pyrolyzed. The pyrolysis often requires significant amount of time at elevated temperatures. The second method

involves heating coal, coal tar or petroleum pitch under pressure. The heating process softens the starting material, causes volatilization of volatile content in the starting material and decomposition of some of the side chains forming gases. The lighter molecules that are produced, in addition to those present, vaporize resulting in significant increase in bulk volume. The volatile matter acts as an imbedded chemical blowing agent similar to that in polymeric foaming. While the vaporization is occurring, the remaining higher molecular weight molecules cross-link (carbonize) to stabilize the bulk structure. Again, this process requires significant lengths of time at elevated temperatures and, depending upon the process conditions, elevated pressure.

The addition of additives known as blowing agents is common for several foaming processes.[46] The blowing agents are used to produce a supersaturated solution upon the reduction of pressure and/or increase in temperature. Because of thermodynamic instability, bubbles, termed cells for foam materials, are formed in the melt. If the cells remain upon solidification of the material, the resulting material is a cellular solid, and is commonly called foam. From a technical standpoint, it is a foam if the reduced bulk density is less than 1/3 that of the starting solid material.[47]

The use of CO_2, N_2, and water as physical blowing agents has gathered much interest as alternatives to chlorofluorocarbons (CFC) and hydrochlorofluorocarbons (HCFC) which have come under increasing environmental regulation due to their ozone depleting chemistry in the atmosphere. CO_2 and N_2 have also received interest due to plasticizing effects (i.e. lowering of the glass transition temperature, softening point, and viscosity) seen during processing, which could reduce processing expenses. The plasticization effect is seen more dominantly with low molecular weight blowing agents and diluents. These effects are due to the influence that blowing agents have on the free volume of the polymer and real dilution effect on the polymer.
There are many similarities between molten pitches and polymer melts. Some of the characteristics that both have in common include macro-organic molecules, molecular weight distributions, and amorphous to semi-crystalline morphologies. Due to the molecular weight range, polymers and pitches both have comparable rheologic profiles with a majority showing shear thinning character. Additionally, process temperature for several polymers falls in the same temperature range as that of several grades of pitch.

One of the primary differences between pitches and polymers is in the molecular skeleton. Most polymers consist of long chains of molecules, with varying degrees of branching and/or side groups, which are often characterized as strings or lines, whereas pitches are primarily composed of napthene aromatics, polar aromatics, and asphaltenes. The molecules in pitches also tend to be more planar or globular in structure than in polymers. In much polymer theory, polymers are often modeled as spherical or globular wrapping forms, particularly for amorphous morphology and in certain solvents. Thus it may be that these polymer models may are suited to modeling pitches as well.

The first objective of the present study is to examine current polymer foaming theory and production practices, specifically the uses of physical blowing agents (gaseous and liquids), the blowing agent solubility and equilibrium fraction and how the physical blowing agents affect the rheology of the melt.

From the examination of polymer theory and practices, an assessment of the applicability of using them to foam pitch is made. This will include a comparison of melt rheology, surface tension, and effects of physical blowing agents on the melt.

Evaluation of the properties of pitches is conducted and compared to various polymers. Samples will also be produced by a batch method to qualitatively compare the effect of variables (temperature, pressure, and pressure-drop rate) on pitch foam and by the extrusion method to verify if extrusion is possible. A test apparatus was constructed for extrusion to verify that pitch foam can be produced in a manner similar to that of polymer extrusion. The experiment will utilize CO_2, N_2, and H_2O as physical blowing agents. The viscosities of the melt samples is calculated from models.

The pitch and foam samples are examined under an optical microscope and by SEM to quantify the morphology and cell structure. The size, size range, shape of the cells, and whether the cells are open or closed in nature are examined. Mechanical properties of the pitch foam will also be examined, but not optimized. The focus of the project is on the production and quantification of cells formed within pitch foam rather than on the evaluation of their mechanical properties. Gibson and Ashby and others[48,49,50] have quantified the mechanical properties of foam from structure and these resources could be used for theoretical evaluation of the mechanical properties.

Also, areas of evaluation and production should be examined to further understand the complexities of pitch foam formation and the properties of pitch as they relate to the melt, process conditions, and blowing agents.

Cellular materials can be composed of numerous materials, including polymers, metals, and ceramics. True cellular solids are usually considered to be materials that are less than 1/3 of the density of the original solid material,[51] ?$_s$. Equation 7 quantifies this effect where, f is the relative density and ?$_f$ is the bulk density of the foamed material. Materials above the 30 % relative density, but still below that of the solid material are properly termed solids containing isolated pores for relative comparison).

$$j = \frac{r_f}{r_s} \quad . \qquad \text{(Equation 7)}$$

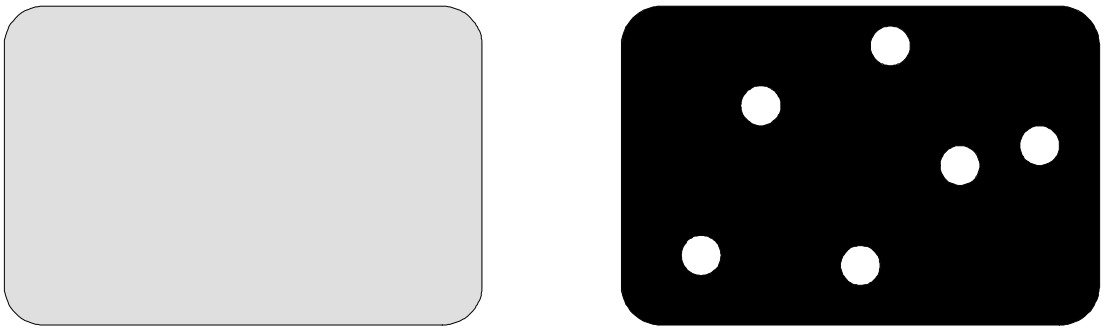

Figure 42. Relative comparison of cellular solid (left) and solids with isolated pores (right).

Cellular solids can be ideally organized into two basic groups. The first consisting of a two-dimensional matrix of polygons, often known as a honeycomb matrix. The other consists of a three-dimensional matrix, and is known as foam. In the literature, foams are often represented as idealized pentagonal dodecahedrons, though this is rarely true in reality. Foam can be further divided into two subgroups, closed cell and open cell. The cell walls or membranes between the cells in closed cell foams remain intact and do not allow flow through the foam. In open cell

foam, the membranes between cells have ruptured leaving a basic skeleton or strut type structure. The cell structure in actual foam is often some combination of open and closed cells which is characterized as percent open or closed cells.

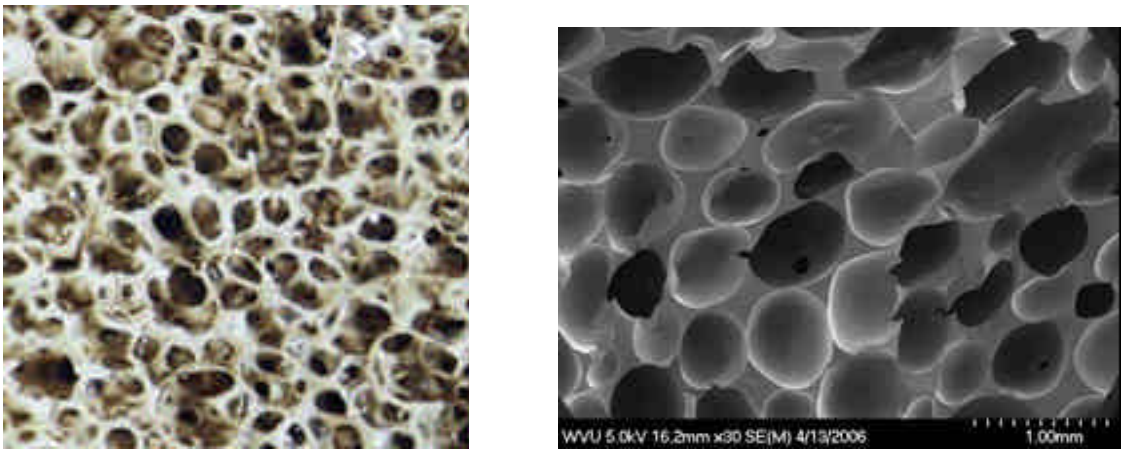

Figure 43. Comparative view of open celled and closed celled foam. Left: open cell alumina foam. Right: closed cell pitch foam produced at West Virginia University.[52]

Both rigid and flexible cellular solids can be produced. The degree of rigidity or flexibility of the cellular solid depends on the solid material's glass transition temperature, chemical composition, polymer backbone, degree of crystallinity, and degree of cross linking.[53] The glass transition temperature, T_g, is the temperature at which some molecules achieve partial mobility within the material. For materials that have T_g above room temperature, it may be possible to produce flexible foam if the proper plasticizers are used to reduce the T_g below room temperature.

Cellular materials are an area of much interest due to their extension of the material properties of the solid. A majority of interest comes from the density reduction and material savings in comparison with marginally diminished strength, Young's Modulus, conductivity and improved energy absorption.

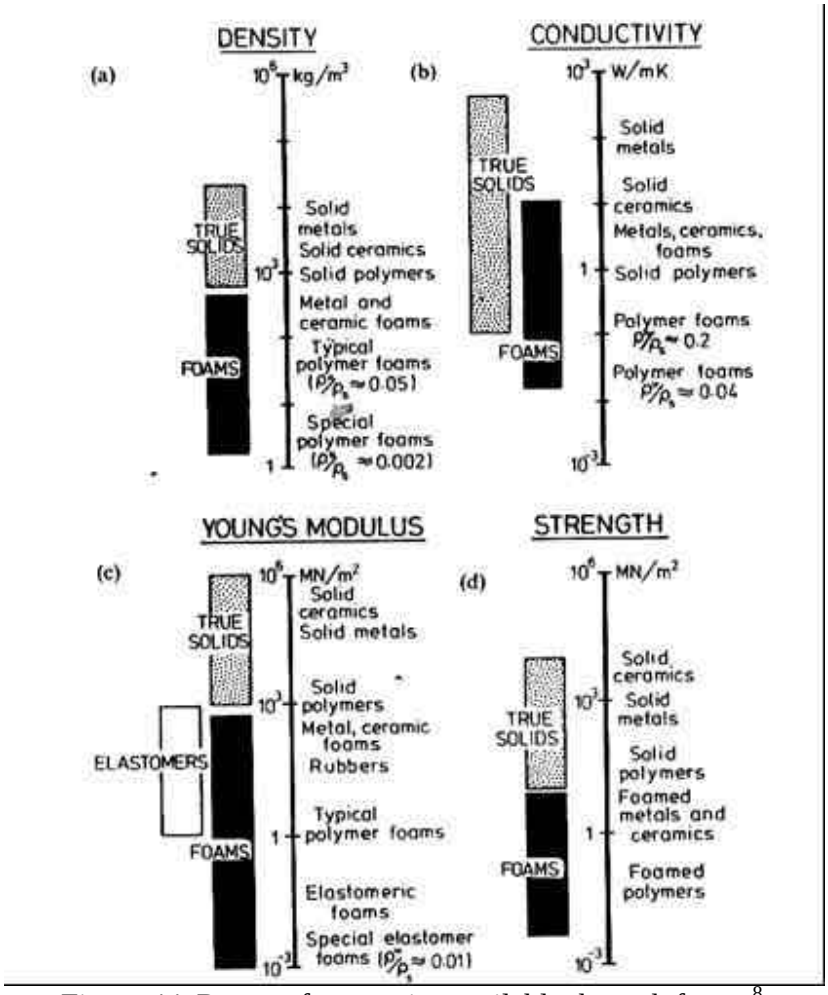

Figure 44. Range of properties available through foams[8].

The increased surface area afforded by foam is also of interest for both catalysis and thermal management. Major areas where these enhanced properties have found application are in thermal insulation, packaging, structural components, and flotation devices. Gibson and Ashby in their text *Cellular Solids,* go into much detail in describing the theoretical basis for understanding and predicting properties of cellular solids and is an excellent reference on the subject.

It is interesting to note that the size, shape, flexibility, and amount of interconnecting cells directly determine the physical properties of the foam, but the application for the foam directs which type of cell structure is desired. For example, a closed cell structure is desirable for thermal insulation while an open cell is desired for acoustic insulation.

Since the advent of polymeric foams by means of batch processes, many continuous processes have been developed to increase production rate and reduce cost. Foam has made inroads into a diverse variety of applications. Due to continued development of foam properties, total demand has steadily increased (Table 3) to over 3.7 million tons in the United States alone in 2001 and this number is expected to continue to increase for the near future. In 1993, foam accounted for 31 % of total polystyrene and 7.7 % of all plastic consumed in Japan.

Table 3. Foam production in the United States (in Millions).

Item	1975[54]	1987[55]	1996[56]	2001[57]
Total Foamed Plastics Demand (millions of lbs.)	2,633	4,558	6,325	7,420
Urethanes	1,330	2,363	3,325	3,910
Polystyrene	600	1,316	1,676	1,900
Other Polymers	703	879	1,324	1,620
Total Foamed Plastics Demand (millions $)	N/A	6,850	12,100	16,200

Table 4. Common foaming technologies and applicable polymers.

Production Method	Applicable Thermoplastics
Extrusion	PS, PVC, PE, PP, PVOH
Molded Beads	PS, PP, PE
Injection Molding	ABS, PC, PPO
Reactive Injection	PU, UF
Mechanical Blending	PU, UF, Elastomers

There are several production methods in use today (Table 4) to manufacture foam from a myriad of polymers and polymer/additive mixtures. Continuous extrusion is a method of producing large quantities of foam quickly usually in slab stock or rod form. This method can mix both physical and chemical blowing agents and other additives into the melt during the processing phase. Injection molding couples the continuous extrusion method with a mold to produce complex foam shapes.

In forming foam, two events must take place sequentially, no matter what the solid matrix may be. The first is the formation of large numbers of bubbles in the melt. This involves increasing the free energy of the foaming material system. The second is stabilization of the melt before the bubbles collapse or escape (i.e. reach the free energy minimum of the foaming material system).

The progression from a homogeneous uniform material into one containing voids with controlled dimensions can be daunting. Naturally produced foams such as sea sponges and cork grow with the voids present, while sea foam is mechanically churned or frothed by wind and wave motion. While natural foams can be interesting and of some use, they often are not available in quantities or qualities that are economically viable. For this reason several industrial production techniques have been developed to introduce gas bubbles into the precursor material. The developed techniques include: mechanical whipping or frothing of a liquid, expansion of dissolved gas(es) in a melt, flash vaporization of low-boiling liquids in a melt, volatilization of gas-producing compounds within a melt, incorporation of insoluble salts into a melt which are later removed, or the incorporation of hollow beads (microspheres)[58] which remain in the final product.

Both the frothing technique and the incorporation of microspheres are of limited usefulness for polymer melts due to processing and cost constraints. The mechanical frothing techniques are usually used with low viscosity liquids that have low energy requirements to stir at high rates. An example of frothing to produce a foam is beating egg whites to form meringue for pies. Incorporating hollow beads or insoluble salts is a sure way of producing solids containing voids. Once the melt is stabilized, the beads or salt remain and can result in additional concerns for each. For the beads, the foam matrix instead of being a single solid phase is now a two-phase

solid in which surface interactions of the two materials need to be considered. For salts, the difficulty becomes the removal of the salts without damaging the foam matrix. Salts have been used successfully in the production metal foams.

A majority of polymeric foam is produced by incorporating soluble gases, low-boiling point liquids, or compounds that decompose to form gases during heating. Theses additives are usually referred to as blowing agents. The purpose of the blowing agent is to saturate the melt with gas at low temperature or elevated pressure. Gases produced by decomposition of molecules in the processing temperature range, are known as a chemical blowing agents, while those added directly to the melt and dispersed by diffusion or mechanical agitation of the melt are called physical blowing agents. The purpose of these additives is to cause a thermodynamic instability (supersaturation state of a gas) within the melt upon temperature rise or pressure drop. Bubbles are formed to bring the system back into a metastable thermodynamic state.

Chemical blowing agents usually decompose to produce CO_2, N_2, CO, H_2O, NH_3, HCHO, SO_2, or some combination thereof. Some common chemical blowing agents are azodicarbonamide (ADC), zinc carbonate, and citric acid derivatives,[59] but just about any compound that has a well-defined decomposition temperature and produces a soluble gas in the processing range can be used.

Physical blowing agents are usually introduced in a continuous process at some predetermined point and mechanically mixed to form a single-phase mixture. At elevated pressures, melts sustain higher equilibrium concentrations of soluble gas. Through an extrusion process, the pressure and/or temperature are reduced to near ambient conditions, which results in a thermodynamic instability (supersaturation) in the melt. If the instability is produced rapidly, bubbles are spontaneously generated following classical homogeneous and heterogeneous nucleation models as in batch liquid processes. The supersaturated gas in the melt expands forming voids, and results in both pressure and temperature reductions to regain thermodynamic equilibrium. The most common physical blowing agents in the polymer foam industry are CO_2, N_2, water, and low molecular weight hydrocarbons. Liquid blowing agents (e.g. water and low molecular weight hydrocarbons) are usually added with the polymer pellets. During processing, both the temperature and pressure are raised. The pressure is raised in order to maintain the blowing agents in a liquid state. For water, this results in the formation of an emulsion. Upon release of pressure, the blowing agents vaporize, and diffuse out of the melt. By controlling the viscosity, blowing agent concentration, and pressure drop rate, the cell structure can be optimized.[60]

It has been shown that the presence of fine, dispersed solid particles, known as nucleating agents, greatly aid in increasing bubble formation by reducing the level of supersaturation needed before bubbles form.[61] This phenomenon has been likened to the addition of boiling chips to aqueous solutions, in that it provides an irregular surface on which bubbles can nucleate. The use of nucleating agents has led to the production of more and smaller cells in foam.

In extrusion processes, in addition to the above nucleation phenomenon, shear nucleation of bubbles can also occur. The shear nucleation can be caused by cavitation of the screw in the melt and cavities along the barrel of the extruder. Shear nucleation has been studied and modeled, and is very much dependent upon the operation and condition of the equipment.

Once a bubble is formed it must satisfy the stability equation (Equation 8), otherwise the gas in the bubble will be reabsorbed into the melt. In Equation 8, ? P is the vapor pressure gradient from the bubble to the melt, ? is the surface tension of the melt, and R is the radius of the bubble. Nucleation of new bubbles will continue till the supersaturation is sufficiently

reduced to favor bubble growth over new bubble formation. At this point, diffusion becomes the dominant means of reducing the remaining supersaturated gas.

$$\Delta P \geq \frac{2\gamma}{R} \quad . \qquad \text{(Equation 8)}$$

Once diffusion becomes dominant, the nucleated bubbles begin to expand till ? P=2?/r. When the gas concentration reaches equilibrium, bubbles can only grow by diffusion of gas from smaller bubbles, were the pressure gradient is greater than in larger bubbles, coalescence of adjacent bubbles, or by the exothermic expansion of the gas in the bubble. These growth mechanisms act to further reduce the free surface energy of the melt system by following Equation 9 where ? F is the surface energy, ? is the surface tension, and A is the total surface area the bubbles.

$$\Delta F = \gamma A \quad . \qquad \text{(Equation 9)}$$

As can clearly be seen from Equations 8 and 9, the surface tension is a significant factor in both the formation of bubbles and the free energy needed for foam systems. By reducing the surface tension of the material melt, the pressure gradient (i.e. the concentration of gas) and the free energy input requirements are reduced resulting in bubble formation sooner and greater transient stability for smaller bubble formation.

Frequently, cells are not spherical in nature. In highly-expanded, open or closed cell foams, the cells exhibit polyhedron structure due to the interaction of adjacent cells. The cell structure is often idealized as pentagonal dodecahedrons for modeling the mechanical properties. Foams formed in a mold or in pressure gradient fields often exhibit ellipsoid-shaped cells. In this case, the ellipsoidal behavior is due to pressure interactions on either side of the cell during growth. The ellipsoidal growth was seen to be retarded through increasing both initial pressure of cell formation and viscosity of the bulk melt.[62]

Several researchers have modeled foam formation and growth to give quantitative insight for production. The foaming process has been simplified into three major events: foam nucleation, foam growth, and cell coalescence with temperature, pressure, surface tension, heat and momentum transfer, diffusion, gas solubility and viscosity as variables. Tomasko et al. correlated many of the variables and their relationship to one another for a CO_2 based blowing of polymer in an extrusion process.[63]

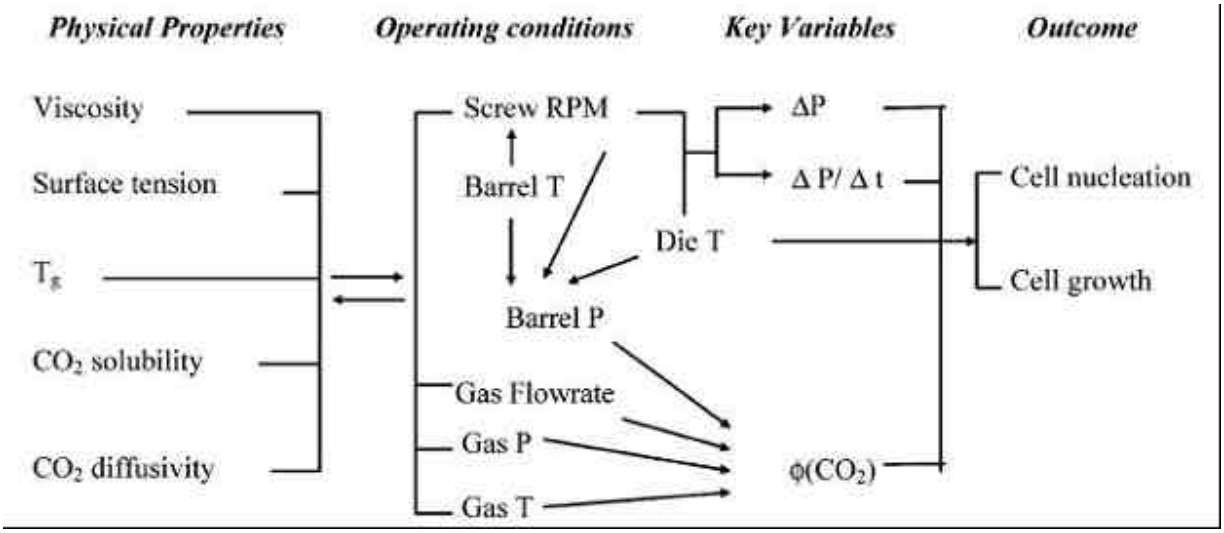

Figure 45. Relationships between parameters in a continuous extrusion foaming process using CO_2 as the blowing agent.[64]

From classical homogeneous nucleation theory, the rate at which invisible gas clusters are energized by effective diffusion governs the nucleation rate.[65] From work by Gibbs, the rate of nucleation can be expressed as

$$N = fc \exp\left(-\Delta G^* / kT\right) \qquad \text{(Equation 10)}$$

where N is the nucleation rate, f is a frequency factor, c is the gas concentration, ? G* is the activation energy to sustain a bubble, and k and T are the Boltzmann constant and the absolute temperature respectively. Further work by Blander and Katz defined the minimum work term, ? G*, and frequency factor, f, into measurable parameters (Equation 11) resulting in Equation 12 for homogeneous nucleation,

$$?G^*_{\text{hom}} = \frac{16p?^3}{3\left(P_b - P_\infty\right)^2}$$

$$f = \left(\frac{2g}{pm}\right)^{0.5} \qquad \text{(Equation 11)}$$

$$N = c\left(\frac{2g}{pm}\right)^{0.5} \exp\left(\frac{-16pg^3}{3kT\left(P_b - P_\infty\right)^2}\right) \qquad \text{(Equation 12)}$$

where ?, P_b, P_1, and m are the surface tension, pressure in the bubble, pressure in the melt, and mass of a gas molecule respectively. Often P_8 is assumed to equal to atmospheric pressure.

S. T. Lee collected and presented a detailed development of nucleation theory.[66] Tomasko et al. in their review presented simplified models in terms of an activation energy, ? G*, for heterogeneous nucleation (Equation 13), though they did not define the frequency factor, f, for the equation.

$$N_1 = c_1 f_1 e^{\left(\frac{-\Delta G^*_{het}}{kT}\right)}$$

$$\Delta G^*_{het} = \frac{16\pi g^3}{3\Delta P^2}\frac{(2+\cos q)(1-\cos q)^2}{4} \quad . \qquad \text{(Equation 13)}$$

For Equations 13, c is the concentration of gas, f is the frequency factor of gas adding to the nucleation site, k is the Boltzmann constant, T is the absolute temperature, ? is the surface tension, ? P is the gas pressure difference, and ? is the contact angle of the melt-particle/gas-phase interface. For single phase polymer melts, only homogeneous nucleation occurs. In melts containing solid particles or two-phase systems, both the homogeneous and heterogeneous equations need to be solved simultaneously.

From the pressure difference, ? P, Blander and Katz developed the concept of superheat, SH, (Equation 14). For low superheat, diffusion is able to reestablish equilibrium before the critical bubble radius is reached thereby limiting nucleation.

$$SH = P_b - P_{1\infty} \quad . \qquad \text{(Equation 14)}$$

In actuality, polymer melt bubble nucleation has been seen to deviate from what is predicted. This is believed due to the polymer being of non-homogeneous character and the thermodynamic-based model's inability to handle the simultaneous pressure and temperature changes on the gas activity and polymer chain mobility. However, when pressure gradients and surface tension dominate, bubble nucleation is in close agreement with homogeneous theory.[67] Some researchers have modified nucleation theory to better predict nucleation rate and added or modified several terms resulting in more complex homogeneous and heterogeneous nucleation equations.

Early models focused on the growth of a single bubble (i.e. a single bubble in an infinite fluid with infinite gas available). This is clearly not the case for foam formation where there are many bubbles with a finite amount of gas. Newer models sought to correct for this problem by using cell or "swarm" bubble growth models. These cell models assume an interaction between the cells in the foam.

Older foaming models usually involve simultaneous solution of the momentum, heat, and mass balances, with a specific rheologic model. The incorporation of gas loss from the foam, blowing agent plasticization, concentration-dependent diffusion, and transient cooling have further improved the models. The models shown below in Equations 15-18 need to be solved simultaneously with appropriate boundary conditions.[68]

Momentum Equation,

$$P_g - P_\infty - \frac{2g}{R} + \int_R^{R_f}\left(t_{gg} - t_{qq}\right)\frac{dr}{r} = 0 \quad . \qquad \text{(Equation 15)}$$

Rheological Equations,

$$t + \frac{h_0 *}{E} t_{(1)} = -h_0 * s$$

$$h_0 * = h_0 \exp^{\left[\frac{E_v}{R_g}\left(\frac{1}{T}-\frac{1}{T_0}\right)\right]} f(c) \quad . \quad \text{(Equation 16)}$$

where f(c) = viscosity reduction factor

Growth of Radius Equation,

$$\frac{d}{dt}\left(r_g R^3\right) = 3 r_p D R^2 \left[\frac{\partial c}{\partial r}\right]_{r=R} \quad . \quad \text{(Equation 17)}$$

Concentration-Dependent Diffusion Equation,

$$\frac{\partial c}{\partial t} + V_r \frac{\partial c}{\partial r} = \frac{1}{r^2}\frac{\partial}{\partial r}\left(D r^2 \frac{\partial c}{\partial r}\right) \quad . \quad \text{(Equation 18)}$$

where $D = (1 + Ac) 10^{-7} e^{\left(B - \frac{c}{T}\right)}$

In the above equations, P_g is initial pressure in a cell, P_8 is the bulk pressure, ? is the surface tension, $t_{??}$ and $t_{??}$ are the normal stress elements in the radial and circumferential directions respectively, $?_0$ is the viscosity, R_f is the cell outer radius, R is the gas-polymer interface radius, r is the radial coordinate, $t_{(1)}$ is the convective time derivative of stress tensor, E is the elastic modulus, s is the rate of strain tensor, E_v is the activation energy for the viscosity equation, R_g is the ideal gas constant, T is the foaming temperature, T_0 is the initial temperature, $?_g$ is the density of the blowing agent, ? is the density of the polymer, D is the diffusion coefficient, c is the blowing agent concentration, t is foam growth time, and lastly V_r is the radial component of velocity.

From inspection, general trends expected are an increase in cell size with increased blowing agent concentration, time dependent concentration (decreasing pressure-drop rate) and reduced viscosity. It is important to remember that the above equations are for growth of a cell from the instant of formation. It is therefore necessary to make some assumptions to solve the equations as cells continue to form until the supersaturation of blowing agent is reduced to favor diffusional growth instead of nucleation.

S.T. Lee et al. have developed a model that approximates experimental results for low density polyethylene with butane as a blowing agent in a continuous extrusion process based on the above equations.[69] It is expected that the general trends captured by their models will be suitable for other systems.

As long as the pressure is sufficient to overcome the critical radius, there is the possibility that as new cells form, that they will do so adjacent to existing cells. Due to pressure difference within the adjacent cell, diffusion occurs from smaller cells (high pressure) to larger cells (low pressure), causing the larger cell to grow while the smaller cell shrinks till it is reabsorbed into the matrix material. This process is known as cell coarsening.[70]

As new cells continue to form and grow, the possibility increases that two or more cells of approximately the same size will come in contact with one another. As a result, a wall or membrane will form between the adjacent cells. As cell growth continues, the separating membrane is stretched thinner and becomes less stable. Eventually, the membrane ruptures resulting in the merger of the two cells into one larger cell as a way for the matrix material to minimize surface free energy. The net result is a reduction in cell number density which is usually undesirable since it adversely affects the thermal and mechanical properties of the foam.[71]

Coalescence and coarsening of cells are difficult to model and this continues to be an area of research. Much of the research focuses on improving melt strength or reducing surface tension thereby increasing the likelihood of adjacent cells surviving until the matrix material stabilizes.[72]

Currently, carbon form is produced using one of two main methods. The first method is to use a pyrolytic polymeric foam and subject it to high temperatures to cause char and cross-linking of the polymer matrix. The other way is to subject coal or pitch to high temperature and pressure, usually between 300-500 °C and 14.7-1500 psia.[73] This process takes advantage of naturally-present lower molecular weight molecules that volatilize during the heating process to create cells in the bulk phase. The resulting material is a cellular carbon which is sometimes referred to as “green” carbon foam. The foam can be further processed by carbonization, graphitization, or subjected to acid or base washes to alter the surface characteristics. Green carbon foams have been treated under inert atmosphere, usually nitrogen, to 300-500 °C. Further heating (600-1600 °C) of green foam under an inert atmosphere often leads to rejection of hydrogen and the fission of side groups on the molecular structure, a process known as calcination. Heating of select carbon foam still further (1700-3000 °C), under inert atmosphere, leads to graphite planes forming in the bulk structure. This last heating is known as graphitization and is usually accompanied by significant alteration of the physical properties of the foam.[74] For example, Figure 46 gives a general overview of the effect on electrical resistivity during heating processes for a graphitizable foam.

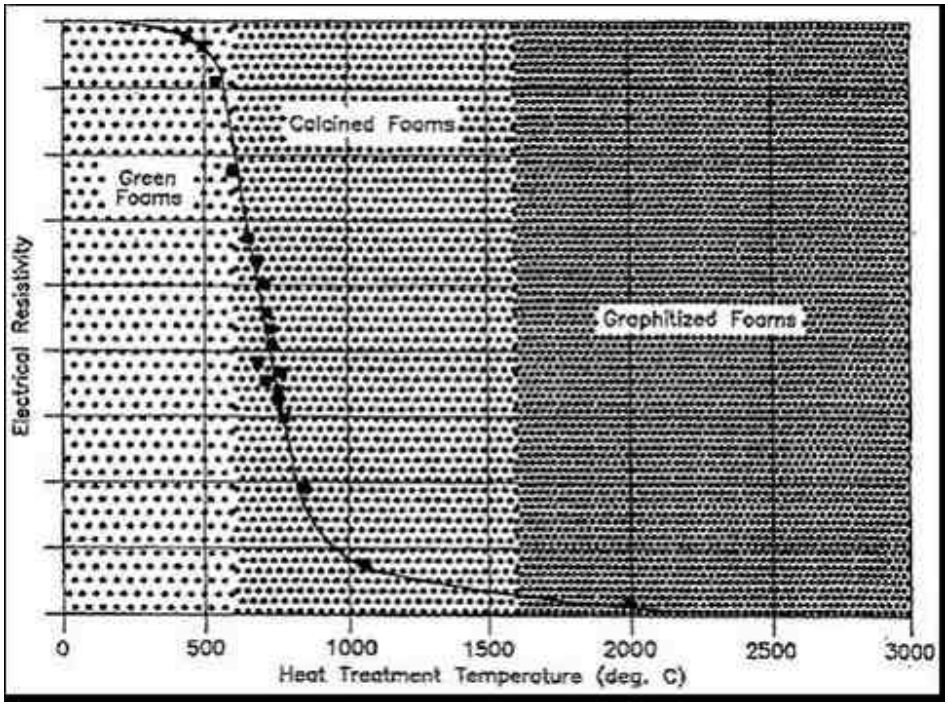

Figure 46. Electrical resistivity versus heat treatment temperature for carbon foam.

2.3.2 Background on Pitch Foam

Similar to polymeric foams, carbon foams retain a significant amount of strength despite the reduction in density of the solid starting material (Figure 46). In addition, other physical properties of carbon foam can be tailored. Most of the tailorability comes from how the carbon molecules are ordered. Foams made from highly graphitic precursors (anisotropic and mesophase pitch) have much higher electrical and thermal conductivity in the same direction as the graphitic plane (Figure 45). The conductivity in the plane of direction is so high that it can rival solid aluminum or copper for heat transfer per weight due to the high surface transfer area. Conversely, the electrical and thermal conductivity for isotropic carbon foams can be similar to that of ceramic insulators due to the absence of a continuous graphitic plane structure.

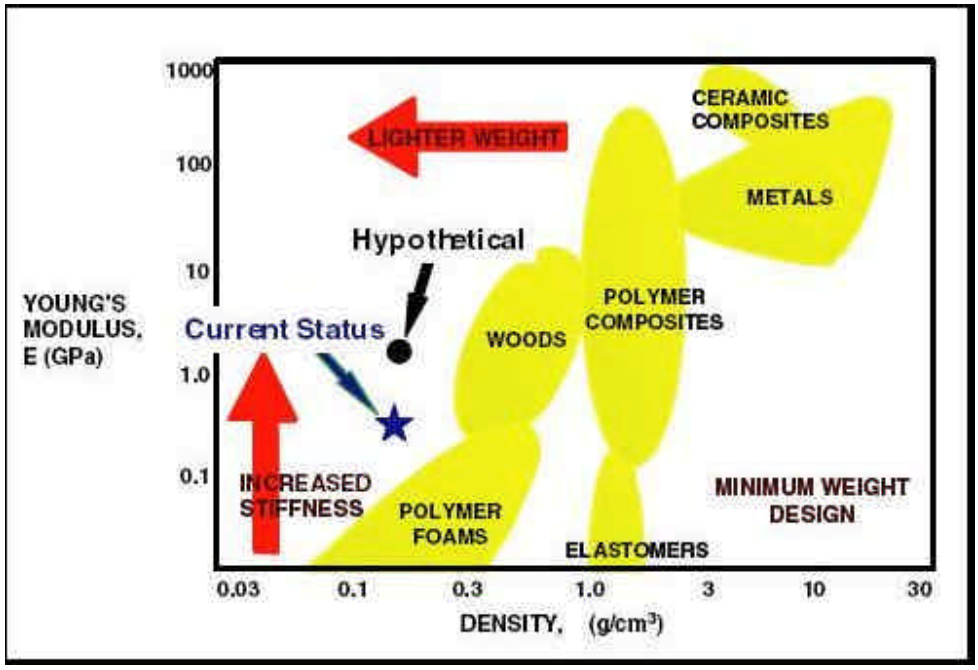

Figure 47. Estimated specific modulus/property chart of pitch-based carbon foam and competing materials.[75]

From the strength-to-weight ratio and the variety of properties of carbon, a number of applications have been proposed. Some of the fields that would take advantage of this mix of properties include transportation, energy, and military industries.

The aerospace, automotive, and transportation industries share many of the same interests in carbon foam and are continually looking for materials that would reduce the weight and cost of their vehicles while maintaining performance. For these industries, the energy absorption properties of carbon foam have been of particular interest for bumpers and replaceable impact absorbing tiles. The large energy absorption is not only due to the strong carbonaceous matrix material, but also the energy necessary to crush the foam structure itself. The automotive industry, along with catalysis researchers, is additionally looking at using carbon foam as a substrate for catalysts and as a catalyst itself through surface modification.

There has even been some interest in using carbon foam in fuel cells. One of the proposals is to use carbon foam for the bipolar plates in proton exchange membrane (PEM) fuel cells.[76] Another is to use the carbon foam as a fuel in high performance direct carbon conversion fuel cells (DCFC).

Bubbles can be formed a number of ways in liquids, but most bubbles do not last long before collapsing or bursting. The key to making a solid foam is to stabilize the molten material to a solid before the cell structure collapses. Controlling rheology and melt strength of the base material is what makes foam production possible. The formation of foam is a complex function of temperature, pressure, surface tension, heat and momentum transfer, diffusion, and viscosity. Most of the listed parameters have a significant effect on the rheology of the molten material that is used. An understanding of how each effect, particularly diluents and temperature, influences the pitch rheology aides tremendously in forming process conditions without much additional trial and error. The first step is to identify the type of long range molecular structure, or

crystallinity, present in the base material. The crystallinity gives a general idea of how the melt rheology behaves and is discussed below.

The arrangement of molecules in a solid material is known as crystallinity. Crystallinity is divided into crystalline and amorphous structure depending upon the degree of long range orientation of the atoms.

Crystalline materials have regular long range lattice orientation of their atoms or molecules. The molecular order leads to defined melting and boiling points. Often polymers considered crystalline rarely have a purely crystalline structure but rather partly crystalline domains.

Amorphous materials, as the name implies, lack long range lattice orientation. This lack of orientation is usually a result of the material having a broad variety of molecules of varying molecular weight. Amorphous materials can also be formed by cooling liquids faster than a minimum thermodynamic orientation can be reached. Due to this irregular structure, amorphous materials do not have defined melting points. Instead, they often undergo a rubbery transition in a material-specific temperature range as they are heated from a solid to a fluid state. The point at which this transition occurs is known as the glass transition temperature, T_g. The glass transition temperature is a reference point that is often used in the calculation of several physical properties of amorphous materials.

The Glass Transition Temperature is a important characteristic in the processing of polymers and pitches. It is used extensively in estimating several rheologic properties of both materials. To begin, the T_g is defined as the point at which an amorphous glassy state transitions to a mobile rubbery state.[77] In the solid state, only intermolecular vibrations of the molecules occur. At the T_g short range intermolecular motion begins along with some molecular slippage. The range of motion in and around the molecules increases until free motion of the entire molecule is achieved forming a liquid solution. There is also a significant increase in the fractional free volume of the system due to the molecular relaxation.[78] Fractional free volume is defined as the fraction of the total volume accessible to solutes of any, even subatomic, size.
Generally, the T_g increases as molecular weight and intermolecular forces increase. The T_g of a material can change over time due to the thermal history of the material. For example, if the material is heated above a temperature at which lower molecular weight molecules begin to escape from the melt, a general rise of the T_g is seen. Heat treatments, depending on the material, can also result in degradation, charring, cross-linking, and cracking of the heavier molecules to further increase the T_g. Eventually, mass loss will occur before the T_g is reached resulting in no melt phase formation. This is one method that is used to stabilize pitch-based products.[79]

The glass transition temperature is usually evaluated through the use of Differential Scanning Calorimetry (DSC), though thermogravimetric analysis, mechanical thermal analysis, coefficient of thermal expansion, and nuclear magnetic resonance imaging can be used and yield similar results. During the T_g, there is a significant change in the heat capacity between the glassy to rubbery state in the material, which is detected with DSC through an increase in energy needed to maintain a constant heating ramp. The inflection point of the heat input curve is then taken as the T_g. This is usually within ±2 °C of the actual T_g.

A simple correlation was developed by Barr et al. for approximating the T_g of pitches from the Mettler Softening Point Temperature, T_{MS}. The Mettler Softening point is a standard ASTM test method (D3104-99 (2005)) for determining the softening point of pitch. It is valid over a temperature range of 50 °C to 180 °C, and gives results comparable to those obtained by ASTM test method D 2319 for temperatures above 80 °C.[0] Barr et al. suggested a linear

correlation between T_g and T_{MS} (Equation 19) where both are in degrees Kelvin. Khandare, at West Virginia University, confirmed the form of the equation, but disagreed for the value of the constant, x. Barr et al. calculated an experimental value of 0.84±0.02 while Khandare obtained a value of 0.89±0.01.[80] Khandare attributed the variation to differences in preparation and measuring techniques (Differential Scanning Calorimetry for Barr and Dilatometry for Khandare).

$$T_g = xT_{MS} \quad . \qquad \text{(Equation 19)}$$

Viscosity, ?, is one of the most influential parameters in forming foam. As shown in Equation 20, viscosity describes a fluid's internal resistance to flow and is commonly thought of as fluid "thickness", where s and ? are the shear stress and shear rate respectively. As such, water would be a "thin" fluid, at ambient temperature and pressure, having a low viscosity, while motor oil would be considered a "thick" fluid due to its higher flow resistance. For foam production, if the viscosity is too high, the material is difficult to process easily and efficiently and stunts cell formation and growth. If, or the other hand, the viscosity is too low, the gas easily escapes and the foam matrix collapses. The viscosity of a melt is influenced by several factors, though the primary ones are temperature, pressure, and amount and nature of the diluent components in the melt.

$$h = \frac{s}{V} \quad . \qquad \text{(Equation 20)}$$

Every fluid has a unique viscosity profile for a give temperature and pressure. Most fall into three general categories: Newtonian, power law (shear thickening or thinning), or Bingham plastic (Figure 48). A Bingham Plastic is ideal for foaming due to the minimum shear stress needed for its deformation. This behavior would permit the foam matrix structure to hold till the matrix material has an opportunity to cool or cure.

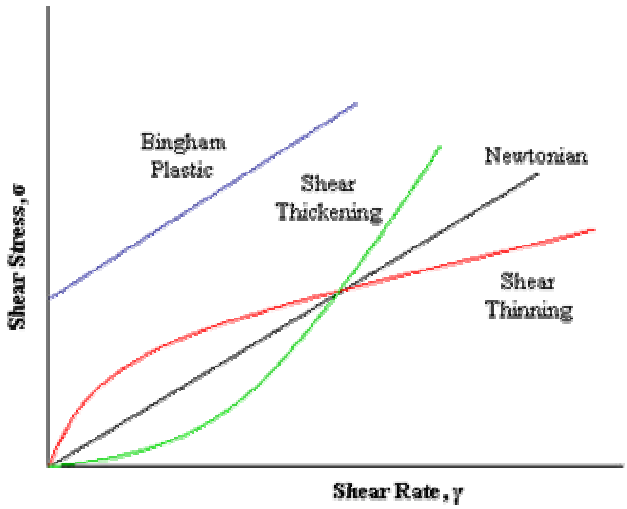

Figure 48. Comparison of viscosity profiles for Bingham plastic, Newtonian, and power law fluids (shear thickening & thinning).

Most polymer and pitch melts exhibit shear thinning behavior. Though shear thinning is less than ideal for foam stabilization, it is still capable of producing high quality foams. The viscosity and melt strength need to be sufficient to allow time for the matrix material to freeze, locking the structure in place.

The viscosity and glass transition temperature of a system diluted with gas are often lower than that of the pure system. This reduction of viscosity and T_g is generally referred to as plasticization of the material and has been attributed to both an increase of the free volume of the material and the real dilution effect of the gas or other plasticizing agent. The plastization behavior has been acceptably modeled for polymers through the work of T.S. Chow and the William-Landel-Ferry Equation (see Equations 24 and 25).

Plasticizing additives for polymers are most commonly phthalates, and they tend to increase the flexibility and durability of hard plastics such as PVC. They are often based on esters of polycarboxylic acids with linear or branched aliphatic alcohols of moderate chain length. Plasticizers work by embedding themselves between the polymer chains, increasing of the free volume and chain slippage, and significantly lowering the glass transition temperature for the plastic thereby making it more flexible.

In time plasticizers diffuse out of the material, returning it to the properties of the pure system. For gases, this diffusion process is fast, especially for light gases, and can be taken advantage of by increasing the freezing rate of melt systems.

Diffusion of gases occurs in most solids and liquids. A natural result is that gases in the material are in equilibrium with the surrounding fluid. The amount of gas that a material is able to take in is unique to the gas and material and is referred to as the solubility of a gas in that material. Being able to rapidly change the solubility of a gas in the melt causing a thermodynamic instability is what makes physical foaming of melts possible.

For most gases, the solubility in a polymer changes at the T_g. Below the T_g, the solubility is usually described by the dual-mode sorption model (Equation 21) which is a combination of Henry's law gas and the Langmuir adsorption equation

$$C = k_H P + \frac{C_L b P}{1 + bP} \quad , \qquad \text{(Equation 21)}$$

where C is the concentration of the gas in the polymer, P is the gas pressure, k_H is the Henry's law constant, and C_L and b are the Langmuir capacity and affinity respectively. [81]

Above the T_g and in the lower pressure regimes, the Langmuir capacity approaches zero resulting in a linear correlation that follows the Henry's law model. Following this, solute gas concentrations can generally be increased by increasing pressure (Figure 49). It is important to note that the Henry's law constant, k_H, is a function of both temperature and total absorbed concentration at high pressures. As the temperature increases, the Henry's law constant decreases, corresponding with a decease in solubility for most materials.

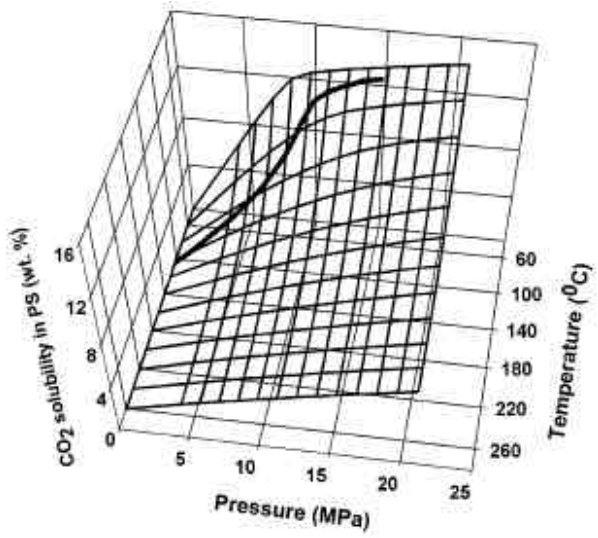

Figure 49. CO2 solubility in polystyrene at different pressures and temperatures (the thick line on the surface is the T_g).[82]

Accurately modeling the solubility of gases in the polymer melt is of great interest in calculating properties of polymer/gas mixtures. This is due to the effect that the diluent gas has on the melt and the resulting temperature dependent viscosity of the melt. Design of equipment and processing of melts has forced the development of correlations between equation of state (EOS) models and solubility for these systems. Reviewing the literature for polymer processing and macromolecules, the Sanchez-Lacombe (S-L), and Panayiotou-Vera (P-V) equations yield fairly accurate predictions for pure polymer melt and diluted melt polymer solutions.[83,84,85,86,87] Both use equilibrium chemical potentials in the melt and gas phases to correlate solubility to the pure phase through a binary interaction parameter. The models and modeling techniques may possibly be extended to pitch as well.

The Sanchez-Lacombe (S-L) EOS (Equation 22) is patterned after the Flory-Higgins (F-H) model that is based on hole theory. In the F-H model, the hole density is fixed by the lattice structure, whereas in the S-L model it is allowed to vary. $\tilde{P}$, $\tilde{T}$, and $\tilde{r}$ are the reduced pressure, temperature and density, respectively. P*, T*, ?* are the characteristic pressure, temperature and density at the critical point of the gas, respectively. R_g is the ideal gas constant, v^* is the characteristic volume of a lattice site, e^* interaction energy, r is the number of lattice sites occupied by a molecule, and M is the molecular weight of the occupying molecule.

$$\frac{\tilde{P}}{\tilde{T}} = \ln(1-\tilde{r}) - \left(1-\frac{1}{r}\right)\tilde{r} - \frac{\tilde{r}^2}{\tilde{T}}$$

$$\tilde{T} = T/T^*; \quad T^* = e^*/\mathrm{R}$$

$$\tilde{P} = P/P^*; \quad P^* = e^*/v^*$$

$$\tilde{r} = r/r^*; \quad r^* = M/(rv^*)$$

(Equation 22)

The Panayiotou-Vera Equation of State (Equation 23) is a modification of the S-L EOS and incorporates concepts developed by Guggenheim. In the Panayiotou-Vera Equation, $\tilde{P}$, $\tilde{T}$, and $\tilde{v}$ are the reduced pressure, temperature and volume, respectively. P*, T*, v^* are the characteristic pressure, temperature and volume at the critical point of the gas, respectively. R_g is the ideal gas constant, Z is a finite coordination number, v^* is the characteristic volume of a lattice site, e^* interaction energy, q is the effective chain length, r is the number of lattice sites occupied by a molecule, ? is the fraction of total external contacts in the system that are mer-mer contacts in a random array of molecules and holes, and N is the number of external contacts present in the system.

$$\frac{\tilde{P}}{\tilde{T}} = \ln\left(\frac{\tilde{v}}{\tilde{v}-1}\right) + \frac{Z}{2}\ln\left(\frac{\tilde{v}+q/r-1}{\tilde{v}}\right) - \frac{?^2}{\tilde{T}}$$

$$\frac{Z}{2}e = P^* v_H = RT^*$$

$$\tilde{v} = \frac{V}{V^*} = \frac{v_{sp}}{v_{sp}^*}; \quad V^* = Nrv_H$$

$$\tilde{T} = \frac{T}{T^*}; \quad \tilde{P} = \frac{P}{P^*}$$

$$q = \frac{(Z-2)r+2}{Z}$$

. (Equation 23)

It is also known from Henry's Law, and has been further verified by experimental work with polymers, that physical properties are also affected by temperature, pressure and diluent concentration. An accurate understanding of the blowing agent/pitch system over a broad range of temperature and pressures is needed to accurately produce a melt system with the appropriate rheologic properties. This is particularly needed in ascertaining the rheologic behavior with blowing agent concentrations below and at equilibrium concentrations in the pitch at elevated temperatures and pressures. Two equations that have been developed to aid in this modeling are the William-Landel-Ferry equation and the Chow correlation.

Below T_g and above the melting temperature, T_m (~T_g+100 °C to 150 °C for amorphous polymers and pitches), amorphous materials follow an Arrhenius-type relationship for the temperature dependence of viscosity. But between T_g and T_m, the viscosity behavior deviates greatly from the Arrhenius-type relation[88,89] (Figure 50). The William-Landel-Ferry Equation

(Equation 24) was developed for this temperature region and accurately describes viscosities of amorphous materials,

$$\log\left(\frac{h}{h_s}\right) = -\frac{c_1(T - T_s)}{c_2 + T + T_s} \quad .^{90,91} \qquad \text{(Equation 24)}$$

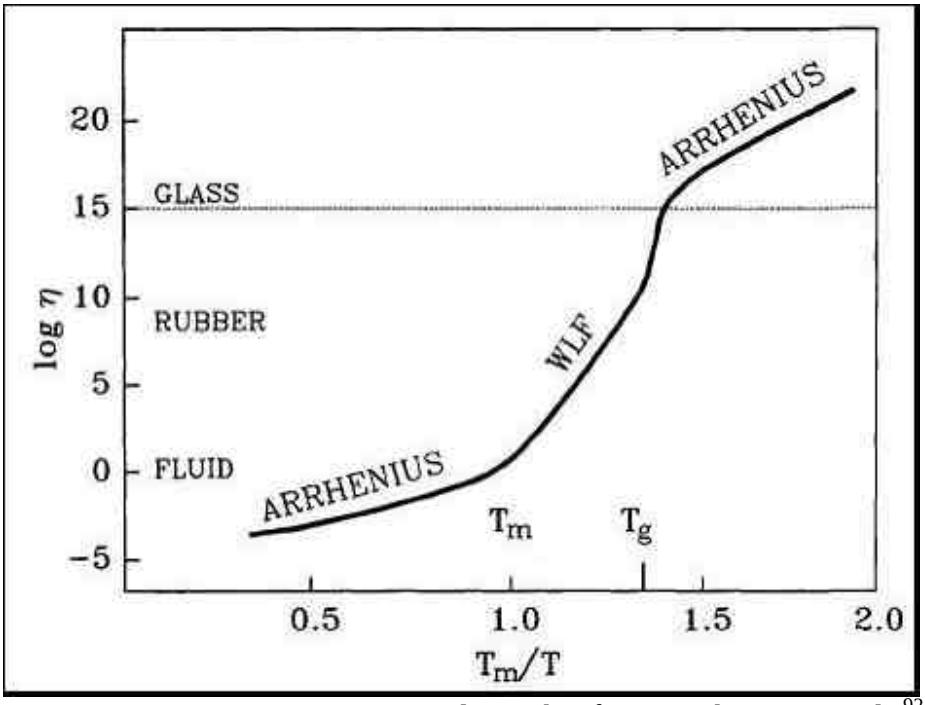

Figure 50. Viscosity-temperature relationship for amorphous materials.[92]

The Williams-Landel-Ferry (WLF) equation was originally developed in 1955 as an empirical equation for amorphous polymers. It has since been shown to accurately model most amorphous materials including pitches. The WLF equation has since been correlated to free volume theory for predicting the viscosity of amorphous materials that are between the T_g and approximately 100-150 °C above the T_g. Beyond 150 °C above the T_g, the effects of free volume become insignificant and Arrhenius type behavior better describes the viscosity observations. In the WFL equation (Equation 24), T_s and $?_s$ are temperature and viscosity respectively at a selected reference temperature $T_g<T_s<T_g+100$ °C, c_1 and c_2 are experimentally determined constants at constant shear rate for the material, T and ? are temperature and viscosity respectively for $T_g<T<T_g+100$ °C. It was been suggested that values of 17.44 and 51.6 for c_1 and c_2 respectively can be used generally for polymer system, but these should be experimentally determined for the best correlation fit.[93]

The presence of gaseous or liquid diluents often alters the T_g of amorphous materials.[94,95] T. S. Chow showed for polymers that the change in T_g could be modeled as a function of the diluent's mass fraction (?) and characteristic parameters of the polymer/diluent mixture. Chow

proposed a model (Equation 25) based on classical and statistical thermodynamics to account for the change in T_g for binary polymer-diluents systems.[96]

$$\ln\left(\frac{T_g}{T_{g0}}\right) = \Psi[(1-q)\ln(1-q) + q\ln(q)]$$
$$q = \frac{M_p}{zM_d}\frac{w}{1-w}; \quad \Psi = \frac{zR}{M_p \Delta C_p} \quad . \qquad \text{(Equation 25)}$$

where T_g and T_{g0} are glass transition temperature with diluent and without diluent respectively, ? is the mass fraction of the diluent, M_p and M_d are the molecular weight of the polymer repeat unit and the diluent respectively, ? C_p is the heat capacity at the glass transition temperature, R_g is the ideal gas constant, and z is a lattice constant. The use of the Bragg-William approximation in the development of the above expression requires ? to be numerically small for best results.[97] As such, this correlation works best with lower molecular weight diluents and small mass fractions of diluent. The lattice constant has been found to usually be 1 or 2 for polymers. The selection of either makes only a minor variation in T_g.

Through the use of the Chow correlation and the WFL equation, the reduced viscosity can be calculated. This is accomplished by shifting the viscosity profile predicted from the WFL equation by the change in the T_g predicted from the Chow correlation. This calculation assumes a lateral shift of the entire viscosity profile and has been shown experimentally to be an acceptable assumption.[98]

Surface tension is an effect within the surface layer of a liquid that causes the layer to behave as an elastic sheet. It is what allows water striders (a small aquatic insect) to stand on the surface of the water. In producing foam, one is attempting to increase the surface area and freeze it in place and surface tension is a measure of the resistance to increase that area. The surface tension is the energy required to increase the surface area of a liquid by a unit amount and is a significant parameter in foam production. Simply put, the higher the surface tension, the more energy is needed to increase the surface area above that of the minimum energetic shape state. The thermodynamic definition of surface tension is the derivative of the Gibbs free energy of the system, G, with respect to area at constant temperature and pressure (Equation 26).[99]

$$g = \left(\frac{\partial G}{\partial A}\right)_{T,P} \quad . \qquad \text{(Equation 26)}$$

Surface tension is an effect within the surface layer of a liquid that causes the layer to behave as an elastic sheet and is due to attraction between the molecules of the liquid, which is a result of various intermolecular forces. In the bulk of the liquid each molecule is pulled equally in all directions by neighboring liquid molecules, resulting in a net force of zero. At the surface there are no liquid molecules on the outside to balance these forces resulting in molecules being pulled inwards by molecules deeper inside the liquid. The surface molecules are then subject to an inward-directed pulling force of molecular attraction which is counteracted by the resistance of the liquid to compression. There may also be a small outward attraction resulting from interaction with the phase interface, but usually this interaction force is negligible.

Using water as an example, it has a relatively high surface tension for its density and is difficult to form suds due to the significance that surface tension plays in minimizing surface energy. By adding soap, a surfactant which lowers surface tension, forming bubbles becomes much easier. Not only does surface tension affect the stability of the matrix, but the nucleation growth, and stability of cells are also affected.

Polymer melts have gathered more interest than pitch melts due to their extensive use in consumer goods. Several studies have found similar rheologic behavior between pitch thermoplastic melts and characterized pitch as a thermoplastic.100,101 The studies have successfully applied viscosity models for polymer melts to pitch melts, such as the William-Landel-Ferry Equation (Equation 24).

Compositionally, polymer and pitch share a number of characteristics such as elemental composition, and molecular weight distributions. From an elemental standpoint, both are macro-organic molecules primarily composed of carbon and hydrogen with other secondary atoms (N, O, S, etc.) incorporated to a lesser extent. In polymers the secondary atoms are often part of the base monomer, where as in pitch, the distribution of these secondary atoms is in a more random arrangement.

The arrangement of the atoms is fairly different between the two with the organic molecules in pitch being more aromatic or globular in structure whereas in polymers the arrangement is more linear or chainlike in nature. Additionally, the average molecular weight of pitch is in the range of 100's-1000's Da whereas that of various polymers is 1000's-1,000,000's Da.[102] In the melt, primary interactions between molecules for the pitch and polymer vary but have similar overall results. Polymers molecules, due to their extremely long length-to-width ratio tend to become entangled with each other. Pitches do not have the same length to width ratio and consequently entanglement of pitch molecules is of less influence than other interactions. Both experience Van der Waals interactions and some hydrogen bonding can occur if polar functional groups are present in the molecular structure.

Despite the variation of dominant interaction between the molecules, many of the measurable physical properties, such as the glass transition temperature, T_g, and rheology are similar. An important physical property in polymer processing is the, T_g. Due to molecular weight distribution there is no defined melting, but rather a change from solid to rubbery then to liquid state. The rheology of pitches and polymers are extremely similar, experiencing shear thinning character in comparable shear fields.

One current application that utilizes the thermoplastic character of pitch is for carbon and graphite fiber production. The distinguishing difference between carbon fiber and graphite fiber is that the former is composed of 90 % or greater carbon, while the later is 99 % or greater carbon.

It should be noted that carbon fibers can be produced from polyarcrylonitrile (PAN), rayon, and pitch. Fibers from the first two are produced by standard synthetic textile methods (i.e. melt spinning, or solution spinning). Pitch-based fibers can be produced by both methods, but are usually produced by melt spinning. The properties of the fiber vary according to the base starting material and treatment. Generally, pitch-based fibers have higher stiffness and thermal conductivity than PAN-based fibers.[103]

Melt spinning fibers usually requires a melt viscosity of between 100 to 2000 poise.[104] To achieve this viscosity range, the pitch is heated above its Mettler Softening point and is forced through a spinneret and drawn onto a spindle. This process often involves extruders to produce

the required pressure to force the melt through the spinneret. A process diagram for general carbon fiber production from pitch is shown in Figure 51.

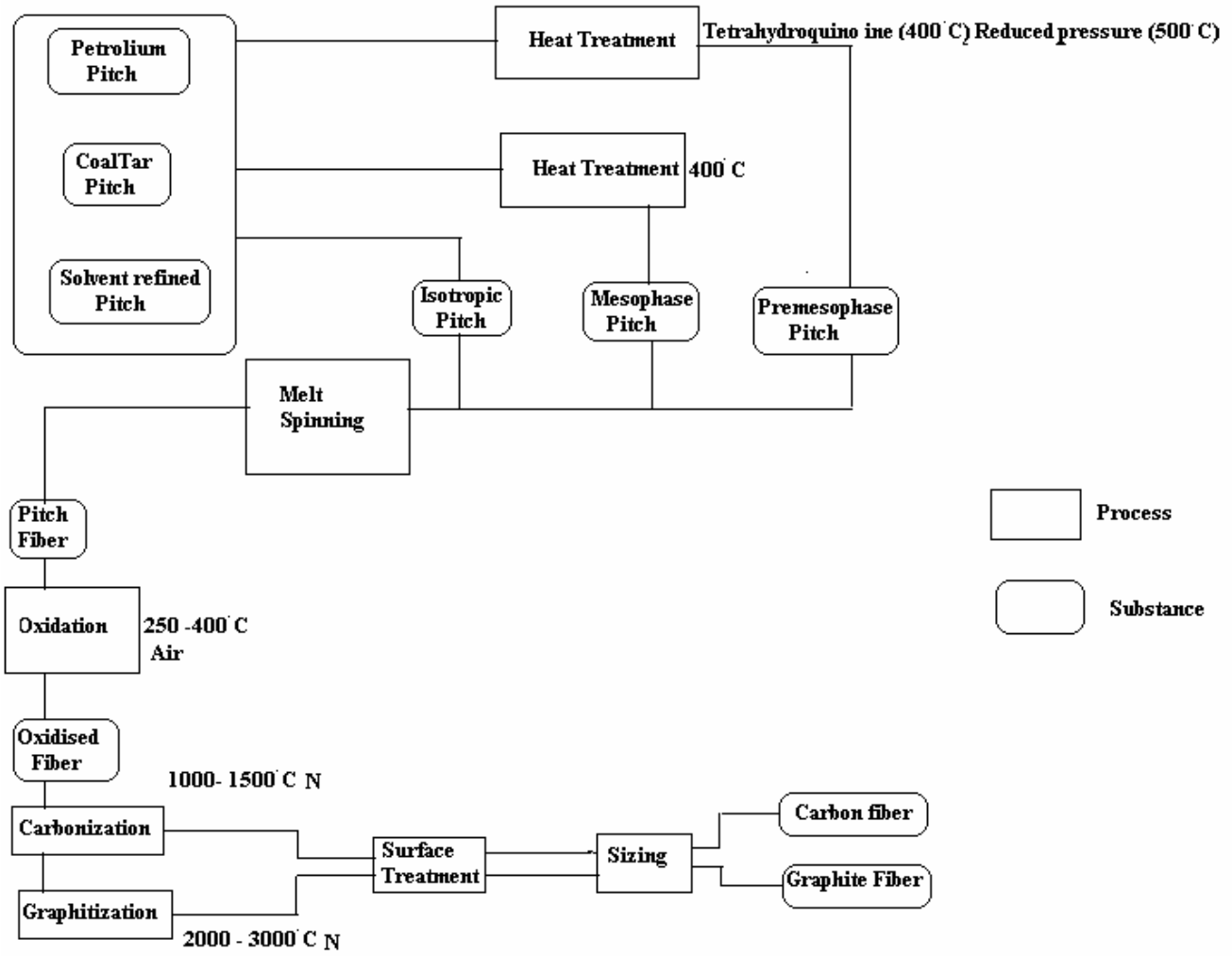

Figure 51. Manufacturing process schematic for pitch-based carbon fibers, for oxidation and graphitization processes, N stands for inert atmosphere (nitrogen). [105]

2.3.3 Experimental

Experimental objectives were first to determine if pitch foam can be produced by use of physical blowing agents, in a manner similar to polymeric foams, and second to determine if pitch foams follow the same general trends in process conditions that are formed for polymeric foams; and third to show that pitch foam could be extruded.

The evaluation of the first objective was a simple proof of concept experiment to see if foaming of pitch in this manner is possible. The design of this experiment was to construct a small pressure vessel, load it with a low softening point pitch, pressurize with inert gas and heat the vessel, then rapidly release the pressure and examine the pitch for cells.

Upon proof of the first objective, the second objective was to evaluate how the variables for pitch production compare to those for polymer foams. This involved evaluation of some of the pitch properties (viscosity, heat capacity, gas solubility, etc.) in comparison to various polymers and then comparing pitch to foamed polymers. From the review of polymer foaming theory, three significant and easily assessable variables were selected and these are temperature, initial pressure and pressure drop rate. This was done with a batch foaming method similar to that preformed by Maio et al.[106] carbon dioxide, nitrogen, and water were selected for consideration as blowing agents.

The temperature is a significant controller for viscosity of pitches and polymers. From polymer foaming theory, the viscosity influences the cell size and cell number density of the foam. By varying the temperature, and thus controlling the viscosity while maintaining constant saturation pressure and pressure drop rate, the general effect of viscosity can be observed and compared. The temperature was varied so that a suitable viscosity range for foaming could be determined and carried out using the 110 °C softening point pitch. This data were then used to achieve a similar viscosity range for the 180 °C softening point pitch.

The initial pressure influences the equilibrium concentration of blowing agent in the melt. From Henry's Law, the concentration of gas dissolved increases proportionately with increasing pressure. By controlling the initial pressure, and thereby controlling the concentration of blowing agent in the melt, the effect of concentration can be observed while holding the temperature and pressure drop rate constant. These experiments were conducted with the 180 °C softening point pitch.

The pressure let down rate is the third variable to be examined. High pressure drop rates in polymer foam, thermodynamically favor new cell nucleation rather than cell growth by diffusion. The pressure drop rate experiments were conducted with the 180 °C softening point pitch.

The experimental tests listed above were conducted using CO_2 as the blowing agent for consistent results. Additionally, N_2 and water were tested as blowing agents in comparison to CO_2 as possible alternate blowing agents.

The size of the pressure vessel was sufficient to accommodate four samples simultaneously. This allows the production of four samples under identical experimental conditions. Thus variations of pitch and foaming additives can be observed. This feature was utilized while observing the effect of talc addition, a nucleating agent in polymeric foam production, to the pitch. A pure pitch sample together with three other samples containing talc mass fractions from 0.2wt % up to 10wt % were foamed simultaneously and examined.

An experimental batch extrusion apparatus was also constructed. The purpose was to show that foaming could be extended to a continuous process with standard foam extrusion equipment. The 110 °C softening point pitch was used in the batch extrusion experimentation.

The pitches selected for testing were a 110 °C softening point and 180 °C softening point coal tar pitch, both supplied by Koppers Industries Inc. The 110 °C pitch arrived as approximately ¾ inch by 1-2 inch cylindrical pellets. The 180 °C pitch arrived as a solid mass in a 5 gallon canister. The pitches were stored under normal atmosphere in a cold room at ~60°F till ground for use.

The 110 °C softening point pitch was ground with dry ice to between 50-60 U.S. mesh size (250- 300µm). The dry ice was used to prevent heat from accumulating in the grinding process, softening the pitch and leading to fowling of the equipment. Once ground, the pitch was stored at ambient conditions till used (less than 1 week).

The 180 °C softening point pitch was ground to a slightly larger mesh size range 40-60 (250-420µm) in the same manner as the 110 °C SP pitch without the addition of dry ice. Once ground, the pitch was stored at ambient conditions till used (less than 1 week).

The heat capacity, glass transition temperature, particulate content, and density of the pitches were experimentally determined. These parameters are significant in describing the rheologic, nucleation and surface tension characteristics which in turn are significant in foam formation for polymers.

Proximate analysis is a test commonly used to determine the amounts of moisture, volatiles, mineral ash, and fixed carbon content of organic materials.[107] The motivation for this test is to determine the solid mineral ash content, which if present, could act as a nucleating agent similar to that of talc or silicate in polymers.

The proximate analysis of the samples preformed in-house on a Flash EA 1112 instrument, manufactured by ThermoQuest. Three representative samples for each pitch were analyzed and the mean average taken. Results are listed on Table 5.

Table 5. Mean average proximate analysis of pitches, weight percent.

Mass Fraction	Fixed Carbon wt %	Moisture wt %	Volatile wt %	Ash wt %
110 °C SP Pitch	54.29±0.12	0.44±0.33	45.23±0.21	0.04±0.07
180 °C SP Pitch	67.84±0.09	0.19±0.26	31.80±0.15	0.17±0.01

Differential scanning calorimetry (DSC) can be used to measure a number of characteristic parameters of a sample. Using this technique it is possible to observe fusion, crystallization, and glass transition temperatures. It is also possible to obtain absolute heat capacity with the aid of a known reference. The purpose of using DCS is to determine the glass transition temperature, verify the Mettler Softening point/glass transition temperture correlation, and to determine the heat capacity of the pitch.

The glass transition temperature and absolute heat capacity were tested on a TA Instruments Q100 Differential Scanning Calorimeter using helium at 25.0ml/min. For the absolute heat capacity, the DSC was calibrated with a sapphire calibration sample supplied by TA Instruments. Sample were prepared, annealed and tested according to the operating manual for the Q100. Results for the heat capacity and T_g are listed in Table 6. Representative plots of DSC heat flow curves for 110 °C softening point coal tar pitch showing T_g and melting point are in Figures 52 and 53.

Table 6. Properties of Koppers Industries Inc. Coal Tar Pitch.

Koppers Industries Inc. Coal Tar Pitch	110°C	180°C
Mettle Softening Point (°C)	111.0	176.4
T_g from DSC (°C)	49.7±2	Not Measured
T_g from Barr et al. Correlation (°C)	49.5±7.7	104.7±9.0
Density (g/cm^3)	1.18	1.32
Abs. Heat Capacity at T_g (J/g°C)	1.26	Not Measured
Surface Tension (dynes/cm)	35.7±3.1	55.9±4.9

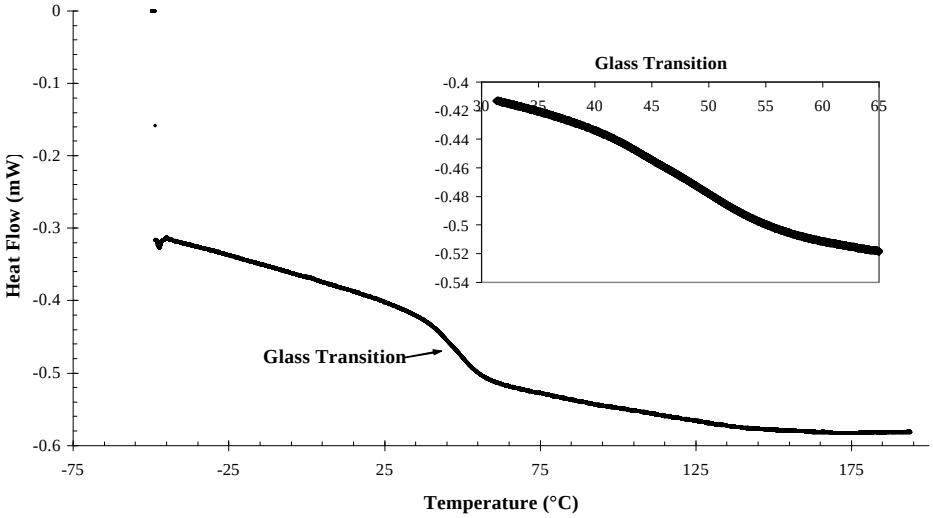

Figure 52. DSC of 110 °C softening point pitch displaying the glass transition.

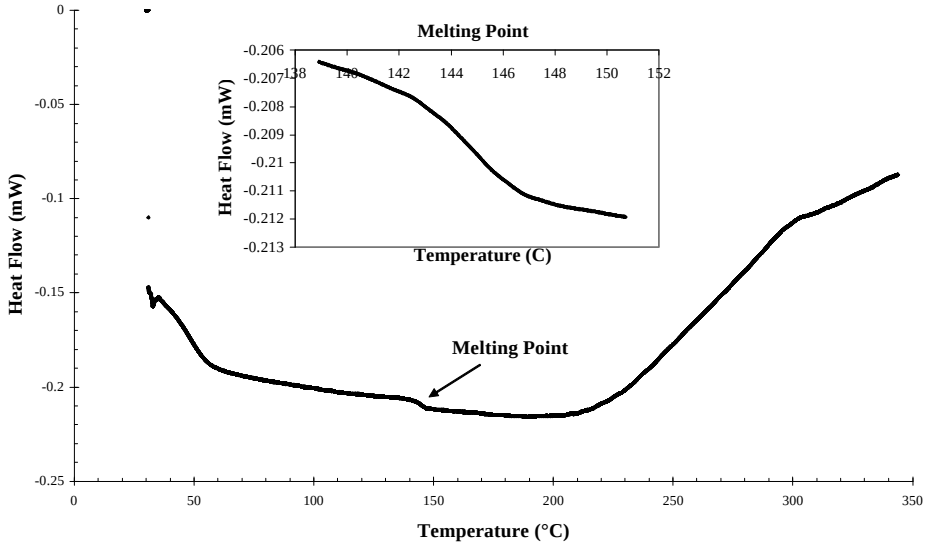

Figure 53. DSC of 110 °C softening point pitch displaying the melting point.

The Mettler softening point is a standard characterization technique for pitches and some other glassy materials. The purpose of this test is to verify the softening point of the pitch as well as to use it in a correlation for the glass transitions temperature.

The pitches were reported to have a Mettler Softening point of ~110 °C and ~180 °C respectively by Koppers Industries Inc. This was verified by use of a Mettler Toledo FP80 controller with FP83 dropping point/softening point measuring cell. Samples for the Mettler Softening point were first annealed and then heated at 2 °C/min in accordance to procedures outline in the unit's operation manual and ASTM D3104-99 (2005).[108] The correlation of Barr et al. was then used to calculate a T_g of 104 °C for the 180 °C softening point pitch and 49 °C for the 110 °C softening point pitch. The Barr et al. correlation was used rather than that of Khandare because, upon attempting to air stabilize the 180 °C softening point pitch at 110 °C, the foam matrix experienced relaxation below the T_g predicted by Khandare. There was good agreement between the Barr et al. correlation and that determined from DSC.

The mass loss during the foaming operation is of interest in determining the mechanism for blowing the foam. Current coal and pitch foaming utilize the inherent volatile mater in the pitch or coal as a blowing agent. This project is seeking to show that the use of soluble gases can produce the same effect with better control. Additionally foam making may be possible for pitch with little or no volatile content.

The mass of the samples and molds were measured and recorded by a Denver Instrument M-310 electronic balance before and after foaming to check the mass loss of the pitch.

The bulk density of the foam is one of the three main foam characteristics, the other two being cell size and cell number density. Consistent control of the bulk density is the one of the primary goals in foam production. The densities of the solid pitches were measured by a volumetric method. The mass of the pitch and volume of distilled water displaced by the pitch in a graduated cylinder for representative samples were recorded. The values listed on Table 6 are the mean average of three samples for the pitches used in this study. The bulk densities of the foam were determined by measuring the dimensions of the sample and calculating its volume. The mass of the foam was recorded by Denver Instrument M-310 electronic balance and divided by the calculated volume to give bulk density. The bulk densities thus determined are approximate as the samples are irregular in shape.

Due to the difficultly in measurement and lack of test equipment, a correlation for surface tension was sought that used readily measurable quantities. D.K.H. Briggs developed a correlation between surface tension and density for coal tar pitch using a modified Macleod's Equation (Equation 27).[109] Briggs found that the surface tension could be calculated to ±8.8 % with a 95 % confidence level for a variety of pitches for a temperature range from 120-220 °C. Using the Briggs correlation, the surface tension for the pitches was calculated and is also listed on Table 6.

$$g = 18.4 r^4 \quad . \text{ (Equation 27)}$$

It was assumed that equilibrium concentrations of CO_2 and N_2 had only slight impact on the surface tension at elevated pressures. This assumption is based on the effect that CO_2 only reduces the surface tension by one order of magnitude for polystyrene at 4500 psia[110] which is well above experimental conditions. A similar reduction of approximately 1 order of magnitude of surface tension is seen for other polymers under similar conditions. Assuming a linear

relationship between pressure induced solubility and surface tension reduction, the reduction of surface tension per 500 psi would be ~2.8 dynes/cm, which is within the initial error for the surface tension of the Briggs correlation at ambient conditions. Additionally, the solubility of CO_2 below the critical pressure is much lower than above the critical pressure (critical pressure of CO_2 1070 psia).

To produce foam, the matrix material must have some melt stability to maintain the cell structure till the bulk material is stabilized. Viscosity is one of the primary means of controlling melt stability. The apparent viscosity of the 110 °C pitch was tested using a Brookfield DV-III Ultra programmable rheometer with a Themocell™ controller and Rheocalc® (ver. 1.3) control software using spindle SC-4 for low viscosity ranges. A Bohlin Instruments Rosand RH2000 capillary rheometer with a 1x16mm capillary was used for the 180 °C SP pitch and for higher viscosity for the 110 °C pitch. Figure 54 shows viscosity curves for 180 °C SP pitch at three different temperatures which clearly demonstrate non-Newtonian behavior.

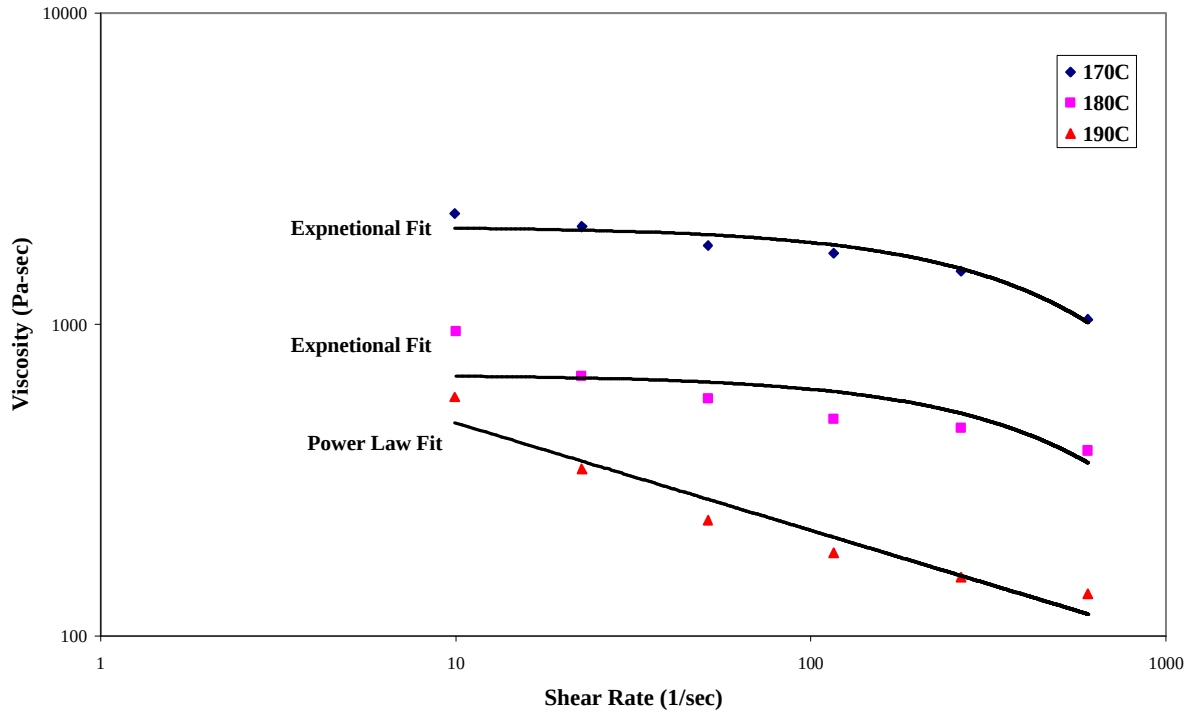

Figure 54. Viscosity curves for 180 °C Softening Point Coal Tar Pitch at 170 °C, 180 °C, and 190 °C.

From the data viscosity at constant shear rate, the constants for the WFL equation (Equation 24) were fitted using Oakdale Engineering's DataFit (version 6.1.10) software. The calculated constants at a shear rate of $10sec^{-1}$ are listed on Table 7. The larger error for the 110 °C pitch is due to variation in the sample data obtained from the Brookfield spindle rheometer which is better suited to low viscosity fluids as apposed to viscous pitches. Figure 55 and Figure 56 show the fits of the data to the WFL model.

Table 7. William-Ferry-Landel Equation constants and error.

	c_1	c_2
110 °C	2.54±1.14	93.3±24.8
180 °C	1.92±0.26	42.9±4.4

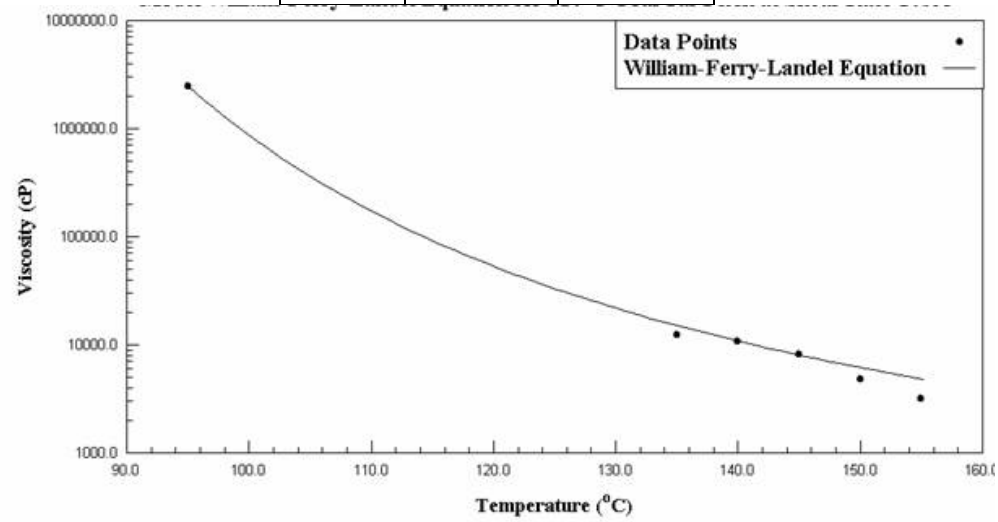

Figure 55. William-Landel-Ferry fit of a 110 °C softening point coal tar pitch at a shear rate of 10sec^{-1} fitted by Oakdale Engineering DataFit version 6.1.10.

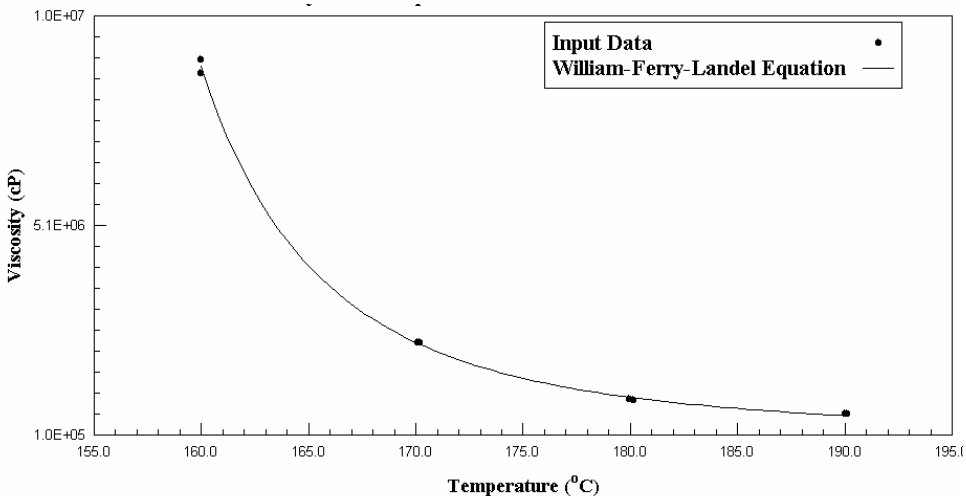

Figure 56. William-Landel-Ferry fit of a 180 °C softening point coal tar pitch at a shear rate of 10sec^{-1} fitted by Oakdale Engineering DataFit version 6.1.10.

Carbon dioxide, nitrogen, and water where selected as blowing agents. Both the CO_2 and N_2 were industrial grade, provided by Airgas Inc. and were used as received. Distilled water was produced by an in-house distillation water system. All experiments to evaluate the effects of temperature, pressure and pressure drop rate were carried out using CO_2 as the blowing agent due to its higher solubility in polymers than N_2. Additionally, the diffusivity for CO_2 is generally lower in most materials than N_2 which is partly due the larger size of the CO_2 molecule. N_2 and

water were tested to see if the process could be repeated for physical blowing agents. Properties of the gases and water are listed in Table 8.

Table 8. Properties of Blowing Agents at 1atm., gas densities are for 20 °C.

Gas	Mol. Wt.	Melting Point (°C)	Boiling Point (°C@1atm)	Vapor Press. at 20°C (psia)	Gas Desn. (g/ml)	Crit. Temp. (°C)	Crit. Press. (psia)
Carbon Dioxide, CO_2	44.01	-56.6	-78.4	844.7	0.0022	31	1070
Nitrogen, N_2	28.01	-214.9	-195.8	N/A	0.0012	-146.9	34
Water, H_2O	18.02	0.00	100.0	17.5	N/A	374.2	218.3

The solubility of gases in pitch varies as a function of composition of the pitch, temperature and pressure. As such, the solubility of blowing agents was not directly measured but a general mass fraction range of CO_2 solubility for heavy petroleum fractions and bitumens was compiled (Table 9). Due to the scope of this research, the solubility of CO_2 in coal tar pitch was assumed to be similar to that of other heavy petroleum products and bitumens[111,112,113] of which pitch is a subcategory. By comparison to other bitumens and heavy petroleum crude at comparable conditions, the weight percent was estimated to be approximately 0.7-0.8wt % at 200 psi and 100 °C. The mass fraction is assumed to be essentially 0 at standard temperature and pressure. This assumption was made due to the low CO_2 concentration (<0.1wt %) naturally present in the atmosphere and linear relationship of Henry's law between solubility and pressure. For bitumens, the linear relationship yields a mass fraction of ~0.05wt % under an atmosphere of pure CO_2 atmosphere at 14.7 psia.

Table 9. Mass fractions CO_2 in select heavy petroleum fractions and bitumens.[114,115,116]

Athabasca Bitumen			Tar Sand Triangle Bitumen			PR Spring Rainbow I Bitumen		
Temp. (°C)	Pressure (psi)	Percent Weight (wt%)	Temp. (°C)	Pressure (psi)	Mass Fraction (wt%)	Temp. (°C)	Pressure (psi)	Percent Weight (wt%)
27C	100	0.31	27C	100	0.44	27C	100	0.36
27C	894	3.62	27C	803	3.19	27C	803	3.18
100C	100	0.28	100C	100	0.36	100C	100	0.43
100C	894	3.37	100C	803	2.94	100C	803	3.02
Inturp. (100C)	200.00	0.72	Inturp. (100C)	200.00	0.73	Inturp (100C)	200.00	0.8
WCLP Fraction			Exxon B Cut 4					
103C	83.5	0.46	200C	109	0.19			
103C	256.3	1.62	200C	265	1.16			
275C	117.6	0.36	298C	102	0.37			
275C	247.0	0.80	298C	264	1.00			
Interp. (200C)	200.0	0.78	Interp. (200C)	200	0.75			

The reduction of T_g due to diluents can be estimated from the Chow Correlation (Equation 25). The reduction in T_g was calculated from the experimental data for the heat capacity and glass transition of the pure pitch (Table 6), and the properties of the blowing agent (Table 8). The repeat molecular weight unit of the pitch, M_p, and lattice constant, z, were assumed to be 81 Daltons and 1 respectively due to the cyclic and aromatic structure of pitch. Normally a value for z is set to 1 or 2 only cause a slight variation in results. The reductions of the T_g due to CO_2 and N_2 diluted pitch systems were calculated and are shown on Table 10.

Table 10. Reduction of glass transition temperature predicted by Chow Correlation.

	Weight Percent of Diluent (wt%)								
	0	0.25	0.5	1.0	2.0	3.0	5.0	10	15
CO_2									
110°C Softening Point Pitch T_g (°K)	323.0	322.7	322.5	322.0	321.0	320.0	318.0	313.1	308.7
180°C Softening Point Pitch T_g (°K)	377.0	376.7	376.4	375.8	374.6	373.5	371.1	365.4	360.3
N_2									
110°C Softening Point Pitch T_g (°K)	377.0	376.5	376.1	375.1	373.3	371.5	368.1	360.4	355.1
180°C Softening Point Pitch T_g (°K)	323.0	322.6	322.2	321.4	319.9	318.3	315.4	308.8	304.2

As can be seen from Table 10, the reduction of T_g decreases only about 1 °C for a CO_2 diluent weight percent of 1.0wt % which is about the equilibrium concentration at the experimental temperature and pressure conditions employed in this work.

Sample preparation for pure ground pitch and samples containing talc are as follows. Approximately 25g of coal tar pitch was weighed into a beaker. An amount of talc was added to the pitch and was varied from 0 to 10 % by weight. The contents of the beaker where transferred to a plastic bag and tumble mixed to provide uniform talc distribution. The pitch/talc mixtures

were placed in 250ml beakers lined with aluminum foil (Figure 57). The foil lining was to aid in removal of the foam samples without damage to the beakers. Sample beakers were placed in a high-temperature pressure vessel (Figure 58) which was then sealed. The pressure vessel was placed in a Paragon TnF-82-3 kiln equipped with a DTC 1000 temperature controller. High-pressure gas fittings were connected to the vessel and the vessel was pressurized with CO_2 to a predetermined pressure. The vessel was then heated to a predetermined temperature at a heating rate of 5 °C/min and held at temperature for 2 hours. Thermal equilibrium was assumed to be reached at the end of the 2 hours. It is unknown if the gas concentration in the melt reached equilibrium concentrations, but the equilibrium concentrations from other heavy petroleum fractions and bitumens provide an upper concentration limit for the pitch. Upon completion of thermal saturation period, the pressure was quickly released via a needle valve in the exit line. The pressure drop rate to atmospheric pressure was varied between 9 and 28psi/sec (62 to 193 kPa/sec) depending upon test conditions. The pressure vessel was removed hot from the kiln and the samples were removed from the vessel as quickly as possible to increase cooling of the samples. Upon solidifying, the samples were removed from the foil-lined beakers for examination and testing.

To test if N_2 was sufficiently soluble to produce foam, the same process as outlined above was repeated, except that N_2 was substituted for CO_2 to pressurize the vessel. To test the possible synergism of water as a blowing agent, liquid water was added to the ground pitch and blended. The pitch/water mixture was placed in the pressure vessel as above and the vessel was pressurized with CO_2 to maintain the water in liquid form until the pressure drop was performed. These samples were then compared to samples prepared using CO_2 alone as the blowing agent.

Figure 57. Batch sample molds.

Figure 58. High temperature pressure vessel.

An apparatus was constructed to test the applicability of pitch foam production by an extrusion process. The apparatus consisted of 1-inch OD stainless-steel tube equipped with pressure fittings and wrapped in heating tape (Figure 59). The apparatus was loaded with between 30-50 grams of pitch and sealed. The apparatus was then pressurized with the desired gas and heated to a predetermined temperature (70-155 °C for 110 °C softening point pitch). The temperature was then held for 30 minutes to allow for thermal equilibrium and gas dissolution. After thirty minutes, a ball valve located at the bottom of the apparatus was opened and the pitch forced out to the atmosphere by the back pressure of the system. This results in near instantaneous pressure release and foam formation. Higher pressures and temperatures were used for this process in comparison to the batch process due to the pressure and lower viscosity needed to force the pitch out of the valve.

Figure 59. Experimental batch extrusion apparatus.

Air stabilization is a process of heating pitch fiber or foam in the presence of oxygen to promote cross-linking and evaporation of volatiles in the pitch thereby increasing the insoluble content, and increasing its softening point and T_g. The hydrogen-to-carbon ratio (H/C) can be used as an indicator of the degree of stabilization.[117] Usually, the stabilization process is continued till softening does not occur before the T_g. Once this occurs, other thermal processes can be carried out without concern of the fibers or foam melting.

Air stabilization was attempted on some of the 180 °C softening point pitch samples. This involved placing the foam samples in an oven at 110 °C for 18 hours, then at 125 °C for 24 hours. No stabilization was attempted on the 110 °C softening point pitch samples due to their low T_g (~50 °C).

One of the driving factors in developing materials is to improve performance per some key variable (i.e. cost, weight, strength, etc.). For foam, some of the important mechanical performance parameters are compressive modulus and strength which relate to how much energy the foam can receive without damage and how much energy can be absorbed by the material and cell structure under impact.

Multiple circular samples were taken from parent samples of foam using a carbide-tipped hole saw with approximately 1inch interior diameter. The top and bottle of the compression

samples are planed flat with and parallel with a carbide-tipped band saw to even the two surfaces. An Instron table-top load frame Model 5869 with a 50kN load cell was used to obtain compressive modulus and strength of some of the pitch foam samples. Currently, there is no standard test method for measuring foam compressive modulus and strength of carbon and pitch foams, therefore the method developed by Carpenter is employed.[118] Data obtained on the foam made in this work are compared with other carbon foams tested by the same method. They are also compared to properties reported by Koppers Industries Inc. and Touchstone Research Laboratory Ltd. for their KFOAM™ and CFOAM® carbon foam products.

2.3.4 Pitch Foam Results

The properties of pitch are in many ways comparable to the properties of polymers (Table 11). One of the significant differences is the presence of volatile content in the pitch. The volatile content does not have a comparison in polymers, but does not seem to affect the processing techniques. The high volatile content is of concern in stabilizing the pitch foam. The pitch also has higher heat capacity than the common polymers listed in Table 11. The higher heat capacity should not affect the processing techniques other than increasing the heat input needed to reach proper processing temperature.

Table 11. Comparison of the two coal tar pitches with some common polymers.[119]

	Pitch 110 S.P.	Pitch 180 S.P.	PVC	PS	PC	PET	PMMA
Density (g/cm^3)	1.18	1.32	1.36	1.05	1.2	1.33	1.18
T_g (°C)	49	104	75	100	148	74	105
? C_p (Cal./g°C)	0.30	Not measured	0.0693	0.0767	0.0585	0.0812	0.0746
M_p (g/mol)	81*	81*	62.5	104	254	192	100

*** assumed repeat unit of pitch from aromatic structure.**

It is documented in the polymer literature that CO_2 and other gases cause a plasticizing effect on polymer melts. Using the same method for calculating the reduction of T_g in polymers, via the Chow correlation, Equation 25, it as shown that the reduction of T_g due to dissolution of CO_2 in pitch under experimental conditions of the present work was approximately 1 °C (Table 10). From the calculations, the plasticization effect due to N_2 was about double that of CO_2 due to its lower molecular weight thought N_2 is less soluble in most polymers. N_2 solubility in polymers is usually about one order of magnitude less than CO_2 under the same conditions. Information concerning the solubility of N_2 in pitch and other heavy organic fractions at elevated temperatures and pressures is basically nonexistent at this time. This lower solubility seen in polymers of N_2 may hold true for pitch as well. For the scope of this research, the plasticization effect of the soluble blowing agent is not significant until the weight percent is ~4 % or more. The general trend shown from the Chow correlation for the 110 °C softening point pitch is approximately a 1 °C reduction in T_g per 1wt % of CO_2 up to 10wt %, at which point the Chow correlation begins to breakdown due to the assumptions in the theory. A weight percent of 4wt %, or greater, may well occur if supercritical CO_2 is used due to superior solvent properties over gaseous CO_2, though the Chow equation may not be applicable for supercritical fluids.

The proximate analysis of the pitch showed measurable amounts of ash, water, and a significant volatile fraction, both of which could have an influence on cell formation. The ash

present in the pitch is likely to act as a nucleating agent similar to talc or other solid particles in polymer melts. The quantities of ash were of the same order of magnitude as most of the talc concentrations added to the pitch. In examination of the samples, no distinguishable difference in cell size or density was detected until the talc mass fraction was greater than one order of magnitude the mass fraction of ash present in the pitch (Figure 62). Normally, a significant difference is not expected in the cell characteristics with the addition of nucleating until its mass fraction is greater than one order of magnitude.

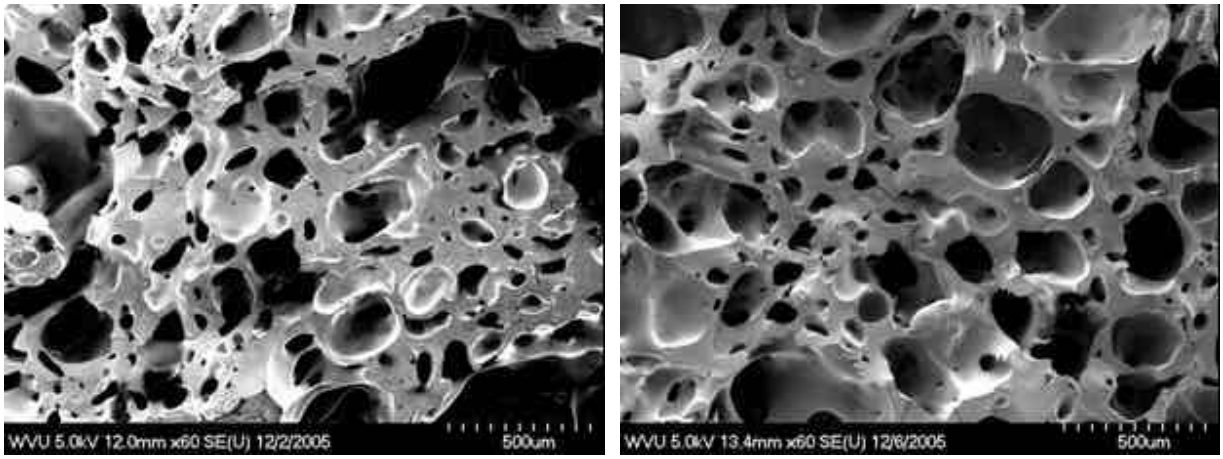

Figure 60. No distinguishable difference between pitch with and without talc for a talc concentration of the same order of magnitude as ash present in the pitch. 110 ℃ softening point pitch foam at 90 °C and 200 psig, Left: no talc, Right: 1.9wt % talc.

Upon removal of pitch foam samples from the pressure vessel, samples were first examined visually. All samples resembled hockey pucks. Most samples had a smooth polished surface. Samples containing high talc mass fraction had a powdery or dusty surface. Samples ranged in height from ~1/2 to 2 inches depending upon processing conditions. Upon cutting the samples, a majority of the cells appear closed with limited interconnection.

Mass measurements of the pitch sample before and after foaming showed an average mass loss of 0.2 % with standard deviation of 0.08 % per sample for the 180 ℃ softening point pitch. Thus, mass loss from the samples during the foaming processing of the samples was negligible. The mass loss is less than 1 % of the volatile content present in the pitch, whereas it is ~100 % of the moisture content present in the 180 °C softening point pitch before addition of any blowing agent addition or foam processing. The mass loss coupled with the large volatile fraction shown by proximate analysis raises the question as to where the mass which is lost is from, and if cell formation and growth maybe due to the mass loss.

Coal tar pitch volatiles are composed of polycyclic aromatic hydrocarbons, PAHs, which primarily consist of benzo(a)pyrene, anthracene, phenanthrene, pyrene, and carbazole. Of the five primary volatile components, only one has a melting point below 155 °C (phenanthrene) with a vapor pressure of 0.005 psia (Table 12), all of which are to low to evaporate under the experimental conditions. The process conditions are also too mild to facilitate cracking of the pitch and no other compounds were added that would evaporate during the heating process.

The vapor pressure of water on the other hand, is 83.7 psia at 155 °C (Table 12). The average mass fraction of water from proximate analysis was 0.19 % (Table 5), practically identical to the mass lost during foaming process.

Table 12. Coal tar pitch volatiles.[120]

Name	Boiling Point (°C)	Melting (°C)	155 °C Vapor Pressure (psia)
Benzo(a)pyrene	495	177	n/a
Anthracene	340	217	n/a
Phenanthrene	328-340	99	0.005
Pyrene	None listed	423	n/a
Carbazole	355	248	n/a
Water	100	0	83.7

The comparison of the temperatures of melting and vapor pressures between coal tar volatiles and water makes it likely that the mass loss is due to evaporation of the moisture at some point during processing, most likely during the final pressure drop to atmospheric pressure.

The minimum quantity of blowing agent need to account for the increase of bulk density change, assuming no diffusion, isothermal conditions, and no relaxation of the foam structure volume, can be calculated from Equation 27. For example, a sample 180 °C softening point pitch foamed at 155 °C, with a final density of 0.66 g/cm^3 (averages quantities for 180 °C pitch foam from all samples), a 97 % increase in volume per unit mass is seen over the starting pitch feedstock. The minimum mass of blowing agent needed per unit mass of pitch was calculated from fluid properties tables from National Institute of Standards and Technology for CO_2, N_2 and water assumed no loss of blowing agent and isothermal conditions are listed on Table 13. From Table 13, the mass fraction of CO_2 needed for the average bulk density reduction is 0.27wt %, which is about 2/5 the estimated equilibrium concentration (0.7-0.8wt %) of heavy petroleum fractions and bitumens at experimental conditions. For water, only a mass fraction of 0.10wt % is needed for the same bulk density reduction. It is highly possible that the moisture present in the pitch is at least partly responsible for cell formation in the pitch. This can be inferred from the significant change in bulk density produced above and below 100 °C for the 110 °C softening point pitch samples (Table 14).

$$\frac{\text{unit mass}}{r_s - r_f} = \text{Blowing Agent Volume Change} \qquad \text{(Equation 28)}$$

Table 13. Mass of blowing agent needed per mass of pitch.

	? Sp. Vol. (ml/g)	Minimum Mass of Blowing Agent/Mass Pitch (g/g)
CO_2 (ml/g)	727.545	0.0027
N_2 (ml/g)	1142.944	0.0017
Water (ml/g)	1932.905	0.0010

It should be noted that a number of samples in the higher temperature tests experienced coalescence of the cell in the center of the samples and formed large voids. This may be due to temperature gradient in the sample during removal, which cause the center of the sample to take longer for stabilization of the cell matrix. Physical jarring during removal coupled with the temperature gradient in the samples may be the cause of the structural collapse and void formation (Figure 61).

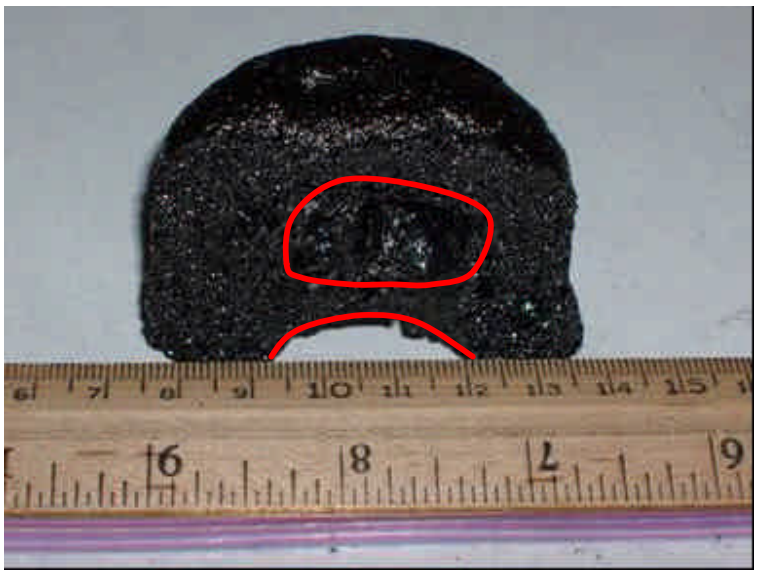

Figure 61. Voids were present in some of pitch foam samples, possibly due to shock during removal from kiln.

The properties of fluids vary but the equations governing the nucleation and growth of cells in fluids are essentially the same for all fluids. For viscous polymers, the effect of temperature, blowing agent concentration and pressure-drop rate on cell nucleation and growth behavior are fairly uniform. This uniformity of viscous polymer melts appears to hold for viscous pitch melts as well. Each of these effects are described below in detail.

As noted previously, temperature is the primary means of controlling viscosity of thermoplastic materials. From inspection of Equation 16 it is evident that viscosity hinders the growth of cells in melts, but aids in the melt stability. As is seen in Equations 10, 13, and 18, temperature also influences the nucleation and diffusion of cells through the exponential term. From Equations 10-13, the increased temperature aids in increasing the number of cells nucleated. In Equation 18, temperature increases the diffusion of the blowing agent thereby increasing cell growth and countering nucleation at lower blowing agent concentrations. With the competing mechanisms associated with increased temperature, generally what is normally seen with polymer foams is an increase in cell size and some reduction of cell number density. By comparing Figures 62 through 64, by increasing the temperature, thereby reducing the viscosity, it can be seen that cell size increases with reduced viscosity, just as is seen in polymer foaming practice.

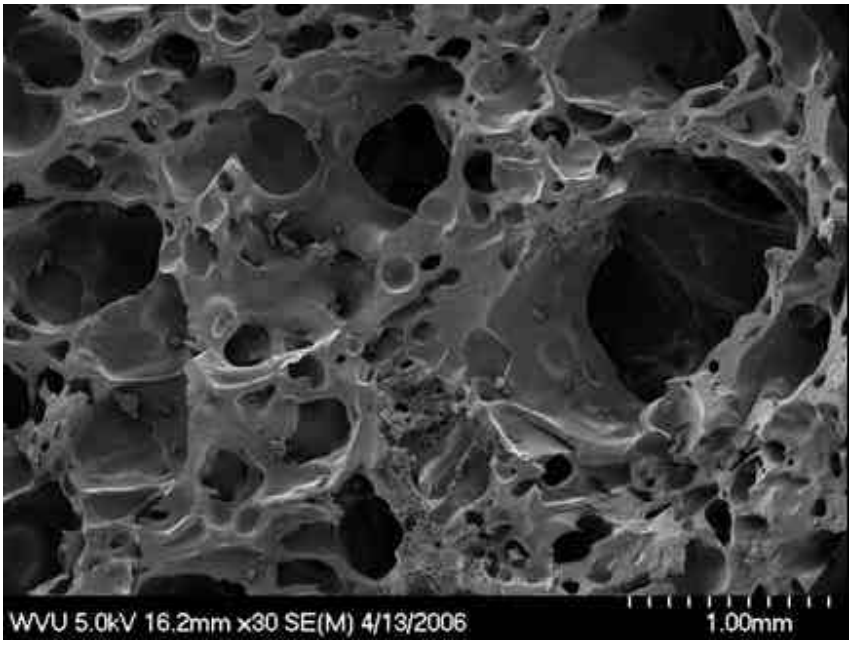

Figure 62. SEM of 110 °C SP pitch foam prepared at 95 °C and 200 psig of CO_2.

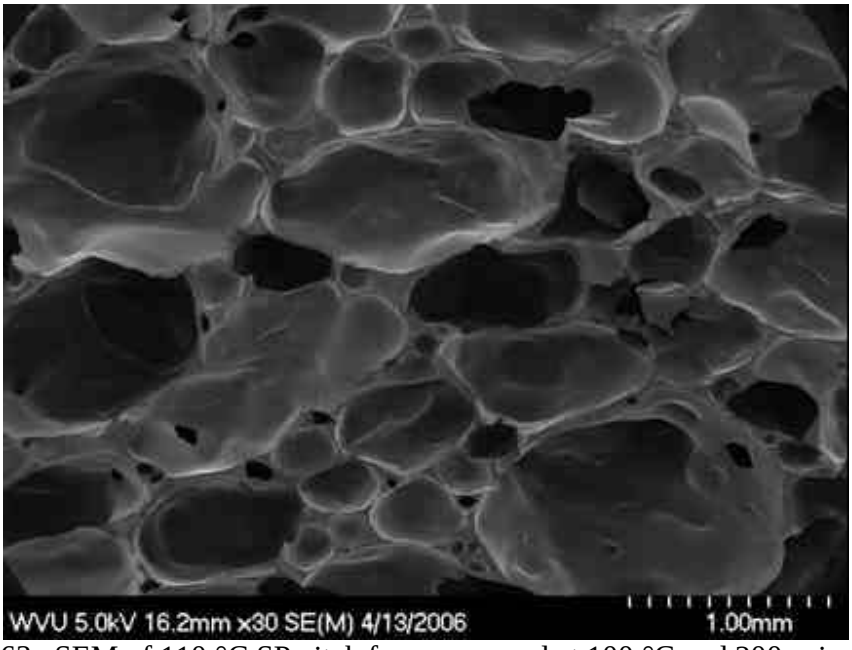

Figure 63. SEM of 110 °C SP pitch foam prepared at 100 °C and 200 psig of CO_2.

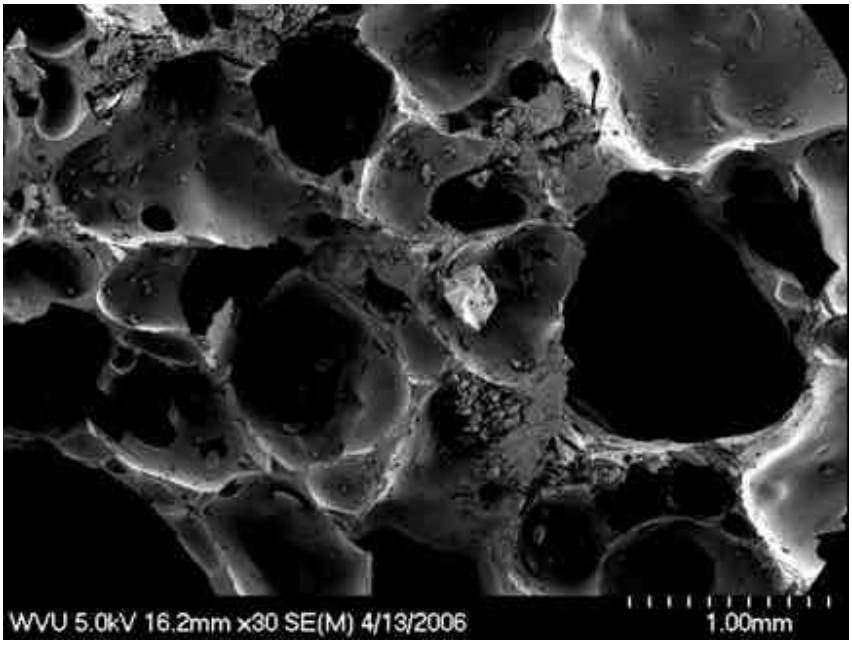

Figure 64. SEM of 110 °C SP pitch foam prepared at 105 °C and 200 psig of CO_2.

Table 14. Bulk density variation of samples at increasing temperature (decreasing viscosity) and cell size range of a 110 °C softening point pitch foamed under 200 psig of CO_2.

Temperature (°C)	Bulk Density (g/cm)	Cell Size (µm)
95°C	0.65±0.08	20-150
100°C	0.27±0.05	40-150
105°C	0.29±0.03	80-140

As noted, the pressure is related to blowing agent concentration in the melt by Henry's Law. From Henry's Law, increasing the gas pressure on a melt increases the equilibrium concentration of the blowing agent in the melt. From Equations 10, 13, 16, and 18, it can be seen that initial blowing agent concentration effects the nucleation and growth of cells. From polymer foaming practice, generally an increase in cell number density or cell size upon conditions within the melt is observed with increased blowing agent concentration.[121] Figure 64 through Figure 67 show an increase in cell density for the experimental conditions. It is interesting to note that variation of the initial pressure had little effect on the density of the samples (Table 15). This may be an artifact of the testing, or the change in blowing agent concentration is not significant enough to affect bulk density.

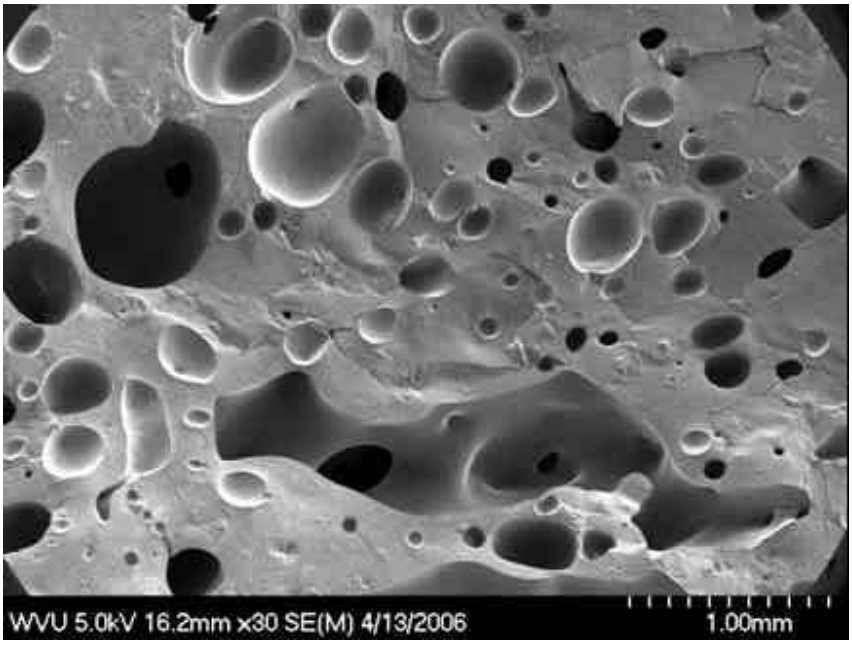

Figure 65. SEM of 180 °C SP pitch foam prepared at 155 °C and 80 psig of CO_2.

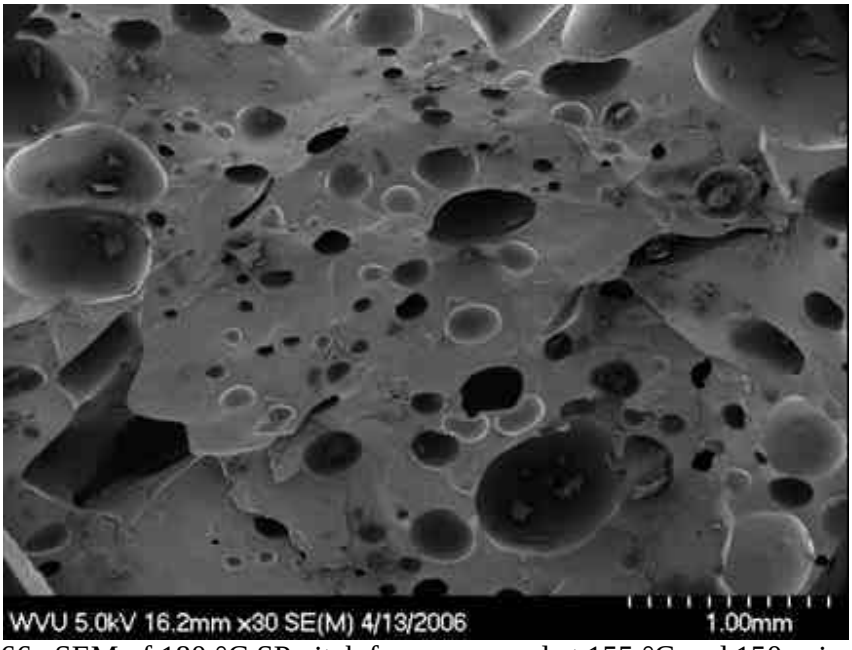

Figure 66. SEM of 180 °C SP pitch foam prepared at 155 °C and 150 psig of CO_2.

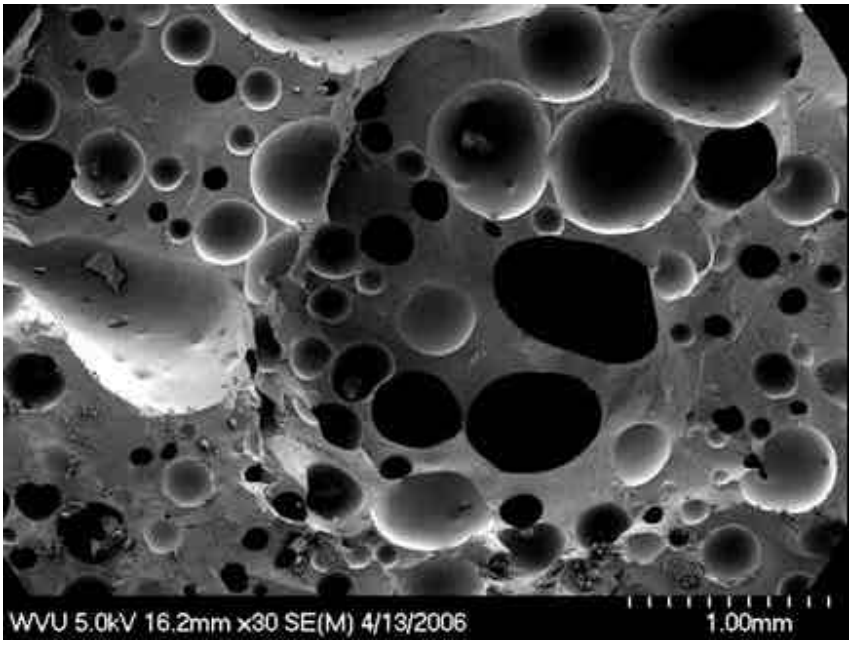

Figure 67. SEM of 180 °C SP pitch foam prepared at 155 °C and 220 psig of CO_2.

Table 15. Bulk density of samples and cell size range with increasing initial pressure of CO_2 of a 180 °C softening point pitch produced at 155 °C and ~16psi/sec pressure-drop rate.

Initial Pressure (psig)	Bulk Density (g/cm)	Cell Size (μm)
80	0.68±0.13	10-70
150	0.69±0.14	10-70
200	0.68±0.06	10-80

In processing of polymeric foams, melt blowing agent systems often undergo pressure-drop rate in the kpsi/sec range and higher. The pressure-drop rate in this examination is of two orders of magnitude less, but variation in cell structure is distinguishable as seen in Figure 68 through Figure 70. Equations 10 and 17 quantitatively show that additional nucleation is favored as opposed to growth of existing bubbles due to diffusion limits at high concentration gradients. The same general trend is seen with polymer processing; that is, with increasing pressure-drop rate, cell size decreases. A slight decrease in bulk density is seen with increased pressure drop rate (Table 16) which is probably due to lower blowing agent loss from the melt during expansion.

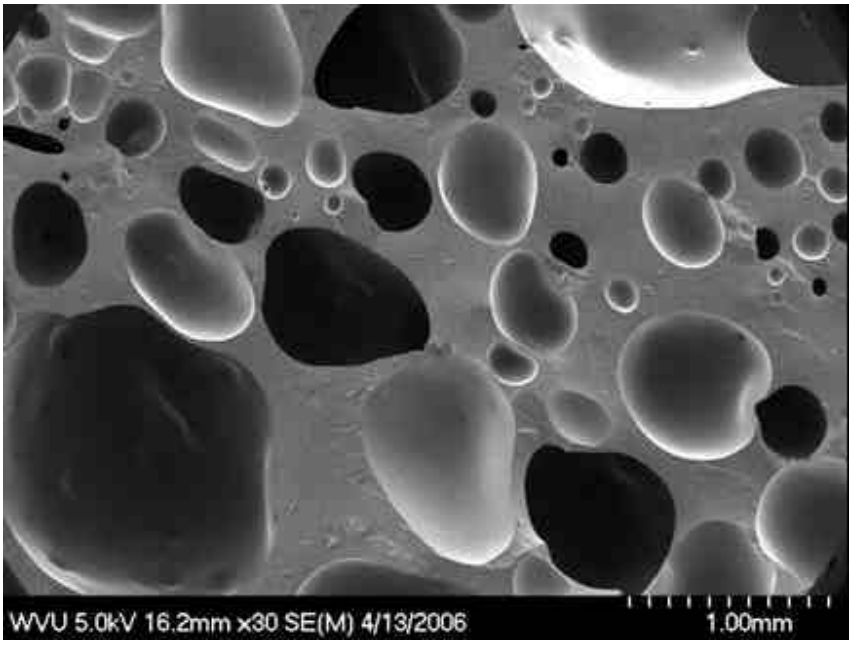

Figure 68. SEM of 180 °C SP pitch foam prepared at 155 °C, 220 psig of CO_2 and pressure drop rated of 8.1psi/sec.

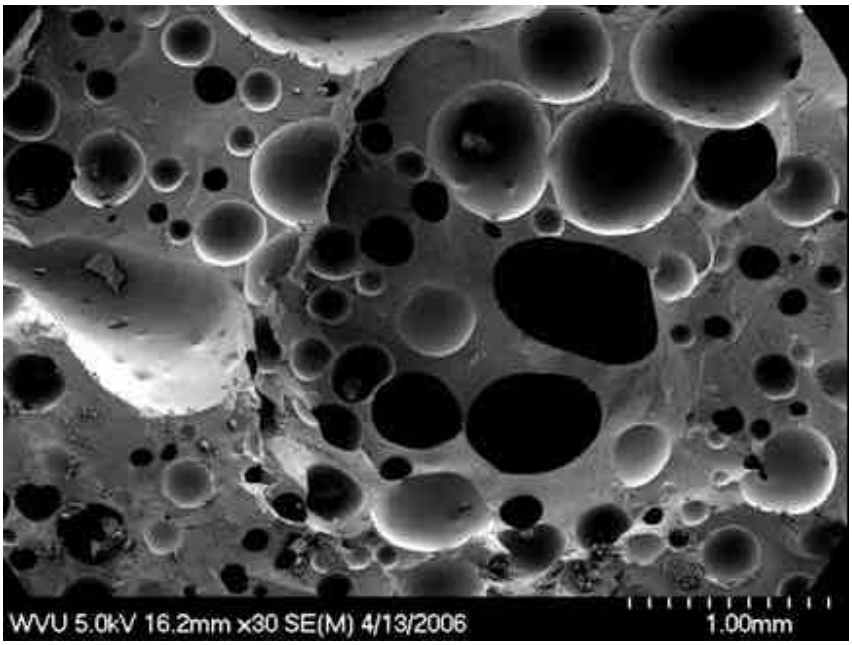

Figure 69. SEM of 180 °C SP pitch foam prepared at 155 °C, 220 psig of CO_2 and pressure drop rated of 13psi/sec.

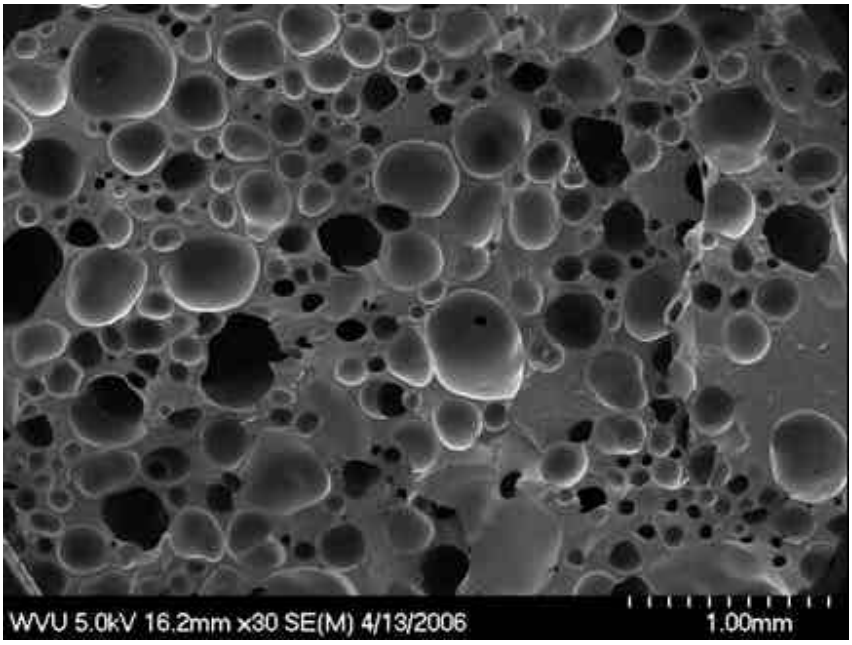

Figure 70. SEM of 180 °C SP pitch foam prepared at 155 °C, 200 psig of CO_2 and pressure drop rated of 15psi/sec.

Table 16. Bulk density variation with pressure drop rate for a 180 °C softening point pitch produced at 155 °C and 200 psig of CO_2.

dP/dt (psi/sec)	Bulk Density (g/cm)	Cell Size (μm)
8.1	0.73±0.12	20-160
13.7	0.64±0.07	10-90
15.0	0.68±0.04	10-50

The addition of H_2O and N_2 were examined to see if they were capable of producing cell formation in pitch. It was found that use of both produced cells in the pitch. As mentioned, moisture present in the pitch may be party responsible for cell formation. The samples produced with N_2 as the blowing agent have smaller cells with higher number density than foam produced with CO_2 under the similar conditions (200 psig, 90 °C for N_2 and 95 °C for CO_2, and ~15psi/sec using a 110 °C softening point pitch, Figure 71 & Figure 72). It is unclear if the cell size and density differences are due to blowing agent concentration, diffusion difference between the blowing agents or some other factor. For the sample containing water, CO_2 was used as to keep the water in the liquid phase until the pressure-drop. The samples processed with CO_2 and water had a larger cell size in comparison to the samples that just used CO_2 as the blowing agent under the similar processing conditions (Figure 73 and Figure 74).

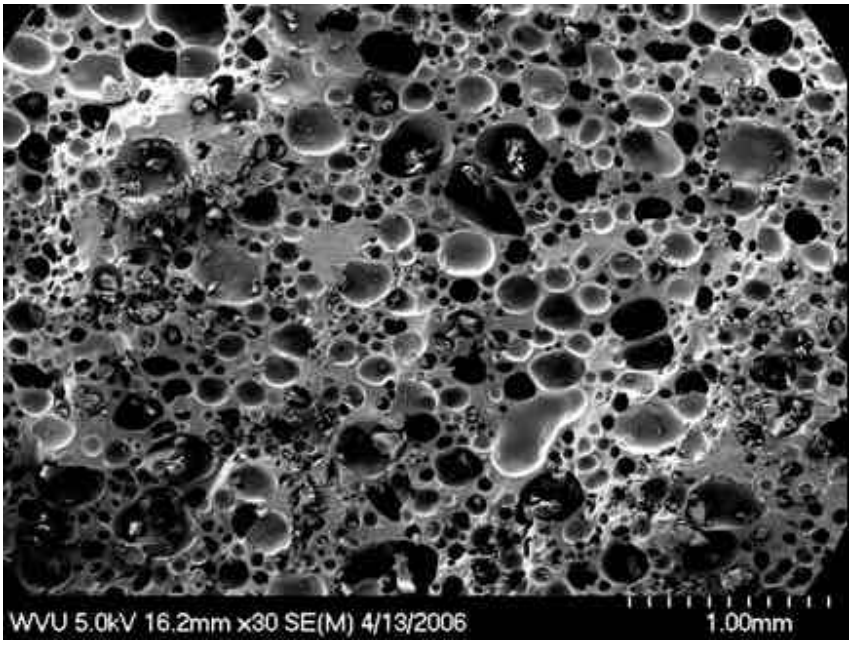

Figure 71. SEM of 110 °C softening point pitch foam produced at 90 °C, dP/dt of 20 psi/sec, and 200 psig N_2.

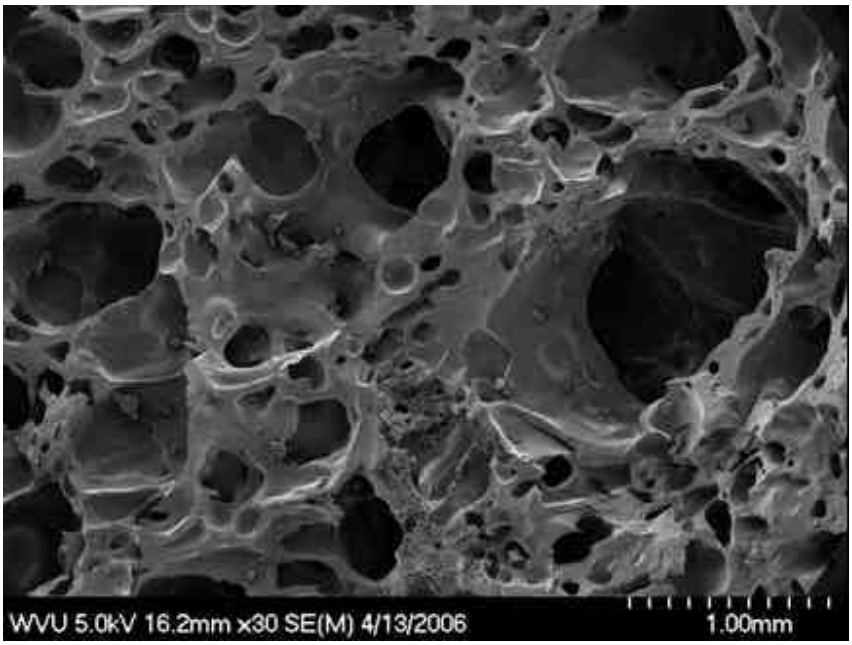

Figure 72. SEM of 110 °C softening point pitch foam produced at 95 °C, dP/dt of 22 psi/sec, and 200 psig of CO_2.

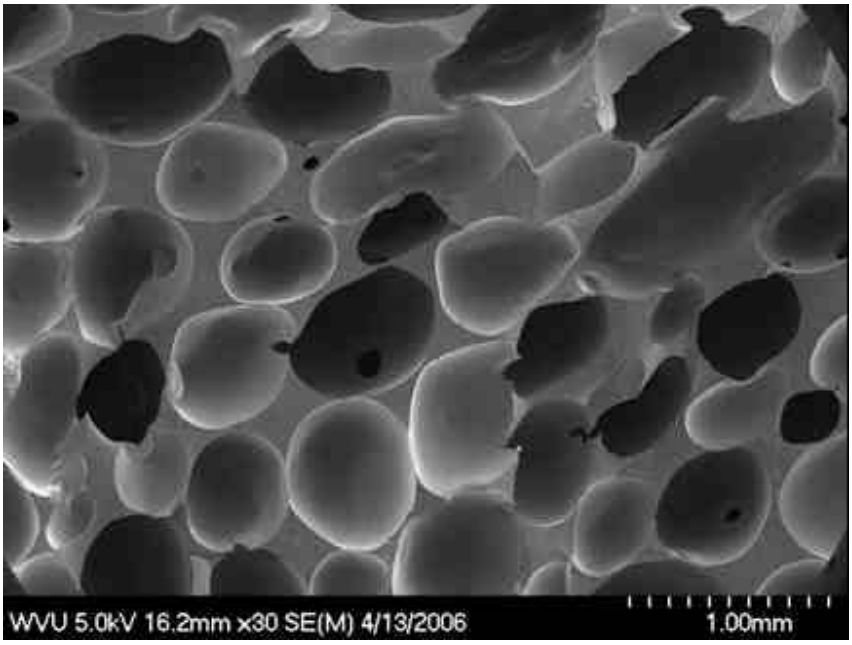

Figure 73. SEM of 180 °C softening point pitch produced at 150 °C, dP/dt of 28psi/sec, and 200 psig CO_2 and 0.3wt % mass fraction water added.

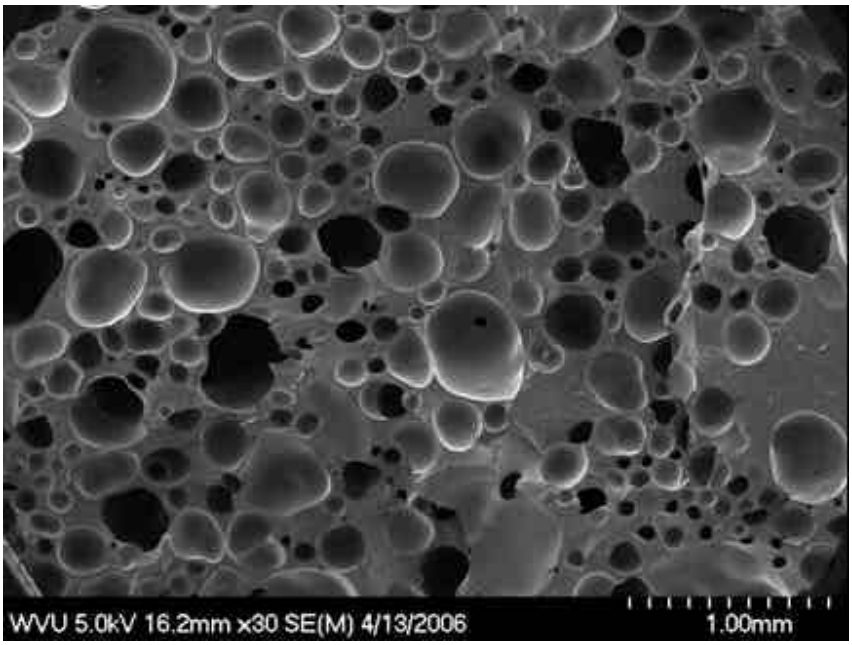

Figure 74. SEM of 180 °C softening point pitch produced at 155 °C, dP/dt of 15psi/sec and 180 psig CO_2.

Pitch foam, like stabilized carbon foam undergoes brittle fracture under load. The initial slope linear of the stress strain curve is the compressive Young's modulus. Elastic deformation occurs until the yield strength at which point cell structure ruptures begins to occur. Samples 1 and 2 show distinct modulus and yield points (Figures 75 and 76), whereas samples 3 and 4 though have no distinct modulus or yield strength (Figures 77 and 78). Once the yield strength is

reached, the stress strain curve plateaus till the cell structure is completely crushed. This region is where a majority of the energy absorption occurs in foams.

Upon complete collapse of cell structure, the solid material undergoes densification and behaves as a solid would. Samples 2-4 experienced complete destruction of cell structure and proceed to the densification phase at approximately 25-30 % strain (Figure 75). The densification of sample 1 did not start till about 40 % strain was reached (Figure 75). Table 17 shows the foam processing conditions, density, measured modulus, and yield strength of four pitch foam samples.

Table 17. Pitch foam process conditions and mechanical properties.

Sample	1	2	3	4
Temperature (°C)	160	155	155	155
Pressure (psi)	200	240	220	200
dP/dt (psi/sec)	28.6	37.3	8.1	33.3
Density (g/cm^3)	0.38±.01	0.52±.01	0.77±.04	0.79±.02
Compressive Strength (MPa)	0.2	0.5	1.4	<1.6
Compressive Modulus (MPa)	8	38	240	<160

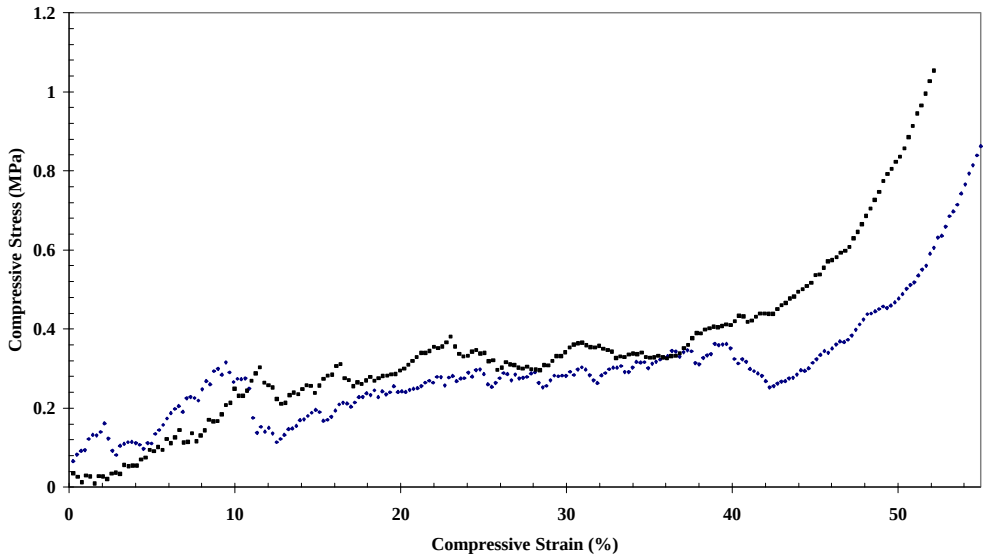

Figure 75. Compressive Stress/Strain Curves for two pitch foam samples from sample 1.

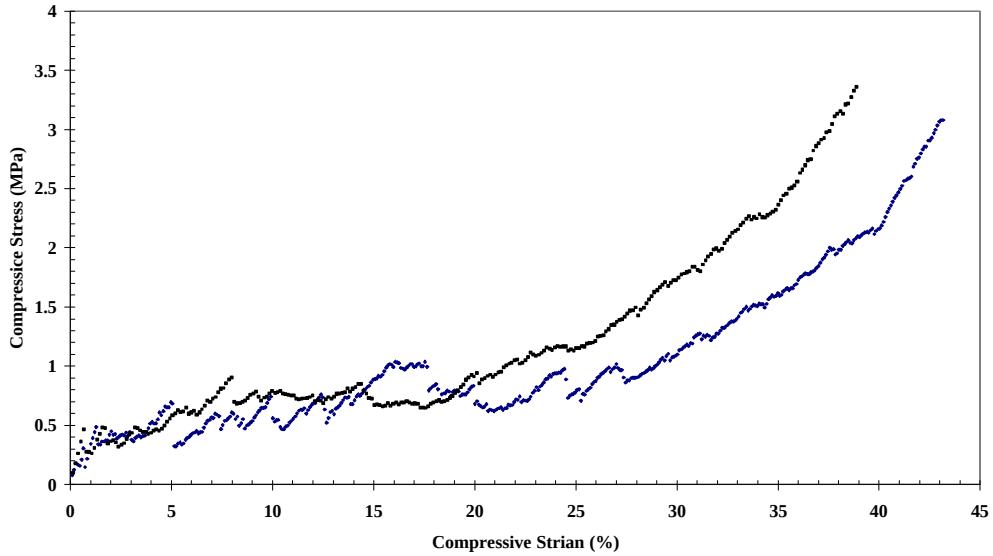

Figure 76. Compressive Stress Strain Curves for two pitch foam samples from sample 2.

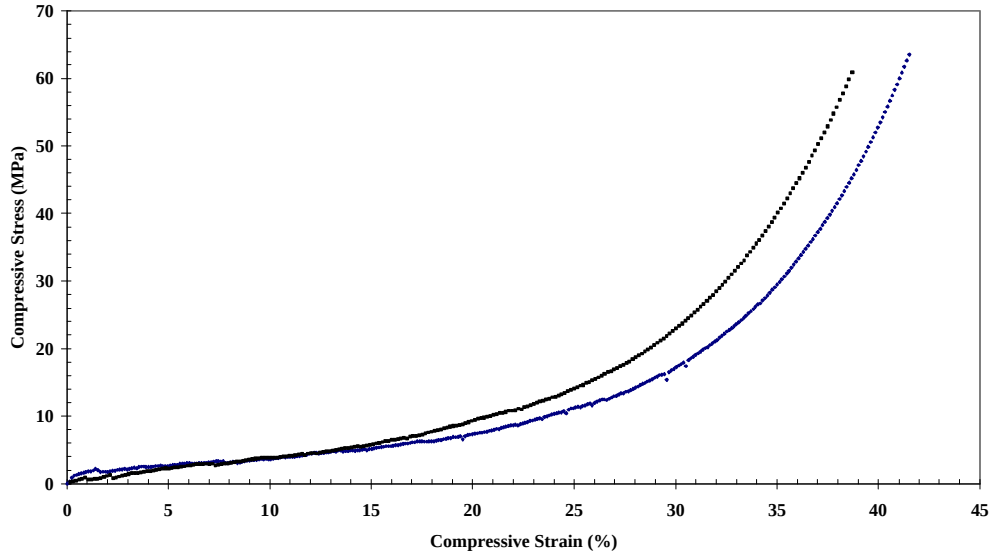

Figure 77. Compressive Stress Strain Curves for two pitch foam samples from sample 3.

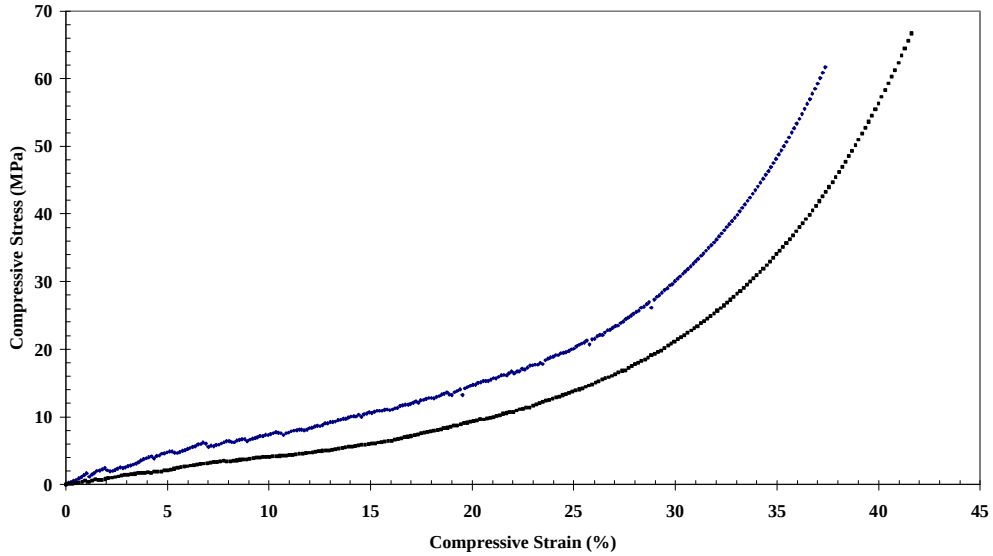

Figure 78. Compressive stress strain cures for two pitch foam samples from sample 4.

The mechanical properties of the pitch foam produced were compared to that of some commercially available carbon foams. There is currently no standard for measuring the mechanical compression properties of carbon foam. As such data provided by the manufacturers are difficult to compare directly. For this reason, data for the commercially available foams was taken from the MS thesis of Steve Carpenter and compared to pitch foam samples using the same test method. Carbon foam samples from Touchstone Research Laboratories (TRL), and POCO for Poco Graphite incorporated were reported. Graphitized carbon foam from Materials and Electrochemical Research (MER) was also reported and are listed on Table 18. The pitch foam showed lower modulus and yield strength then that of similar density carbon and graphite foams. Optimizing the cell structure and stabilizing to form green foam from the pitch foam would probably yield quantities that are closer to those commercially available.

Table 18. Comparison of sample pitch foams.

Specimen	Bulk Density (g/cm^3)	Modulus (MPa)	Yield Strength (MPa)
Ultramet	0.16	41	0.7
TRL	0.30	142	6.2
Sample 1	**0.38**	**8**	**0.2**
MER	0.50	81	1.5
Sample 2	**0.52**	**38**	**0.5**
POCO	0.62	142	2.2
Sample 3	**0.77**	**240**	**1.4**
Sample 4	**0.80**	**<160**	**<1.6**

As stated earlier, there is no standard method for testing the mechanical compressive properties of carbon and graphite foams. Direct comparison of pitch foam and commercially available carbon foam can not be made, though the quantities are listed on Table 19.

.

Table 19. Comparison of properties of foam samples.

	Bulk Density (g/cm^3)	Compressive Strength (MPa)	Compressive Modulus (MPa)
Touchstone CFOAM 17	0.27	6.2	550
Pitch Foam Sample 1	**0.38**	**0.2**	**8**
Koppers Carbon Foam Grade L1a	0.39	1.1	119
Touchstone CFOAM 25	0.40	>15	830
Koppers Carbon Foam Grade D1	0.46	2.5	396
Koppers Carbon Foam Grade L1	0.49	3.4	307
Pitch Foam Sample 2	**0.52**	**0.5**	**38**
Pitch Foam Sample 3	**0.77**	**1.4**	**240**
Pitch Foam Sample 4	**0.80**	**<1.6**	**<160**

Using experimental apparatus in Figure 59, pitch foam extrusion was attempted with the 110 ℃ softening point pitch. Higher temperatures and gas pressures were used in the extrusion process than in the batch process in order to force pitch melt thought the valve. The process was successful in producing and extruded pitch foam Figure 78. It can be seen from Figure 79 that the pitch experiences swells significantly through the extrusion valve. Supercritical CO_2 conditions were also achieved in the apparatus by adding dry ice during loading. Under supercritical conditions, pitch was successfully extruded at a significantly lower temperature (70 °C) then the 110 ℃ softening point of the pitch, though little cell expansion was achieved. Little qualitative data could be gleaned other than an upper range of foam melt stability before collapses due to the variability of flow and pressure-drop rate variations between runs. The upper limit temperature of melt stability for the 110 ℃ softening point pitch was ~130 ℃ witch corresponds to a undiluted viscosity of approximately 250 poise via the WFL equation.

Figure 79. Extrusion test with a 110 °C softening point pitch extruded at approximately 106 °C.

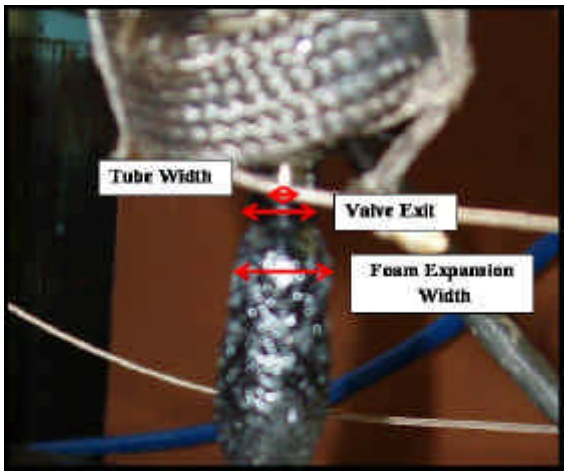

Figure 80. Foam expansion upon exiting the experimental extrusion apparatus at 106C and 540 psig on N_2 of a 110 °C softening point pitch (original poor quality).

Stabilization was attempted only for the foam made from the 180 °C softening point pitch to its higher T_g in comparison to the 110 °C pitch. The samples were heated to only 6 °C above the T_g calculated from Barr et al. correlation, but experienced relaxation of the bulk foam matrix. Heating above the T_g allows relaxation of the foam matrix leading to cell collapse. The 180 °C pitch experienced noticeable relaxation of the bulk structure prior to significant reduction of the volatile content. Higher softening point pitch or an alternative method to stabilizing in air for

18hr at 110 °C then 24hr at 125 °C is needed to stabilize the 180 °C pitch without loss of foam structure.

2.3.5. Summary of Pitch Foam Results

The characteristics of coal tar pitch and petroleum based pitch melts, mimic those of thermoplastic polymer melts. This similar behavior extends to foaming of the melts using physical blowing agents. The solubility of CO_2 and N_2, possibly coupled with moisture present in the pitch, at elevated pressures in coal tar pitch melts was sufficient at experimental conditions to reach the critical radius of bubble formation and resulted in cell formation upon thermodynamic instability (sudden pressure drop). The use of water as a physical blowing agent was also shown to be feasible as a phase change physical blowing agent. Cell structure, qualitatively, followed that of polymeric melts for the variables of viscosity, blowing agent concentration, and pressure drop rate are summarized on Table 20. The uses of physical blowing agents is a viable alternative rout for producing pitch foam that can be further processed into carbon foam through additional heat treatments. The mechanical properties at room temperature for the unoptimized cell structure pitch foam were lower then those for similar bulk density carbon and graphite foams.

Table 20. Quantitative analysis of tested variables and effects.

	Cell Density	Cell Size
Viscosity	Proportional	Inverse
Blowing Agent Conc.	Proportional	Inverse
Pressure Drop Rate	Proportional	Inverse

Thus, it has been shown from this study that pitch foam can be produced in a similar manner to other thermoplastics. Areas of further interest include: possible modification to current polymer foam models to model pitch foam, investigation into the composition of pitch and how it effects foaming characteristics, the solubility and diffusion of gases in pitch for superior blowing agent selection, the use of additives and fillers to modify properties and foaming characteristics, the use of continuous foam production, and cost analysis in comparison to current carbon foam production methods.

Bubble formation, mass, and momentum theory is fairly well developed for foaming viscous fluids. However, spontaneous cell formation and growth in a continuous dynamic process, as in extrusion, is far less developed. The test also showed that the control parameters character of the foam follows the general trend predicted polymer foaming models. More strenuous control of experimental variables is needed to compare polymer foaming models to pitch beyond a quantitative analysis and optimization.

Additional research is needed to bring this concept to maturity and commercialization. Specifically, at present little is known about how the composition of pitch affects the character of pitch foams. Additional study is needed to compare the foam characteristics of foam produced from various pitch sources (coal and petroleum).

There are limited data available for the solubility of gases in pitch. The limited amount of solubility information extends to other heavy petroleum and bitumens to a lesser degree. In this investigation, the solubility of CO_2 was assumed to be approximately equivalent to heavy petroleum fractions and bitumens. Additional information as to the solubility and diffusivity of CO_2 and other blowing agents would aid in the selection of process conditions and other blowing agents.

This study primarily used CO_2 as the blowing agent. Both water and N_2 were tried as blowing agents and were successful in produced foam, though the presence of moisture in the pitch may have contributed to cell formation. Other soluble gases and phase changing liquids may be better suited for cell formation in pitch. Some gases that may be of interest for further investigation include light hydrocarbons and hydrofluorocarbons.[122]

As with polymers, the addition of additives can significantly alter the properties foam. Three areas of additives of interest are fillers, surfactants, and stabilizers which are disused below.

A common practice with polymers and cement is to add fillers. The addition of fillers is often done for one of two reasons, first is to reduce the quantity of matrix material needed, and second to modify the matrix properties. Some fillers of possible interest in pitch foam are: carbon black, refractory metals, and carbon fibers and nanotubes. Using carbon black could be of interested in modifying the electrical conductivity characteristics of the foam. The addition of refractory metals by themselves is not of much interested, but with appropriate processing it may be possible to form carbides within the foam. The addition of carbon fibers and nanotubes are of interest in possibly modifying the mechanical and conductivity characteristics of the foam. With the addition of any filler the surface interactions and wetting characteristics of the filler with the pitch need to be considered.

It is known from polymer foam theory that the surface tension performs a significant role in cell formation, growth and melt stability. Adding surfactants might be a way of improving the foaming characteristic of pitch. Numerous surfactants have been developed for various petroleum products to reduce surface tension. Incorporating some of them into a pitch melt may result in reduced surface tension and improved foaming characteristics.

One of the difficulties encountered in this examination was the air stabilization of the pitch foam. Because of the low softening point, the foam structure would collapse when reheated above the T_g. Normally, in air stabilization the material being treated is heated to 135 °C or more and slowly increased. To attempt this, a pitch would need a softening point approximately 210 °C to hold the foam structure. The addition of cross-linking agents to the pitch may be a way to lower the temperature of stabilization for pitch foams. A possible experiment in evaluating possible cross-linkers in polymers is DSC. Often, the cross-linking process in polymers is exothermic. The resulting variations in heat flow are readily detectabe by DSC.[123,124,125]

This study showed that pitch foam can be extruded. The logical next step would be to attempt production of pitch foam in a continuous extrusion process. Melt processing techniques currently used with pitch fiber production would aid in identifying areas of divergence between pitch and polymer for a continuous foaming process.

The ultimate test of the proposed production method is the economic feasibility of commercial production. The ability to use commercially available processing equipment designed to foam polymers to produces pitch foam would probable be advantageous. The additional heat treatment of pitch foam may reduce the benefit by producing pitch foam by this technique.

2.4. Anisotropic Coke

Highly oriented coke, referred to as needle coke, is used for the production of graphitized steel electrodes. The name needle coke is due to the characteristic needle-like striations that clearly dominate the texture of the material. Needle coke that meets stringent industrial standards commands a price of several hundred dollars per ton. The principal requirement for needle coke is that the CTE must be 2.0 parts per million per degree ^{o}F or below (1).

Table 1 Desired properties of Needle Coke

Property	Value	Unit	Notes	Purpose
CTE	< 2.0			prevents spalling
Sulfur	<0.6	wt %		prevents puffing during graphitization
ash	< 0.3	wt %		causes voids during graphitization
coarse sizing	> 6	mm		
fines	<1	mm		
density	> 78	g/100ml	4/6 mesh test	
real density	2.13	g/cc		

Delayed coking is used to produce needle coke today. That is, hot desulfurized decant oil is pumped into the coking drums. During this process the thermal cracking temperature is reached but coking is "delayed" until the feedstock reaches the coke drums. In the drums hot volatile gases are emitted from the decant oil. The gases form bubbles which rise through the coking feedstock thereby stretching the coke as it begins to form. The temperature gradients as well as the internal stresses caused by the hot gases causes the coke to form oriented (anisotropic) crystalline structures, known as needle coke.

An alternate coking technique was demonstrated by Peter Stansberry and Alfred Stiller at the benchtop scale. At the time of this writing, a provisional patent has not been obtained, so details of the concept will be deferred to the next quarterly report. Nevertheless, figure 1 shows a microscopic image of the coke produced using the alternate method. It can be seen that there are oriented layers that formed parallel to one another, indicative of an anisotropic material.

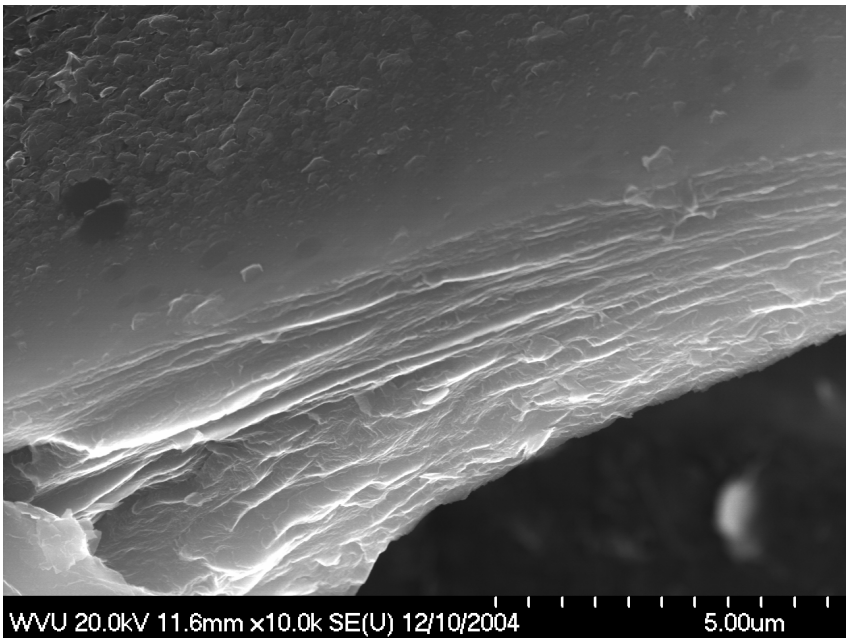

Figure 81 SEM image of oriented coke layers, indicating a high degree of anisotropy.

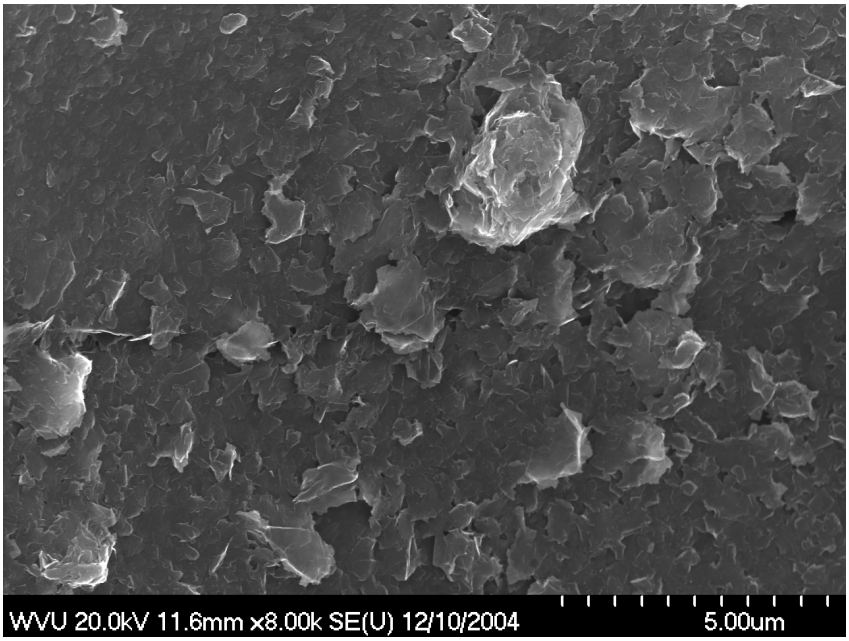

Figure 82. SEM image of an amorphous coke structure.

Figure 83. Test stand including reactor designed to enhance anisotropy of coke.

References.

[1] Chong Chen, Jinsheng Gao, Yongjie Yan; "Role of Noncovalent Bonding in Swelling of Coal"; (1998 American Chemical Society, 10.1021/ef970065w)

[2] Hessley, Reasoner, and Riley; page 4 of "Coal Science, an Introduction to Chemistry, Technology, and Utilization"; John Wiley & Sons, New York

[3] Fessenden, Fessenden, "Organic Chemistry"; Fifth Edition, Brooks/Cole Publishing Company, 1994

[4] Fessenden, Fessenden, "Organic Chemistry"; Fifth Edition, Brooks/Cole Publishing Company, 1994

[5] Fessenden, Fessenden, "Organic Chemistry"; Fifth Edition, Brooks/Cole Publishing Company, 1994

[6] Wiser, W. H. , "Schematic Representation of Structural Groups and Connecting Bridges in Bituminous Coal." 1978

[7] Petrakis, L., Grandy, D.W. "Coal Analysis, Characterization, and Petrography," J. Chem. Ed., 57, 691-692 (1980)

[8] "Coal Research Tutorial", Argonne National Laboratories, Chemistry Division, http://chemistry.anl.gov/carbon/coal-tutorial/nomenclature.html

[9] Hessley, Reasoner, and Riley; page 83 of "Coal Science, an Introduction to Chemistry, Technology, and Utilization"; John Wiley & Sons, New York

[10] Stiller, Alfred; "US patent # 4,272,356"; June 9, 1981

[11] Stiller, Alfred; "US patent # 4,272,356"; June 9, 1981

[12] Wiser, W. H. , "Schematic Representation of Structural Groups and Connecting Bridges in Bituminous Coal." 1978

[13] Toshimasa Takanohashi, Masashi Iino; "Investigation of Associated Structure of Upper Freeport Coal by Solvent Swelling"; Energy & Fuels 1995, 9, 788-793

[14] GAF Corporation, Chemical Division, *M-Pyrol—N-Methyl-2-Pyrrolidone*, New York, NY 1972.

[15] Toshimasa Takanohashi, Masashi Iino; "Investigation of Associated Structure of Upper Freeport Coal by Solvent Swelling"; Energy & Fuels 1995, 9, 788-793

[16] A. Marzec, M. Juzwa, K. Betlej, M. Sobkowiak; "BITUMINOUS COAL EXTRACTION IN TERMS OF ELECTRON-DONOR AND –ACCEPTOR INTERACTIONS IN THE SOLVENT/COAL SYSTEM"; Fuel Processing Technology, 2(1979) 35-44

[17] Chong Chen, Jinsheng Gao, Yongjie Yan; "Role of Noncovalent Bonding in Swelling of Coal"; (1998 American Chemical Society, 10.1021/ef970065w)

[18] A. Marzec, M. Juzwa, K. Betlej, M. Sobkowiak; "BITUMINOUS COAL EXTRACTION IN TERMS OF ELECTRON-DONOR AND –ACCEPTOR INTERACTIONS IN THE SOLVENT/COAL SYSTEM"; Fuel Processing Technology, 2(1979) 35-44

[19] Oele, A. P., Fuel, Vol. 30, pg.169, 1951.

[20] Dryden, I. G. C., *Fuel*, Vol. 30, pg39, 1951.

[21] Ana Maria Mastral, Maria Teresa Izquierdo, Begona Rubio; "Network swelling of coals"; FUEL, 1990, Vol 69, July

[22] Bland, Brian, "Design, Construction, and Evaluation of Coal Extraction Pilot Plant to Manufacture Coal Based Carbon Pitch"; Masters Thesis, West Virginia University, 2000

[23] Toshimasa Takanohashi, Masashi Iino; "Investigation of Associated Structure of Upper Freeport Coal by Solvent Swelling"; Energy & Fuels 1995, 9, 788-793

[24] Douglas Brenner; "In situ microscopic studies of the solvent-swelling of polished surfaces of coal"; FUEL, 1983, Vol 62, November

[25] Toshimasa Takanohashi, Masashi Iino; "Investigation of Associated Structure of Upper Freeport Coal by Solvent Swelling"; Energy & Fuels 1995, 9, 788-793

[26] George D. Cody, Jr., John W. Larsen, Michael Siskin; “Anisotropic Solvent Swelling of Coals”; Energy & Fuels, Vol. 2, No. 3, 1988

[27] George D. Cody, Jr., John W. Larsen, Michael Siskin; “Anisotropic Solvent Swelling of Coals”; Energy & Fuels, Vol. 2, No. 3, 1988

[28] George D. Cody, Jr., John W. Larsen, Michael Siskin; “Anisotropic Solvent Swelling of Coals”; Energy & Fuels, Vol. 2, No. 3, 1988

[29] George D. Cody, Jr., John W. Larsen, Michael Siskin; “Anisotropic Solvent Swelling of Coals”; Energy & Fuels, Vol. 2, No. 3, 1988

[30] George D. Cody, Jr., John W. Larsen, Michael Siskin; “Anisotropic Solvent Swelling of Coals”; Energy & Fuels, Vol. 2, No. 3, 1988

[31] Jose M. Rincon, Sergio Cruz; “Influence of preswelling on liquefaction of coal”; (FUEL, 1988, Vol 67, August)

[32] Jose M. Rincon, Sergio Cruz; “Influence of preswelling on liquefaction of coal”; (FUEL, 1988, Vol 67, August)

[33] Jose M. Rincon, Sergio Cruz; “Influence of preswelling on liquefaction of coal”; (FUEL, 1988, Vol 67, August)

[34] Jose M. Rincon, Sergio Cruz; “Influence of preswelling on liquefaction of coal”; (FUEL, 1988, Vol 67, August)

[35] Jorge M. Olivares, Nikolaos A Peppas; “THE EFFECT OF TEMPERATURE TREATMENT ON PENETRANT TRANSPORT IN COAL”; Chem. Eng. Comm. 1992, Vol. 115, pp. 183-204

[36] Jorge M. Olivares, Nikolaos A Peppas; “THE EFFECT OF TEMPERATURE TREATMENT ON PENETRANT TRANSPORT IN COAL”; Chem. Eng. Comm. 1992, Vol. 115, pp. 183-204

[37] Douglas Brenner; “Microscopic in-situ studies of the solvent induced swelling of thin sections of coal”; FUEL, 1984, Vol 63, September

[38] Jorge M. Olivares, Nikolaos A Peppas; “THE EFFECT OF TEMPERATURE TREATMENT ON PENETRANT TRANSPORT IN COAL”; Chem. Eng. Comm. 1992, Vol. 115, pp. 183-204

[39] Toshimasa Takanohashi, Masashi Iino; “Investigation of Associated Structure of Upper Freeport Coal by Solvent Swelling”; Energy & Fuels 1995, 9, 788-793

[40] Micromeretics sales brochure for Autopore 9220 mercury porosimeter

[41] A. Marzec, M. Juzwa, K. Betlej, M. Sobkowiak; “BITUMINOUS COAL EXTRACTION IN TERMS OF ELECTRON-DONOR AND –ACCEPTOR INTERACTIONS IN THE SOLVENT/COAL SYSTEM”; Fuel Processing Technology, 2(1979) 35-44

[42] A. Marzec, M. Juzwa, K. Betlej, M. Sobkowiak; "BITUMINOUS COAL EXTRACTION IN TERMS OF ELECTRON-DONOR AND –ACCEPTOR INTERACTIONS IN THE SOLVENT/COAL SYSTEM"; Fuel Processing Technology, 2(1979) 35-44

[43] Gallego, Nidia C., James W. Klett, "Carbon Foams for thermal management", Carbon, vol.41, 2003, 1461 1466.

[44] Frisch, Kurt C., James H. Saunders, Plastic Foams Vol. 1 & 2, Marcel Dekker Inc., New York, USA, 1972.

[45] Spradling, Drew M., R. Andrew Guth, "Carbon Foams", Advanced Materials & Processes, vol. 161 issue 11 2003, 29-31.

[46] Evans, David editor, Handbook of Polymer Foams, Rapra Technology Limited, Shawbury, UK, 2004.

[47] Gibson, Lorna J., Micheal E. Ashby, Cellular Solids: Structure and Properties, 2 Edition, Cambridge University Press, Cambridge, UK, 1997.

[48] Gibson, Lorna J., Micheal E. Ashby, Cellular Solids: Structure and Properties, 2 Edition, Cambridge University Press, Cambridge, UK, 1997.

[49] Choi, S., B.V. Sankar, "Fracture Toughness of Carbon Foam", Journal of Composite Materials, vol.37, no.23, 2003, 2101-2116.

[50] Sihn, Sangwook, Ajit K. Roy, "Modeling and prediction of bulk properties of open-cell carbon foam", Journal of the Mechanics and Physics of Solids, vol.52, 2004, 167-191.

[51] Gibson, Lorna J., Micheal E. Ashby, Cellular Solids: Structure and Properties, 2 Edition, Cambridge University Press, Cambridge, UK, 1997.

[52] Latartech Holdings LTD, http://www.latartech.com/page7.phtml, Accessed: April 2006.

[53] Frisch, Kurt C., James H. Saunders, Plastic Foams Vol. 1 & 2, Marcel Dekker Inc., New York, USA, 1972.

[54] Frisch, Kurt C., James H. Saunders, *Plastic Foams Vol. 1 & 2*, Marcel Dekker Inc., New York, USA, 1972.

[55] Lee, S. T. editor, *Foam Extrusion: Principles and Practice*, Technomic Pub. Comp., Pennsylvania, USA, 2000.

[56] Lee, S. T. editor, *Foam Extrusion: Principles and Practice*, Technomic Pub. Comp., Pennsylvania, USA, 2000.

[57] Lee, S. T. editor, *Foam Extrusion: Principles and Practice*, Technomic Pub. Comp., Pennsylvania, USA, 2000.

[58] Frisch, Kurt C., James H. Saunders, Plastic Foams Vol. 1 & 2, Marcel Dekker Inc., New York, USA, 1972.

[59] Evans, David editor, Handbook of Polymer Foams, Rapra Technology Limited, Shawbury, UK, 2004.

[60] Maio, E. Di, G. Mensitieri, G., S. Iannace, L. Nicolais, W. Li, R.W. Flumerfelt, "Structure Optimization of Polycaprolactone Foams by Using Mixtures of CO2 and N2 as Blowing Agents", Polymer Engineering and Science, vol.45, 2005, 432-441.

[61] Beechem, Thomas, Khalid Lafdi, Ahmed Elgafy, "Bubble Growth Mechanism in Carbon Foams", Carbon, vol. 43, 2005, 1055-1064.

[62] Beechem, Thomas, Khalid Lafdi, Ahmed Elgafy, "Bubble Growth Mechanism in Carbon Foams", Carbon, vol. 43, 2005, 1055-1064.

[63] Tomasko, David L., Hongbo Li, Dehua Liu, Xiangmin Han, Maxwell J. Wingert, L. James Lee, Kurt W. Koelling, "A Review of CO2 Applications in the Processing of Polymers", Industrial Engineering Chemical Research, vol.42, 2003, 6431-6456.

[64] Tomasko, David L., Hongbo Li, Dehua Liu, Xiangmin Han, Maxwell J. Wingert, L. James Lee, Kurt W. Koelling, "A Review of CO2 Applications in the Processing of Polymers", Industrial Engineering Chemical Research, vol.42, 2003, 6431-6456.

[65] Lee, S. T. editor, Foam Extrusion: Principles and Practice, Technomic Pub. Comp., Pennsylvania, USA, 2000.

[66] Lee, S. T. editor, Foam Extrusion: Principles and Practice, Technomic Pub. Comp., Pennsylvania, USA, 2000.

[67] Lee, S. T. editor, Foam Extrusion: Principles and Practice, Technomic Pub. Comp., Pennsylvania, USA, 2000.

[68] Lee, S. T. editor, Foam Extrusion: Principles and Practice, Technomic Pub. Comp., Pennsylvania, USA, 2000.

[69] Lee, S. T. editor, Foam Extrusion: Principles and Practice, Technomic Pub. Comp., Pennsylvania, USA, 2000.

[70] Pop-Iliev, Remon, Fangyi Liu, Guobin Liu, Chul B. Park, "Rotational Foam Molding of Polypropylene with Control of Melt Strength", Advances in Polymer Technology, vol. 22, 2003, 280-296.

[71] Pop-Iliev, Remon, Fangyi Liu, Guobin Liu, Chul B. Park, "Rotational Foam Molding of Polypropylene with Control of Melt Strength", Advances in Polymer Technology, vol. 22, 2003, 280-296.

[72] Pop-Iliev, Remon, Fangyi Liu, Guobin Liu, Chul B. Park, "Rotational Foam Molding of Polypropylene with Control of Melt Strength", Advances in Polymer Technology, vol. 22, 2003, 280-296.

[73] Kearns; Kristen M., United States Patent 5,961,814, Oct. 5 1999.

[74] Rogers, Darren, Kenneth, World Intellectual Property Organization, WO 03/072348 A1, 2003.

[75] Beechem, Thomas, Khalid Lafdi, Ahmed Elgafy, "Bubble Growth Mechanism in Carbon Foams", Carbon, vol. 43, 2005, 1055-1064.

[76] Spradling, Drew M., R. Andrew Guth, "Carbon Foams", Advanced Materials & Processes, vol. 161 issue 11 2003, 29-31.

[77] Campbell, D., R.A. Pethrick, J.R. White, Polymer Characterization: Physical Techniques, 2nd Edition, Stanley Thornes Pub. Ltd., Cheltenham, UK, 2000.

[78] Rand, B., "Pitch precursors for advanced carbon materials – Rheological aspects", Fuel vol.66, 1987, 1491-1503.

[79] Rand, B., "Pitch precursors for advanced carbon materials – Rheological aspects", Fuel vol.66, 1987, 1491-1503.

[80] Khandare, Pravin M. Characterization of Mesophase Pitch Materials from Petroleum and Coal-Derived Precursors: Kinetics and Rheology at Elevated Temperatures. Ph.D. Dissertation, West Virginia University, 1995.

[81] Tomasko, David L., Hongbo Li, Dehua Liu, Xiangmin Han, Maxwell J. Wingert, L. James Lee, Kurt W. Koelling, "A Review of CO2 Applications in the Processing of Polymers", Industrial Engineering Chemical Research, vol.42, 2003, 6431-6456.

[82] Tomasko, David L., Hongbo Li, Dehua Liu, Xiangmin Han, Maxwell J. Wingert, L. James Lee, Kurt W. Koelling, "A Review of CO2 Applications in the Processing of Polymers", Industrial Engineering Chemical Research, vol.42, 2003, 6431-6456.

[83] Tomasko, David L., Hongbo Li, Dehua Liu, Xiangmin Han, Maxwell J. Wingert, L. James Lee, Kurt W. Koelling, "A Review of CO2 Applications in the Processing of Polymers", Industrial Engineering Chemical Research, vol.42, 2003, 6431-6456.

[84] Garg, Ashok, Esin Gulari, Charles W. Manke. "Thermodynamics of Polymer Melts Swollen with Supercritical Gases", Macromolecules, vol. 27, 1994, 5643-5653.

[85] Royer, Joseph R, Joseph M. DeSimone, Saad A. Khan, "High-Pressure Rheology and Viscoelastic Scaling Predictions of Polymer Melts Containing Liquid and Supercritical Carbon Dioxide", Journal of Polymer Science, vol. 39, 2001, 3055-3066.

[86] Danner, Ronald P., Martin S. High, Handbook of Polymer Solution Thermodynamics, American Institute of Chemical Engineers, New York, 1993.

[87] Gerhardt, Linda J., Ashok Garg, Charles W. Manke, Esin Gulari, "Concentration-Dependent Viscoelastic Scaling Models for Polydimethylsiloxane Melts with Dissolved Carbon Dioxide", Journal of Polymer Science: Part B: Polymer Physics, vol.35, 1998, 1911-1918.

[88] Frisch, Kurt C., James H. Saunders, Plastic Foams Vol. 1 & 2, Marcel Dekker Inc., New York, USA, 1972.

[89] Royer, Joseph R, Joseph M. DeSimone, Saad A. Khan, "High-Pressure Rheology and Viscoelastic Scaling Predictions of Polymer Melts Containing Liquid and Supercritical Carbon Dioxide", Journal of Polymer Science, vol. 39, 2001, 3055-3066.

[90] Rand, B., "Pitch precursors for advanced carbon materials – Rheological aspects", Fuel vol.66, 1987, 1491-1503.

[91] William, M. L., R.F. Landel, J.D. Ferry, "The Temperature dependence of relaxation mechanisms in amorphous polymers and other glass-forming liquids", Journal of the American Chemical Society, vol.77, 1955, 3701-3707.

[92] Frisch, Kurt C., James H. Saunders, Plastic Foams Vol. 1 & 2, Marcel Dekker Inc., New York, USA, 1972.

[93] Rand, B., "Pitch precursors for advanced carbon materials – Rheological aspects", Fuel vol.66, 1987, 1491-1503.

[94] Royer, Joseph R, Joseph M. DeSimone, Saad A. Khan, "High-Pressure Rheology and Viscoelastic Scaling Predictions of Polymer Melts Containing Liquid and Supercritical Carbon Dioxide", Journal of Polymer Science, vol. 39, 2001, 3055-3066

[95] Royer, Joseph R., Yvon J. Gay, Joseph M. Desimone, Saad A. Khan, "High-Pressure Rheology of Polystyrene Melts Plasticized with CO2: Experimental Measurement and Predictive Scaling Relationship", Journal of Polymer Science: Part B: Polymer Physics, vol.28, 2000, 3168-3180.

[96] Chow, T.S., "Molecular Interpretation of the Glass Transition Temperature of Polymer-Diluent Systems", Macromolecules, vol.13, 1980, 362-364.

[97] Chow, T.S., "Molecular Interpretation of the Glass Transition Temperature of Polymer-Diluent Systems", Macromolecules, vol.13, 1980, 362-364.

[98] Tomasko, David L., Hongbo Li, Dehua Liu, Xiangmin Han, Maxwell J. Wingert, L. James Lee, Kurt W. Koelling, "A Review of CO2 Applications in the Processing of Polymers", Industrial Engineering Chemical Research, vol.42, 2003, 6431-6456.

[99] Garland, Carl W., Joseph W. Nibler, David P. Shoemaker, Experiments in Physical Chemistry 7ed, McGraw-Hill Comp., New York, 1996.

[100] Rand, B., "The Thermal Processing and Rheological Behavior of Pitch", Design and Control of Structure of Advanced Carbon Materials for Enhanced Performance. Kluwer Academic Publishers, Netherlands, 2001, 135-150.

[101] Fair, W.F. Jr., "The Asphalt Symposium Part I", Industrial Engineering & Chemistry, vol.55, 1966, 26-27.

[102] Campbell, D., R.A. Pethrick, J.R. White, Polymer Characterization: Physical Techniques, 2nd Edition, Stanley Thornes Pub. Ltd., Cheltenham, UK, 2000.

[103] Traceski, Frank T., "Assessing Industrial Capabilities for Carbon Fiber Production", Acquisition Review Quarterly, Spr. 1999, 179-194.

[104] Tadmor, Zehev, and Costas G. Gogos, Principles of Polymer Processing, John Wiley & Sons, Inc., New York, 1979.

[105] Hegde, Raghavendra R., Atul Dahiya, M. G. Kamath, Carbon Fibers, http://www.engr.utk.edu/mse/pages/Textiles/CARBON%20FIBERS.htm, updated Apr. 2004, accessed Feb. 2006.

[106] Maio, E. Di, G. Mensitieri, G., S. Iannace, L. Nicolais, W. Li, R.W. Flumerfelt, "Structure Optimization of Polycaprolactone Foams by Using Mixtures of CO2 and N2 as Blowing Agents", Polymer Engineering and Science, vol.45, 2005, 432-441.

[107] Speight, James G., Handbook of Petroleum Product Analysis, Wiley & Sons, Inc., Hoboken, New Jersey, 2002.

[108] American National Standards Institute, ASTM D3104-99 (2005).

[109] Briggs, D.K.H., "The Surface Tension of Coal Tar Pitch", Fuel, vol.43, 1964, 439-43.

[110] Tomasko, David L., Hongbo Li, Dehua Liu, Xiangmin Han, Maxwell J. Wingert, L. James Lee, Kurt W. Koelling, "A Review of CO2 Applications in the Processing of Polymers", Industrial Engineering Chemical Research, vol.42, 2003, 6431-6456.

[111] Schwarz, Barry J., John M Prausnitz, "Solubilities of Methane, Ethane, and Carbon Dioxie in Heavy Fossil-Fuel Fractions", Industrial Engineering and Chemical Research, vol. 26, 1987, 2360-2366. .

[112] Deo, Milind D., Chia J. Wang, and Francis V. Hanson, "Solubility of Carbon Dioxide in Tar Sand Bitumen: Experimental Determination and Modeling", Industrial Engineering and Chemical Research, vol.30, 1991, 532-536.

[113] Riazi, M.R., and J.H. Vera, "Method to Calculated the Solubilities of Light Gases in Petroleum and Coal Liquid Fractions on the Basis of their P/N/A Composition", Industrial Engineering and Chemical Research, vol.44, 2005, 186-192

[114] Schwarz, Barry J., John M Prausnitz, "Solubilities of Methane, Ethane, and Carbon Dioxie in Heavy Fossil-Fuel Fractions", Industrial Engineering and Chemical Research, vol. 26, 1987, 2360-2366.

[115] Deo, Milind D., Chia J. Wang, and Francis V. Hanson, "Solubility of Carbon Dioxide in Tar Sand Bitumen: Experimental Determination and Modeling", Industrial Engineering and Chemical Research, vol.30, 1991, 532-536.

[116] Riazi, M.R., and J.H. Vera, "Method to Calculated the Solubilities of Light Gases in Petroleum and Coal Liquid Fractions on the Basis of their P/N/A Composition", Industrial Engineering and Chemical Research, vol.44, 2005, 186-192.

[117] Rand, B., "The Thermal Processing and Rheological Behavior of Pitch", Design and Control of Structure of Advanced Carbon Materials for Enhanced Performance. Kluwer Academic Publishers, Netherlands, 2001, 135-150.

[118] Lide, David R., editor, CRC Handbook of Chemistry and Physics 1997ed, 1997.

[119] Chow, T.S., "Molecular Interpretation of the Glass Transition Temperature of Polymer-Diluent Systems", Macromolecules, vol.13, 1980, 362-364.

[120] NIST Standard Reference Database 69, June 2005 Release: NIST Chemistry WebBook. http://webbook.nist.gov/chemistry/.
Deformation Mechanisms in Materials, <www.ems.psu.edu/~green/564-535.html>, Accessed March 2006.

[121] Park, Chul B., Lewis K Cheung, "A Study of Cell Nucleation in the Extrusion of Polypropylene Foams", Polymer Engineering and Science, vol.31, no.1, 1997, 1-10.

[122] Evans, David editor, Handbook of Polymer Foams, Rapra Technology Limited, Shawbury, UK, 2004.

[123] Dean, John A., The Analytical Chemistry Handbook, New York, McGraw Hill, Inc., 1995, 15.1-15.5.

[124] Pungor, Erno, A Practical Guide to Instrumental Analysis, Boca Raton, Florida, 1995, 181-191.

[125] Skoog, Douglas A., F. James Holler and Timothy Nieman, Principles of Instrumental Analysis, Fifth Edition. New York, 1998, 905-908.